INDUCED POLARIZATION OF METALLIC MINERALS, A STUDY OF ITS CHEMICAL BASIS

by

Yed Esaie Angoran

Ingénieur Civil des Mines

Nancy, France (1970)

SUBMITTED IN PARTIAL FULFILLMENT OF THE REQUIREMENTS

FOR THE DEGREE OF

DOCTOR OF PHILOSOPHY

at the

MASSACHUSETTS INSTITUTE OF TECHNOLOGY

September 1975
(i.e. February, 1976)

Signature of Author _____
Department of Earth & Planetary Sciences

Certified by _____
Thesis Supervisor

Accepted by _____
Chairman, Departmental Committee on Graduate Students

Archives
MASS. INST. TECH.
DEC 17 1975
LIBRARIES

INDUCED POLARIZATION OF METALLIC MINERALS, A STUDY OF ITS CHEMICAL BASIS

by

YED ESAIE ANGORAN

Submitted to the Department of Earth and Planetary Sciences in September, 1975, in partial fulfillment of the requirements for the degree of Doctor of Philosophy.

ABSTRACT

The mechanism of induced polarization of metallic minerals, widely used in mining geophysical exploration, is studied from the electrochemical standpoint. The approach leads to investigations of linear electrode impedance spectra in various chemical environments involving wide ranges of Eh and pH in a variety of solutions. It is shown through the generalized inversion of the electrical equivalent circuit that the electrode impedance is dominated by a Warburg impedance term in agreeement with Madden's results (Madden, 1961). This implies that the electrode impedance is controlled by diffusion processes in the solution and/or along the electrode surface. It is shown that when in the solution, cupric and sulfide ions could be active at the electrodes, i.e. control the electrode impedance. In the presence of such active species, surface phenomena are not important and the electrode impedance is explainable on the basis of the active species concentration. However, in the absence of active species, surface phenomena become important. The electrode impedances are not usually dependent on the concentration of the ionic species, chlorides (Cl^-), sulfates ($SO_4^{=}$), carbonates ($CO_3^{=}$), nitrates (NO_3^-), hydroxides (OH^-), iron (Fe^{++}), calcium (Ca^{++}), potassium (K^+), sodium (Na^+), and hydronium (H^+). It is also observed that the electrode impedance is heavily dependent on the surface condition of the electrode. A theory of surface diffusion impedance is proposed to explain the measured electrode impedances whereby major ionic species carry the Faradaic current in the solution while diffusion processes along the electrode surface contribute substantially to the impedance. The importance of the

surface condition of the electrode is demonstrated by depolarization experiments which dramatically lower the surface diffusion impedance. It is shown that in a chloride environment, copper and iron electrode impedances drop after limited impression of anodic current. For sulfide electrodes, however, the depolarization occurs as a result of impression of cathodic current. Insight into the electrodes' reactions is gained through electron microprobe analyses of the electrodes. In particular, it is shown that intensely depolarized copper electrodes have taken up chlorine while depolarized sulfide electrodes are substantially depleted of sulfur. Several hypotheses are proposed for the electrode processes which are consistent with the experimental observations. These studies indicate that the IP responses will not show anomalous behavior in the range of natural environments to be normally expected.

Thesis Supervisor: Theodore R. Madden

Title: Professor of Geophysics

ACKNOWLEDGEMENTS

To Professor Madden, I would like to express my deepest gratitude for his advice and assistance, both human and scientific. It is my hope that this thesis represents at least a reflection of his inspiration. For his limitless supply of patience and his penetrating physical insight, working under Ted's guidance has been an instructive and pleasurable experience.

I would like to thank Professor J. Dickey and Professor J. Edmond for making their laboratory facilities available to me. I also thank Professor R. Burns, who kindly made some x-ray diffraction patterns for me and Professor P. Hurley, who gave me the initial mineral samples.

I am grateful also to Dr. David Davies, who was my advisor in seismology while he was at M.I.T.

I sincerely thank Judy Ungermann for accepting to type this thesis.

Finally, immesurable gratitude is due to my parents, Yed Robert Angoran and Awell Madeleine Tètè for their continuing moral support, having suffered so patiently my long stays away from home.

This research has been partially supported by The National Science Foundation Grant No. GA-41748, while the author has held a scholarship from the Government of the Ivory Coast.

TABLE OF CONTENTS

		Page
CHAPTER 0		13
0.1	Introduction	13
0.2	Plan of the Thesis	16
CHAPTER I	THEORY OF IP, AN ELECTROCHEMICAL APPROACH	18
1.1	Madden's Linear Electrode Impedance Theory and Extensions	18
1.2	Faradaic Impedance and Equivalent Circuit for Simple Electrode Reaction	23
1.3	Concentration of Active Species	33
1.4	Surface Diffusion Impedance	34
1.5	Generalized Inversion Scheme	37
CHAPTER II	METHOD OF ANALYSIS	40
2.1	Chemical Environment in Terms of Eh and pH	42
2.2	Eh-pH Diagrams	46
2.2.1	Eh-pH Diagrams for Copper in Aqueous Solutions	47
2.2.2	Eh-pH Diagrams for Iron in Aqueous Solutions	54
2.2.3	Stability Fields of Copper Oxides and Sulfides	56
2.2.4	Stability Fields of Iron Oxides and Sulfides	56
2.3	Experimental Set-Up	58
2.3.1	Geometry of Cell and Electrodes Configuration	60
2.3.2	Experimental Conditions and Their Control	63

Table of Contents

		Page
2.3.3	The Impedance Comparator	66
2.3.4	Methods of Measurement	68
2.4	Typical Results of Measurements	68
2.5	Equivalent Circuit Fitting	69
CHAPTER III	EMPIRICAL CLASSIFICATION OF IONIC SPECIES AND ELECTRODES REACTIONS	84
3.1	Excursion in the Eh-pH Diagrams	85
3.2	Active and Inactive Ionic Species	86
3.2.1	Active Behavior of Cupric Ions and Associated Reactions	87
3.2.2	Active Behavior of Sulfide Ions and Associated Reactions	96
3.2.3	Exceptional Case of Active Behavior of H^+ Ions	99
3.3	Ionic Diffusion from Electrodes: the Wagner Analogy	99
3.3.1	The Warburg Series	111
3.3.2	The Wagner Analogy of Ionic Diffusion in Electrodes	112
CHAPTER IV	DEPOLARIZATION EXPERIMENTS	117
4.1	Critical Role of the Surface Condition	117
4.2	A Closer Look into the Surface Diffusion Contribution to the Electrode Impedance	122
4.3	Depolarization Experiments on Copper, Iron, and Sulfide Electrodes	134
4.3.1	Depolarization of Copper Electrodes	135
4.3.2	Depolarization of Iron Electrodes	136
4.3.3	Depolarization of Sulfide Electrodes	137

Table of Contents

		Page
4.3.4	Electrode Reactions in Light of the Electron Microprobe Analysis	148
4.4	Chloride and Activated Metals Reactions	157
4.4.1	Catalytic Behavior of Metallic Chlorides	158
4.4.2	Induced Activated Metals on Sulfide Electrodes	161
CHAPTER V	SUMMARY AND CONCLUSIONS WITH IMPLICATIONS FOR MINERAL EXPLORATION	166
5.1	Implications for Electrical Exploration of Minerals	168
5.2	Suggestions for Further Research	173
APPENDIX A	INVERSION OF THE ELECTRODE IMPEDANCE SPECTRUM BY THE GENERALIZED INVERSE THEORY	177
REFERENCES		182
LIST OF SYMBOLS		187

LIST OF FIGURES

		Page
Figure 1.1	Electrode Impedance Model with 4 Parameters	27
Figure 1.2	Electrode Impedance Model with 8 Parameters	30
Figure 1.3	Electrode Surface Structure (adapted from Neumann and Neumann, 1972)	35
Figure 1.4	Electrode Impedance Model with Surface Diffusion	38
Figure 2.1	Duality of Oxidation and Reduction Processes at Electrodes	43
Figure 2.2	Eh-pH Diagram of Copper in Chloride Environment (adapted from Pourbaix, 1973)	48
Figure 2.3a	Eh-pH Diagram of Copper in Chloride Environment (adapted from Pourbaix, 1973)	52
Figure 2.3b	Stability Fields of Solids Involved in Copper Reactions in Chloride Environments	53
Figure 2.4	Eh-pH Diagram of Iron in Chloride Environment (adapted from Pourbaix, 1973)	55
Figure 2.5	Eh-pH Diagram of Copper Sulfides (adapted from Garrels and Christ, 1965)	57
Figure 2.6	Eh-pH Diagram of Iron Sulfides (adapted from Garrels and Christ, 1965)	59
Figure 2.7	Schematic of the Experimental Set-Up	65
Figure 2.8	Schematic of the Impedance Comparator	67
Figure 3.1	Warburg Impedance as a Function of Eh-pH for Copper in (KCl, $CuSO_4$)	88
Figure 3.2	Warburg Impedance as a Function of Eh-pH for Chalcocite in $CuSO_4$ Solution	91

List of Figures

		Page
Figure 3.3	Warburg Impedance as a Function of Eh-pH for Chalcocite in (KCl, $CuSO_4$) Solution	92
Figure 3.4	Warburg Impedance as a Function of Eh-pH for Covellite (i) in (KCl, $CuSO_4$) Solution	93
Figure 3.5	Warburg Impedance as a Function of Eh-pH for Covellite (ii) in (KCl, $CuSO_4$) Solution	94
Figure 3.6	Warburg Impedance as a Function of Eh-pH for Covellite in $CuSO_4$ Solution	95
Figure 3.7	Warburg Impedance as a Function of Eh-pH for Chalcocite (i) in Na_2S Solution	97
Figure 3.8	Warburg Impedance as a Function of Eh-pH for Chalcocite (ii) in Na_2S	98
Figure 3.9	Warburg Impedance as a Function of Eh-pH for Diamond-Polished Copper in KCl Solution	100
Figure 3.10	Warburg Impedance as a Function of Eh-pH for Covellite in KCl Solution	101
Figure 3.11	Warburg Impedance as a Function of Eh-pH for Chalcocite in KCl Solution (i)	102
Figure 3.12	Warburg Impedance as a Function of Eh-pH for Chalcocite in KCl Solution (ii)	103
Figure 3.13	Warburg Impedance as a Function of Eh-pH for Pyrrhotite in KCl Solution	104
Figure 3.14	Warburg Impedance as a Function of Eh-pH for Covellite in Na_2SO_4 Solution	105
Figure 3.15	Warburg Impedance as a Function of Eh-pH for Chalcocite in Na_2SO_4 Solution	106
Figure 3.16	Warburg Impedance as a Function of Eh-pH for Chalcocite in Na_2CO_3 Solution (i)	107
Figure 3.17	Warburg Impedance as a Function of Eh-pH for Chalcocite in Na_2CO_3 Solution (ii)	108

List of Figures

		Page
Figure 3.18	Warburg Impedance as a Function of Eh-pH for Copper in Na_2CO_3 Solution	109
Figure 3.19	Warburg Impedance as a Function of Eh-pH for Copper in $Ca(NO_3)_2$ Solution	110
Figure 3.20	Wagner's Experimental Set-Up	113
Figure 3.21	Equivalent Circuit of the Electrochemical Analogy of Wagner's Oxidation Mechanism	113
Figure 4.1	Warburg Impedance as a Function of Eh-pH for Diamond-Polished and Paper-Polished Copper in KCl Solution	119
Figure 4.2	Warburg Impedance as a Function of Eh-pH for Diamond-Polished Covellite in KCl Solution	120
Figure 4.3	Warburg Impedance as a Function of Eh-pH for Diamond-Polished Chalcocite in KCl Solution.	121
Figure 4.4	Comparison of Amplitude Behavior of a One-Dimensional Surface Diffusion Impedance and CW Branch Impedance	131
Figure 4.5	Comparison of Phase Behavior of a One-Dimensional Surface Diffusion Impedance and a CW Branch Impedance	132

LIST OF TABLES

		Page
Table 2.1	Effect of Concentration on Warburg Impedance for Nickel Electrodes	40
Table 2.2	Effect of pH on Warburg Impedance for Graphite Electrodes	41
Table 2.3	Warburg Impedances for Various Electrodes	41
Table 2.4	Diffusion Lengths (μm) as a Function of Frequency and Diffusivities	61
Table 2.5	Copper Electrode Impedance	71
Table 2.6	Iron Electrode Impedance	71
Table 2.7	Covellite Electrode Impedance	72
Table 2.8	Chalcocite Electrode Impedance	72
Table 2.9	Chalcopyrite Electrode Impedance	73
Table 2.10	Pyrrhotite Electrode Impedance	73
Table 2.11	Pyrite Electrode Impedance	74
Table 2.12	Equivalent Circuit Fitting of Copper Electrode Impedance	76
Table 2.13	Equivalent Circuit Fitting of Iron Electrode Impedance	77
Table 2.14	Equivalent Circuit Fitting of Covellite Electrode Impedance	78
Table 2.15	Equivalent Circuit Fitting of Chalcocite Electrode Impedance	79
Table 2.16	Equivalent Circuit Fitting of Chalcopyrite Electrode Impedance	80
Table 2.17	Equivalent Circuit Fitting of Pyrrhotite Electrode Impedance	81
Table 2.18	Equivalent Circuit Fitting of Pyrite Electrode Impedance	82
Table 3.1	Warburg Impedance Associated to Active Ionic Species	86

List of Tables

		Page
Table 4.1	Depolarization Experiments on Copper Electrodes	138
Table 4.2	Depolarization Experiments on Iron Electrodes	139
Table 4.3	Depolarization Experiments on Covellite Electrodes	141
Table 4.4	Depolarization Experiments on Chalcocite Electrodes	142
Table 4.5	Depolarization Experiments on Pyrite Electrodes	143
Table 4.6	Depolarization Experiments on Chalcopyrite Electrodes	144
Table 4.7	Depolarization Experiments on Pyrrhotite Electrodes	145
Table 4.8	Electron Microprobe Analyses of Chalcocite Electrodes	151
Table 4.9	Electron Microprobe Analyses of Covellite Electrodes	152
Table 4.10	Electron Microprobe Analyses of Chalcopyrite and Pyrrhotite Electrodes	153
Table 4.11	Electron Microprobe Analyses of Pyrite Electrodes	154
Table 4.12	Electron Microprobe Analyses of Pyrite and Copper Electrodes	155
Table 4.13	Electron Microprobe Analyses of Copper and Brass Electrodes	156
Table 5.1	Eh-pH of Natural Waters in Mining Districts	170
Table 5.2	Comparison of Background Electrode Impedances for Sulfide Electrodes	172

CHAPTER 0

0-1 Introduction

The concept of induced polarization (IP) is far from new. Since its introduction into the geophysical literature by Conrad Schlumberger (Schlumberger, 1920) it has been the subject of various investigations and has proved quite successful in unveiling many sulphide ore deposits. All investigators agree that the IP phenomenon arises from electrochemical reactions prompted within the ore body by the inducing current applied.

Conrad Schlumberger felt the phenomenon was essentially electrolytic with ionic transport imbalancing the regions where the current electrodes were buried. Discouraged by their unsuccessful experiments in the field, the Schlumberger brothers dropped the subject of IP which remained buried for several years.

The first important revival of the subject came from Bleil's doctoral dissertation in 1948 stamped by the seal of confidentiality until 1953 (Bleil, 1953). Bleil conducted field and laboratory investigations of IP in the time domain. In the laboratory, he simulated metallic minerals in the ground by setting a metallic target in an electrolyte and demonstrated the associated IP effect. From the decay curves of IP obtained, he suggested that diffusion processes and chemical reactions played a dominant role in the phenomenon. In the field, Bleil

conducted a survey over an amphibolite dyke, a pyrrhotite outcrop and a magnetite ore body and he showed successful delineations of the targets (Bleil, 1953).

Almost simultaneously, but independently, Harold Seigel was conducting pioneering field surveys under the instigation of Arthur Brant from Newmont Exploration Limited (Brant, 1959). His extensive field experience, backed by laboratory models, led him to adopt a phenomenological approach. He formulated a mathematical representation of the IP phenomenon regardless of the chemistry involved, as the result of charging the medium with a volume distribution of current dipoles the strength of which was proportional both to the primary current and to the "chargeability" of the medium (H. Seigel, 1959). The chargeability is defined as a property of the medium which includes all the polarization effects therein, and depends also on the charging time with a saturation effect for, say, over 10 seconds. A similar approach was developed in Russia by V. A. Komarov and his coworkers (Komarov et al., 1966).

Several researchers have contributed to the phenomenological study of the IP method since the mid-50's. Prominent among these studies are the works by Hallof (1957, 1966), Madden et al. (1957, 1958, 1959, 1967), Madden (1967), the Newmont Exploration Company (Wait et al., 1959), Sumi (1959, 1961), Bacon (1965), Bertin (1968), Seigel et al. (1968), Bertin and Loeb (1969), Zonge et al. (1972), Patella (1972), Swift (1973), Van Voorhis et al. (1973).

It was also discovered as far back as Schlumberger (1920) that there could be an IP effect even without any metallic minerals present. In most of such occurrences, the IP effect was ascribed to clay minerals contained in the medium. Richard Frische and Haro von Buttlar (1957) developed a mathematical model using the electrostatic potential difference created by a distribution of current dipoles in the polarizable volume overlain by a non-polarizable overburden. The method was used for groundwater exploration. Almost simultaneously, laboratory and field measurements conducted by Vacquier et al. (1957) suggested that acquifers contaminated by clay minerals could be IP targets. Henkel and Van Nostrand (1957) and Henkel (1958) described, always on the basis of clay minerals, the resulting IP as due to an induced electromotive force modifying the effective resistivity of the polarizable earth materials involved. The existence of IP due to non-metallic minerals (Schlumberger, 1920), clay minerals in particular, was a complicating factor in the exploitation of the IP method in prospecting for metallic minerals.

In 1953, under the instigation of Prof. P. M. Hurley of the Department of Geology and Geophysics at MIT, a group of graduate students led by T. R. Madden initiated a study of the IP phenomenon and its mechanism. The project produced several theses, among which are Phil Hallof's doctoral thesis on the phenomenology of IP (Hallof, 1957), Don Marshall's doctoral thesis on

the mechanism of IP in rock-bearing membrane systems (Marshall, 1959), and Ted Madden's doctoral thesis on IP in rock-bearing metallic minerals (Madden, 1961).

The prominent characteristic of the project was the innovation of the variable frequency method in addition to the conventional time domain transient measurements in IP investigations. In particular, Madden, in his thesis, expanded the linear electrode impedance concept, generalizing thereby the excellent theory of Faradaic admittance expounded by David C. Grahame (1952). The application of the electrode impedance theory to the study of the IP mechanism was a necessary step exhibiting the electrochemical nature of the IP phenomenon.

0-2 Plan of the Thesis

The present thesis is an extension of Madden's, which attempts to delve more specifically into the chemistry involved in the IP mechanism.

The first chapter will be a cursory review with appropriate extensions of the basic elements in Madden's thesis, which is a necessary background for the understanding of this thesis. As in Madden's thesis, the fundamental tool throughout this study is the electrical equivalent circuit of the electrode impedance. Specific elements of the circuit represent specific elementary processes in the electrode reactions. The resolution of these elements will therefore shed light on the mechanism governing the electrode reactions. From the values of the elements, estimates of the concentration of the active species

as well as the capacitance associated with the electrical double layer at the electrode and the exchange current densities involved will be derived.

The second chapter concerns essentially the method of analysis and interpretation of the data obtained after inversion. Here will be introduced relevant elements of electrochemistry which will shed light on reactions and species whose concentrations have been derived by the method of Chapter I.

The third chapter will attempt to classify active and inactive ionic species under ordinary conditions on the basis of the electrode impedance spectra coupled to specific chemical environments. Plausible reactions will be identified for specified active species.

The fourth chapter emphasizes the critical role of the electrode surface condition. It is shown how limited anodic oxidation of copper and iron depolarizes the electrodes resulting in a dramatic drop of the electrode impedance. At sulfide electrodes, however, it is cathodic reduction of the electrode which induces the depolarization. The implications of these depolarizations are investigated in light of analysis of the electrode surfaces using the electron microprobe of the MIT Department of Earth and Planetary Sciences.

The fifth chapter will essentially give suggestions for areas where further research may be needed to increase our understanding of phenomena associated with IP. Special attention is given to non-linear regimes in specific environments.

CHAPTER I

Theory of IP, an Electrochemical Approach

Electrical conduction in rocks arises through a complex mixing of ionic conduction within fluids (electrolytes) in intricately interconnected pore systems, and electronic conduction through metallic minerals blocking possible pore passageways within the rock. The transition from ionic to electronic conduction of current at the solution/metallic mineral interface will occur through electrochemical reaction at the electrode. This reaction requires an additional voltage (overvoltage) which is responsible for the transient voltage decay (IP) observed when the driving voltage is shut off.

Since it takes a finite amount of time to build up the overvoltage, the impedance of a rock containing metallic minerals will be frequency-dependent. A way to understand the IP mechanism in rock systems will thus be tantamount to understanding the low frequency behavior of the impedance across a solution/metal interface, and its control by the chemical environment. The method could then be extended to semi-conducting minerals of geological interest.

1.1 Madden's Linear Electrode Impedance Theory and Extensions

We outline here results which Madden derived in his thesis (Madden, 1961) and which are indispensable for the understanding of this present thesis.

The ionic conduction in the solution is due to the motion

of charged species under any electric field and/or concentration gradient present. The charge transfer across the solution/metal interface occurs by means of electrochemical reactions at the electrode. These reactions put some constraints on the motion of species in the solution. The electrode kinetics will therefore consist of a set of equations describing the motion of the species in solution supplemented by a set of boundary conditions prompted by the electrode reactions. Diffusion processes along the surface or through the volume of the electrode may also be involved.

If p represents the concentration of positive ionic species and n the concentration of negative species all assumed univalent, the fundamental equations of motion are

$$\frac{\partial p}{\partial t} = D_p \frac{\partial^2 p}{\partial x^2} - \mu_p \frac{\partial (pE)}{\partial x}$$

$$\frac{\partial n}{\partial t} = D_n \frac{\partial^2 n}{\partial x^2} + \mu_n \frac{\partial (nE)}{\partial x}$$

with Poisson's equation

$$\frac{\partial E}{\partial x} = \frac{F}{\varepsilon} (p - n)$$

and Einstein's relation

$$\frac{\mu}{D} = \frac{F}{RT}$$

For small current density and no static electrical field, the fundamental equations can be linearized:

Let $p = p_0 + p_1(x,t)$ $\qquad p_1 \ll p_0$

$n = n_0 + n_1(x,t)$ $\qquad n_1 \ll n_0$

Put $D_n = \sigma D_p \equiv \sigma D$; $\mu_n = \sigma\mu_p \equiv \sigma\mu$; $p_0 = n_0 = C_0$

Assuming sinusoidal time dependence, $p_1(x)$ and $n_1(x)$ are both found to be of the form $A_1 e^{-r_1 x} + A_2 e^{-r_2 x}$, with

$$r_1^2 = \frac{2\mu C_0 F}{\varepsilon D} + \frac{j\omega}{D}\frac{1+\sigma}{2\sigma} \equiv K^2(1+\delta)$$

$$r_2^2 = \frac{j\omega}{D}\frac{1+\sigma}{2\sigma} \equiv K^2\delta, \qquad \text{with } K^2 = \frac{2\mu C_0 F}{\varepsilon D}$$

at low frequency. r_1^{-1} is a measure of the diffuse zone (of order 100 Å) expanding with dilution (decreasing C_0) while r_2^{-1} is a measure of diffusion distance (or order 10^{-3} cm) increasing with decreasing frequency. Thus $p_1(x)$ and $n_1(x)$ are the sum of two exponential terms: one decays very rapidly away from the electrode and is frequency-independent (contribution to diffuse layer); the other decays over a much larger distance and depends on frequency. The changes $p_1(x)$ and $n_1(x)$ depend on two arbitrary constants which are determined from the boundary conditions at $x = 0$, describing the flow of current as a result of the electrochemical reactions: the positive ions p flow into the solution carrying a fraction α_p of the total current i_∞ in solution while the negative ions n flow out of the solution carrying a fraction α_n. The amplitudes of $p_1(x)$ and $n_1(x)$ are thus found as a function of α_p, α_n, ω and the diffusion

parameters of p and n. The knowledge of α_p and α_n enables the computation of the diffuse layer impedance. In particular for an ideally polarized electrode (no reactions at the electrode, i.e. $\alpha_p = \alpha_n = 0$) the diffuse layer impedance is a simple capacitance in series with the solution resistance.

When only one active species q reacts at the electrode, it is assumed that this species also obeys the diffusion equation. Putting $q = q_0 + q_1(x)$, assuming equal mobilities and diffusivities for all the species in solution, the change $q_1(x)$ is also a sum of the same two exponentials as $p_1(x)$ and $n_1(x)$. More precisely,

$$q_1(x) = \frac{(\alpha-1)i_\infty}{2Fj\omega}\frac{r_1 q_0}{C_0} e^{-r_1 x} + \frac{\alpha i_\infty}{2FDr_2}\left(2 - \frac{q_0}{C_0}\right) e^{-r_2 x} \qquad (1.1\text{-}1)$$

with the electric field

$$E = E_\infty - \frac{(\alpha-1)i_\infty}{\varepsilon j\omega} e^{-r_1 x}$$

where α stands for the complex fraction of the total current carried by the reaction involving q. This equation represents the balance between the Faradaic current involving charge transfer at the electrode and the non-Faradaic current involving the fixed and diffuse layer capacitance. The Faradaic current $i_\alpha = \alpha i_\infty$ depends on the reaction rate, i.e. changes in the concentrations of the active species as well

as the potential drop across the fixed layer: $i_\alpha = F(C_i, V_f)$. For very small current densities, we can approximate it to a first order Taylor expansion

$$i_\alpha = i_{\alpha 0} + \frac{\partial f}{\partial V_f} V_f + \frac{\partial f}{\partial C_i} \Delta C_i + \text{higher order terms} \qquad (1.1\text{-}2)$$

with $i_{\alpha 0} = 0$ because of the equilibrium between electrode and solution.

The theory of reaction rates (Eyring, Glasstone and Laidler, 1939) assumes that for a reaction

$$\sum_{i=1}^{n} \nu_i A_i \rightleftarrows \sum_{i=1}^{m} \nu'_i A'_i$$

the forward and backward rates are, respectively

$$\text{forward rate} = \frac{kT}{h} \prod_{j=1}^{n} [A_j]^{\nu_j} e^{-\frac{\Delta \vec{G}_0^{\dagger}}{RT}}$$

$$\text{backward rate} = \frac{kT}{h} \prod_{j=1}^{m} [A'_j]^{\nu'_j} e^{-\frac{\Delta \overleftarrow{G}_0^{\dagger}}{RT}}$$

where $[A_i]$ stands for the activity of the species A_i; k is the Boltzmann constant, h is Planck's constant. $\Delta G^{\dagger}$ stands for some form of free energy change involving activated complex and which will be approximated by $\bar{\alpha} F V_f$ for the forward reaction and $(1-\bar{\alpha}) F V_f$ for the backward reaction, V_f being the voltage drop across the fixed layer.

At equilibrium, the forward rate is equal to the backward rate, which is a definition of the exchange current density i_0. In the linear expansion, the reaction rates become

$$\text{forward rate} = i_0[1 + \frac{\bar{\alpha}F}{RT} V_f + \sum_{i=1}^{n} \nu_i \frac{\Delta[A_i]}{[A_i]}]$$

$$\text{backward rate} = i_0[1 - \frac{(1-\bar{\alpha})FV_f}{RT} + \sum_{i=1}^{m} \nu_i' \frac{\Delta[A_i]}{[A_i]}]$$

The Faradaic current is represented by the net rate (forward rate - backward rate) which is

$$i_\alpha = i_0[\frac{F}{RT} V_f + \sum_{i=1}^{n} \nu_i \frac{\Delta[A_i]}{[A_i]} - \sum_{i=1}^{m} \nu_i' \frac{\Delta[A_i']}{[A_i']}] \qquad (1.1\text{-}3)$$

The comparison between Equations (1.1-3) and (1.1-2) enables the extraction of α and $\frac{\partial f}{\partial c_i}$ in terms of the exchange current density i_0, thereby allowing the determination of the Faradaic impedance in terms of reaction rate parameters.

1.2 Faradaic Impedance and Equivalent Circuit for Simple Electrode Reaction

The equivalent circuit method will be the fundamental tool throughout this study. We present first Madden's derivation for the case of a simple reaction of the type

$Q \rightleftarrows \bar{X}$ (unit activity)

The Faradaic current becomes, from Equation (1.1-2)

$$i_\alpha = \alpha i_\infty = \frac{V_f}{\theta} - \beta q_1$$

Furthermore, since V_f acts across the fixed layer, the displacement current will be

$$(1-\alpha) i_\infty = j\omega C_f V_f$$

At the electrode, the active species concentration change is

$$q_1 = q_1(0) = \frac{i_\infty}{2F} \left[\frac{(\alpha-1) r_1 q_0}{j\omega C_0} + \frac{2 - \frac{q_0}{C_0}}{Dr_2} \right]$$

so that replacing q_1 in the Faradaic current expansion, we get the Faradaic impedance

$$Z_\alpha = \frac{V_f}{\alpha i_\infty}$$

$$= \frac{\frac{\beta (2 - \frac{q_0}{C_0})}{2F\sqrt{j\omega D}}}{\frac{1}{\theta} + \beta \frac{q_0 K C_f}{2 C_0 f}}$$

with $K^2 = \frac{2 C_0 F^2}{\varepsilon RT}$

The Faradaic impedance is the sum of two terms:

$$Z_\alpha = R_1 + Z_w$$

with

$$R_1 = \frac{1}{\frac{1}{\theta} + \beta \frac{q_0 K C_f}{2 C_0 F}} \simeq \theta$$

$$Z_w = \frac{\frac{\beta(2 - \frac{q_0}{C_0})}{2F\sqrt{j\omega D}}}{\frac{1}{\theta} + \beta \frac{q_0 K C_f}{2 C_0 F}} \simeq \frac{\beta\theta(2-\frac{q_0}{C_0})}{2F\sqrt{j\omega D}}$$

By comparing the above expansion of the Faradaic current with the expression of the net reaction rate [Equation (1.1-3)], we get

$$\theta = \frac{RT}{Fi_0}$$

$$\beta = \frac{i_o}{q_o}$$

and

$$\theta\beta = \frac{RT}{q_0}$$

independent of the exchange current density.

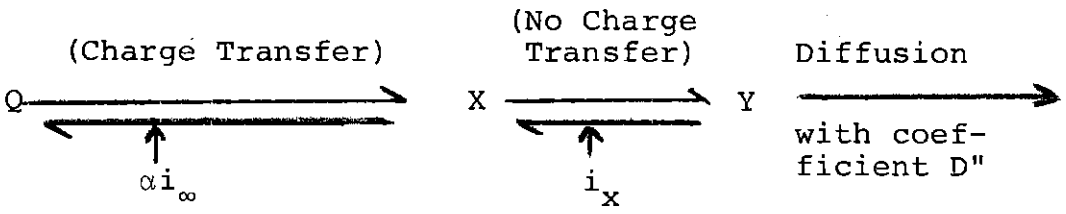
We obtain, therefore,

$$Z_w \simeq \frac{RT}{q_0 F^2 \sqrt{j\omega D}} \qquad (1.2\text{-}1)$$

The first term, R_1 is a reaction resistance associated to the reaction at the electrode; the second term, Z_w, is called a Warburg impedance characteristic of diffusion of active species from the solution towards reaction zones at the electrode. The Faradaic impedance is in parallel with the fixed layer capacitance. The theory provides some dependence on zeta potential

and diffuse layer capacitance. We have to add naturally the solution resistance R_s so that the equivalent circuit of the electrode impedance for the elementary process considered is as shown in Figure 1.1.

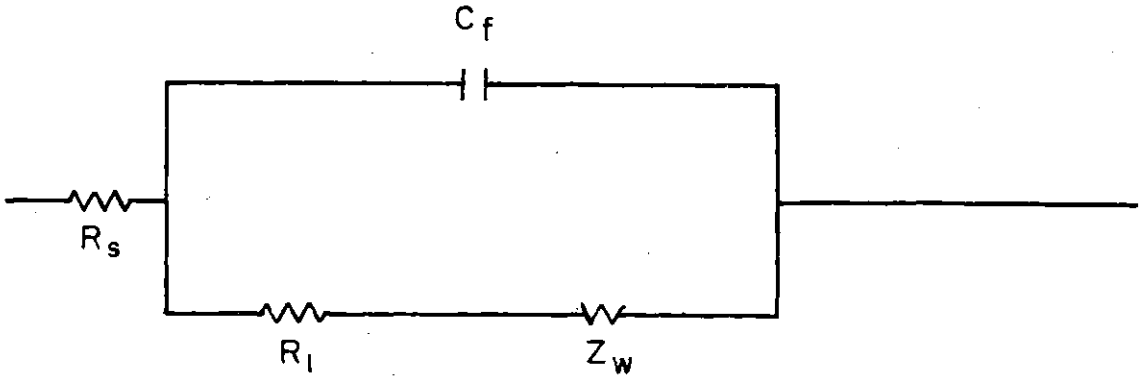
To demonstrate the general feature and usefulness of the equivalent circuit representation, we derive it for a complex reaction chain



The active species Q reacting at the electrode take a current αi_∞, while the product X reacting in turn requires a current i_x. We have

$$i_x = -\xi \Delta X + \nu \Delta Y \qquad (a)$$

and



Equivalent circuit for reaction

$Q \rightleftharpoons \overline{X}$

Figure 1.1 Electrode Impedance Model with 4 Parameters. C_f=fixed layer capacity; R_l=reaction resistance; Z_w=Warurg impedance; R_s = solution resistance.

$$\alpha i_\infty = \frac{V_f}{\theta} - \beta q_1 + \gamma \Delta X \qquad (b)$$

The time rate of change of ΔX is

$$j\omega \Delta X = - \frac{\alpha i_\infty}{F} + \frac{i_x}{F} \qquad (c)$$

while the time rate of change of ΔY which diffuses away is

$$j\omega \Delta Y = - \frac{i_x}{F} - D'' r_2 \Delta Y \qquad (d)$$

(c) and (d) give $j\omega \Delta X + [j\omega + D'' r_2] \Delta Y = - \frac{\alpha i_\infty}{F}$

(a) and (c) give $(j\omega + \frac{\xi}{F}) \Delta X - \frac{\eta}{F} \Delta Y = - \frac{\alpha i_\infty}{F}$

These two equations give immediately ΔX:

$$\Delta X = - \frac{\alpha i_\infty}{F} \; \frac{\frac{\eta}{F} + j\omega + D'' r_2}{j\omega \frac{\eta}{F} + (j\omega + \frac{\xi}{F})(j\omega + D'' r_2)}$$

Putting ΔX back into (b), we get

$$\alpha i_\infty \left[1 + \frac{\gamma}{F} \; \frac{\frac{\eta}{F} + j\omega + D'' r_2}{j\omega \frac{\eta}{F} + (j\omega + \frac{\xi}{F})(j\omega + D'' r_2)} \right] = \frac{V_f}{\theta} - \beta q_1$$

which is of the form

$$\alpha i_\infty = \frac{V_f}{\theta''} - \beta'' q_1$$

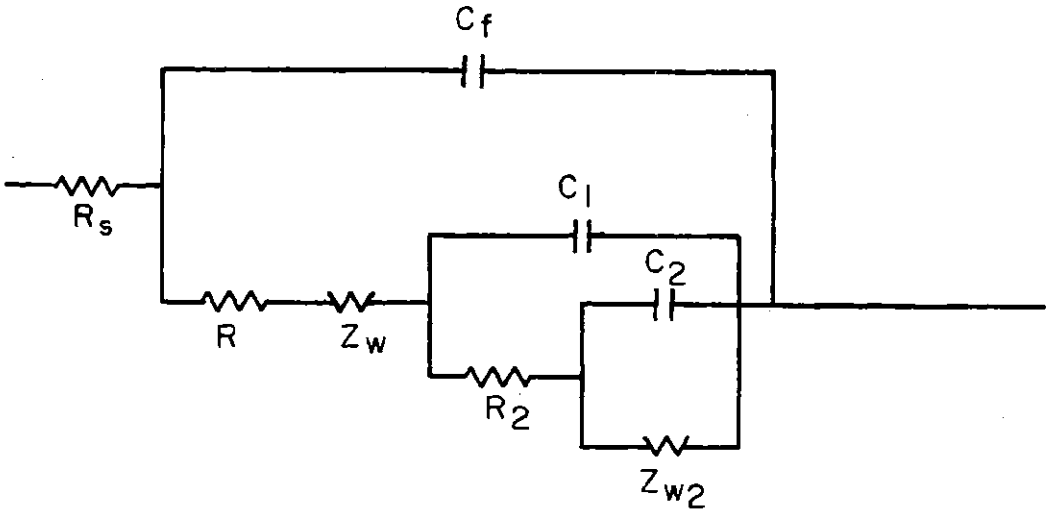
Thus we get, using the analogy with the previous derivation of the Faradaic impedance

$$Z_\alpha = R\left[1 + \frac{\gamma}{F}\,\frac{\frac{\eta}{F} + j\omega + D''r_2}{j\omega\frac{\eta}{F} + \left(j\omega + \frac{\xi}{F}\right)(j\omega + D''r_2)}\right] + \frac{\beta\left(2 - \frac{q_0}{C_0}\right)R}{2F\sqrt{j\omega D}}$$

$$= R + Z_w + \cfrac{1}{\frac{j\omega F}{R\gamma} + \cfrac{1}{R\frac{\gamma}{\xi} + \cfrac{1}{\frac{j\omega\xi F}{\eta R\gamma} + \frac{\sqrt{j\omega D''F\xi}}{\eta R\gamma}}}}$$

C_1 R_2 C_2 Z_{w_2}

The equivalent circuit is clearly exhibited in this form in Fig. 1.2.



Equivalent circuit for reaction chain

$$Q \rightleftharpoons X \rightleftharpoons Y \xrightarrow[\text{coefficient D}]{\text{Diffusion with}}$$

Figure 1.2 Electrode Impedance Model with 8 Parameters. R_S=solution resistance; R, R_2=reaction resistances; C_f, C_1,C_2 = capacities; Z_w, Z_{w2} = Warburg impedances.

As remarked by Madden, the equivalent circuit for any reaction chain follows a simple pattern which can be written down immediately. At each point of the reaction chain, the accumulation of the products represents a capacitance to the electrode. The escape of these products occurs either by diffusion, represented by a Warburg impedance, or by reaction, represented by a resistor. The products of this reaction simulate the preceeding steps. If several species contribute to independent reaction chains, the corresponding impedances act in parallel. A different result holds, however, for the case where several species are involved in the same reaction.

We start with the expression of the Faradaic current

$$i_\alpha = f(C_i, V_f)$$

with the expansion for small current density

$$i_\alpha = \frac{\partial f}{\partial V_f} V_f + \sum_i \frac{\partial f}{\partial C_i} \Delta C_i$$

As we did in Equation (1.1-3), we write

$$\alpha i_\infty = \frac{V_f}{\theta} - \sum_i \beta_i \Delta p_i$$

where p_i represent active species. As computed by Madden (Madden, 1961, op. cit., p. 37)

$$\Delta p_i = \frac{i_\infty}{2DF}\left[\frac{C_i(\Sigma_j \alpha_{p_j} + \Sigma_j \alpha_{n_j} - 1)}{C r_1 \delta} + \frac{\alpha_i(2 - \frac{C_i}{C})}{r_1\sqrt{\delta}}\right]$$

where C_i stands for the initial concentration of p_i, $\delta = \frac{r_2^2}{K^2}$, r_2 and K are defined in Section 1.1.

Assuming all the voltage drop occurs across the fixed layer, the displacement current across the fixed layer capacitance is

$$(1 - \sum_j \alpha_{p_j} - \sum_j \alpha_{n_j}) i_\infty = j\omega C_f V_f$$

α_{p_j} and α_{n_j} represent the fraction of the total current i_∞ carried respectively by species p_j and n_j. We will use α_i if the distinction is not essential. $C = \Sigma C_i$; $\alpha = \Sigma \alpha_i$ The above expression of αi_∞ in comparison with Equation (1.1-3) gives $\beta_i = \frac{i_0 \nu_i}{C_i}$. Using the expression of the displacement current in the Faradaic current, we get

$$\alpha i_\infty = \frac{V_f}{\theta} + \sum_i \frac{KC_f V_f \beta_i C_i}{2FC} - \sum_i i_\infty \frac{\beta_i \alpha_i (2 - \frac{C_i}{C})}{2F\sqrt{j\omega D}}$$

yielding

$$Z_\alpha = \frac{V_f}{\alpha i_\infty} \equiv R + \sum_i Z_{w_i}$$

with

$$R = \frac{1}{\frac{1}{\theta} + \sum_i \frac{\beta_i C_i KC_f}{2FC}} \qquad \text{and} \quad Z_{w_i} = R \frac{\beta_i \alpha_i (2 - \frac{C_i}{C})}{2\alpha F\sqrt{j\omega D}}$$

The equivalent circuit for the case of multiple active species contains, therefore, a Warburg impedance which is the sum of Warburg impedances relative to each active species.

1.3 Concentration of Active Species

In the Faradaic impedance, the Warburg term depends prominently on the concentration of active species present. The Warburg impedance is related to the concentration q_0 of active species by

$$q_0 = \frac{2.5 \times 10^{-2}}{W\sqrt{f}} \text{ moles/l}$$

(Madden, 1961, op. cit.), where the Warburg impedance has been put in the form

$$Z_w \equiv W e^{-j\frac{\pi}{4}}$$

This simple relation giving the concentration q_0 once the Warburg impedance is known is quite important. We shall see later how the Warburg impedance is determined in practice from the electrode impedance spectrum. Whenever a magnitude of Warburg impedance is given without specifying a frequency, it means that an angular frequency $\omega = 1$ has been assumed.

We may also note that in the previous paragraph the presence of several active species is expressed by a series of Warburg impedances. Since each Warburg term is inversely proportional to the corresponding species concentration, a good working approximation will just be to ascribe the equivalent concentration to a minor constituent whose presence is essential for the electrode reaction. We shall see later how this scheme helped us identify some active species in our experimental investiga-

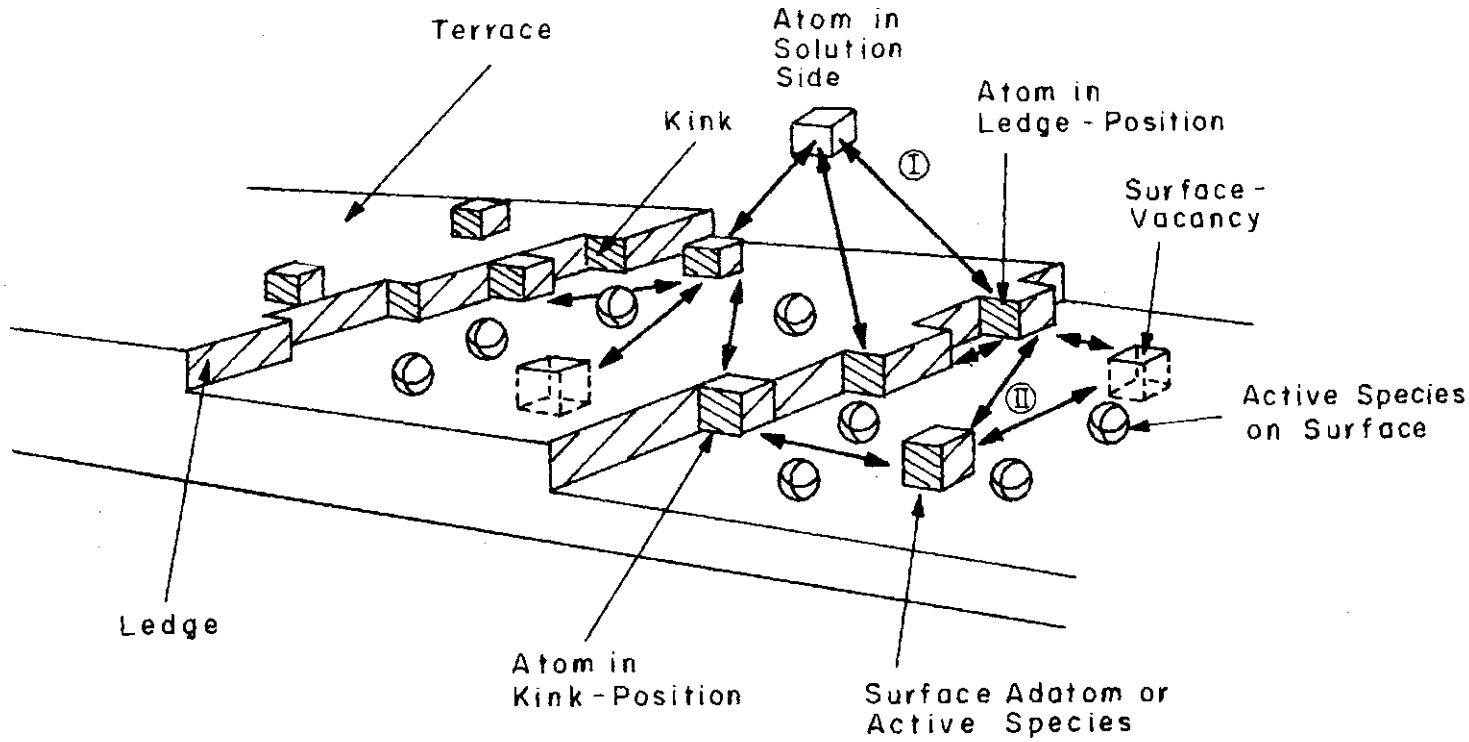
tion of electrode processes.

1.4 Surface Diffusion Impedance

The reactions considered in the previous sections occur in the vicinity of the electrode surface. It is therefore likely that the surface condition will be a factor which must be taken into consideration. However the complexity of the surface geometry defies any thorough treatment of all the possible phenomena which might occur at the surface.

The surface of the electrode can be pictured as an area of adsorption of species in addition to ad-atoms of the metal all of which can diffuse on the surface if any concentration gradient is initiated due to possible reactions of surface species. The usual Terrace-Ledge-Kink (TLK) model of surface structure as used in surface diffusion studies (Neumann and Neumann, 1972) and crystallization processes (Vetter, 1967) may help visualize the phenomena at the electrode surface.

Figure 1.3 shows several paths of possible reactions where some analogy to crystallization processes could be easily drawn. The reaction pathways can be divided in two groups: one group involves the crossing of the double layer between electrode and solution, and these are precisely the cases investigated in the previous sections. The second group of paths is restricted to the surface. We assume for simplicity a cylindrical symmetry around an "active center" initiating the reactions leading to surface diffusion. For an initial concentration



Electrode processes : Possible reactions pathways and associated diffusion

Figure 1.3

C_0 of species, the reaction prompted by the active center leads to diffusion along the surface such that we have the equations

$$\frac{\partial C}{\partial t} = D\nabla^2 C$$

$$C = C_0 \text{ at } r = \infty$$

If we put

$$C = \frac{C-C_0}{C_0}$$

then we get

$$\frac{\partial C}{\partial t} = D\nabla^2 C$$

$$C = 0 \text{ at } r = \infty$$

Assuming sinusoidal time dependence, we have the transformed equation

$$\frac{d^2C}{dr^2} + \frac{1}{r}\frac{dC}{dr} - \frac{j\omega}{C} C = 0$$

This yields the solution

$$C = H_0^{(2)}\left[\sqrt{\frac{-j\omega}{D}}\ r\right]$$

where

$H_0^{(2)}(z)$ is Hankel's function of the second kind of order zero.

We define therefrom the surface impedance as proportional to

$$Z_s = \frac{\Delta C}{\partial C/\partial r}$$

$$= \frac{H_0^{(2)}\left[\sqrt{-\frac{j\omega}{D}}\ r_0\right]}{\sqrt{-\frac{j\omega}{D}}\ H_1^{(2)}\left[\sqrt{\frac{-j\omega}{D}}\ r_0\right]}$$

r_0 represents a typical surface diffusion distance which must be very small if we consider the estimates of surface dif-

fusion coefficients of the order 10^{-6} - 10^{-8} cm^2/sec (Oriani and Frankenthal, 1962). We observe that this impedance looks like a Warburg impedance at high enough frequency. At low frequency, it becomes resistive logarithmically with respect to frequency. This impedance is in series with the Warburg impedance in the solution so that the equivalent circuit for the reaction

$$Q \rightleftharpoons X \xrightarrow{\text{Surface Diffusion}}$$

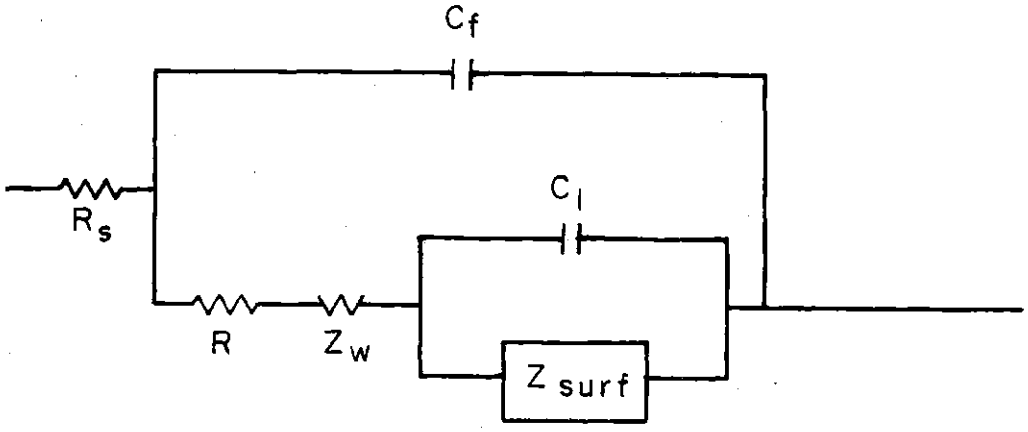
can be drawn as in Figure 1.4.

1.5 Generalized Inversion Scheme

The purpose of the Inversion is to resolve the values of the elements contained in the equivalent circuit adopted in representing the electrode processes and simulating the electrode impedance spectra. We use essentially a generalized inversion scheme whose particularity consists in logarithmic variations of the parameters (Madden, 1972). The chief advantage of the logarithmic variation is that the procedure weights the data uniformly and takes advantage of the positive nature of the parameters.

Let $Z_i(\omega_i, P_1, P_2, \ldots P_m) \equiv |Z_i(\omega_i, \underline{P})| e^{j\phi(\omega_1, \underline{P})}$

be the impedance model, i.e. given by the electrical equivalent circuit whose parameters P_j we want to determine. The procedure consists in assigning initial values to P_j and adjusting them iteratively using a kind of "steepest descent" correction:



Equivalent circuit for reaction

$Q \rightleftharpoons X$ Surface Diffusion $\longrightarrow$

Figure 1.4 Electrode Impedance Model with Surface Diffusion. R_s=solution resistance; R=reaction resistance; C_f,C=capacities; Z_w=Warburg impedance; Z_{surf}= surface diffusion impedance.

$$\text{Log}\ \frac{Z^{\text{mod}}(\omega_k, \underline{P})}{Z^{\text{obs}}(\omega_k, \underline{P})} = \sum_{i=1}^{m} \frac{\partial \text{Log} Z^{\text{mod}}(\omega_k, \underline{P})}{\partial \text{Log}\ P_i}\ \Delta\text{Log}\ P_i \quad k=1,\ldots n$$

This system of n complex equations with the m unknowns $\Delta\text{Log}\ P_i$ gives in splitting into amplitude and phase functions 2n equations with m unknowns $\Delta\text{Log}\ P_i$. We make spectra measurements at sufficient number of frequencies (n large enough) so that the system is overdetermined. We then evaluate $\Delta\text{Log}\ P_i$, i = (1, ... m) and compute the corrected values for P_i which are the new values to be used in the system, and iterate the procedure until convergence. In Appendix A we show the details of the fitting procedure using the generalized inversion which we call the "ε^2 method" suppressing small eigenvalues leading to instabilities.

It is essential to note that the parameters we have found determine the elements in the electrical equivalent circuit used as our model for the <u>whole</u> frequency range of measurement. The method provides also a resolution matrix which exhibits the most significant paramters.

Chapter II

Method of Analysis

The equivalent circuit fitting procedure was successfully used by Madden to simulate the impedance spectra of different electrodes in various environments. A remarkable feature which emerged from the results of his experimentation (Madden, 1961) was that the electrode impedance behavior was dominated by the Warburg term in the circuit. Furthermore, this Warburg impedance element was surprisingly insensitive to solution concentration as well as the pH of the solution.

The insensitivity to concentration is demonstrated by Table 2.1, where nickel electrode impedances have been analyzed. Table 2.2 demonstrates the insensitivity to pH for graphite electrode, and Table 2.3 the quasi-uniformity of results obtained with different electrodes.

Concentration of KCl moles/l	Warburg Impedance $\Omega x\ cm^2$	Effective Concentration Ci moles/l
.01	4170	$.6 \times 10^{-5}$
.005	4210	$.595 \times 10^{-5}$
.002	4770	$.525 \times 10^{-5}$
.001	4720	$.53 \times 10^{-5}$
.0005	4380	$.57 \times 10^{-5}$
.0001	4950	$.505 \times 10^{-5}$

Table 2.1 Effect of concentration on Warburg Impedance (Madden, 1961) for Nickel Electrodes

Concentration of KCl moles/l	pH	Warburg Impedance $\Omega \times cm^2$	Effective Concentration Ci moles/l
.014	7	1610	1.55×10^{-5}
.01	10	1150	2.2×10^{-5}
.01	3.8	1210	2.1×10^{-5}

Table 2.2 Effect of pH on Warburg impedance for graphite electrodes (Madden, 1961)

Electrode	Warburg Impedance $\Omega \times cm^2$	Effective Concentration Ci moles/l
Stainless Steel	3960	$.65 \times 10^{-5}$
Nickel	670	3.7×10^{-5}
Graphite	1610	1.55×10^{-5}
Copper	1270	2×10^{-5}
Pyrite	805	3.1×10^{-5}

Table 2.3

These results seem to imply that the electrode impedance is controlled by some minor constituents whose concentrations in the solution are of the order of 10^{-5} mole/l. Therefore it appeared mandatory that more controlled experimentation with special reference to the chemical environment be undertaken in

order to unveil those active species involved in the electrode processes.

A great deal is known about the stability fields of ionic species in aqueous solutions from the standpoint of corrosion processes (Pourbaix, 1966) as well as geochemical environments (Garrels and Christ, 1965).

2.1 Chemical Environment in Terms of Eh and pH

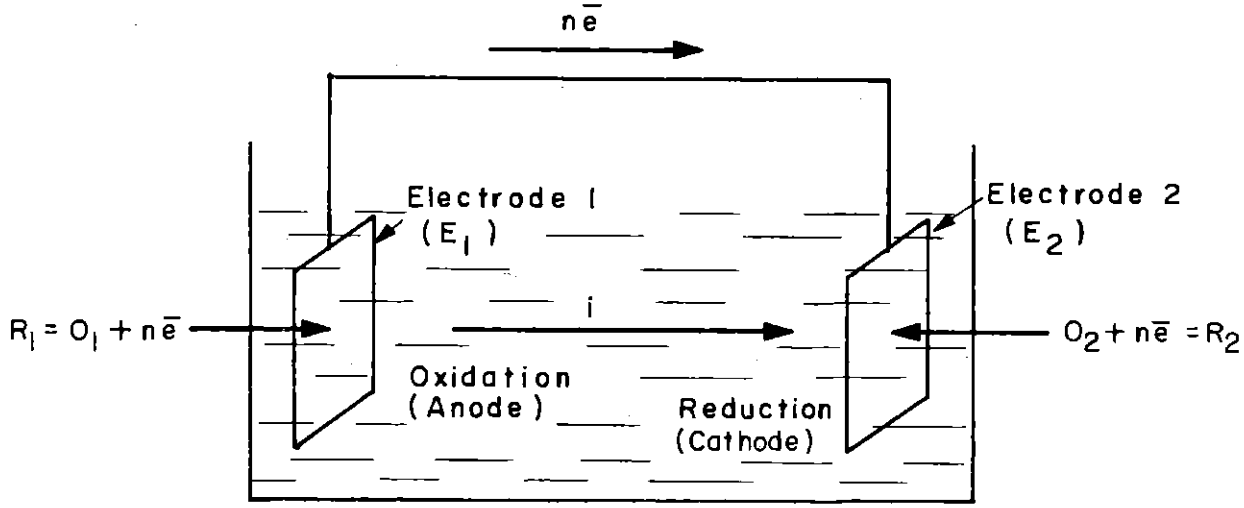
The last twenty years have witnessed a rapid increase in the use of Eh-pH diagrams for the study of stability relations among mineral species in natural environments. The success encountered by the method stems from the relative elegance, simplicity, and effectiveness with which it describes chemical environments. It is, however, important to note that the oxidation potential, Eh, and the pH of a system result from an overall electrochemical balance of all species present in the environment. Basic references are to be found in Garrels and Christ (1965), Pourbaix (1973), and Antropov (1972).

Charge transfer reactions are always redox (reduction-oxidation) type reactions. Any such reaction can be split into two half-cell reactions of the form represented in Figure 2.1.

Reduced state = oxidized state + $n\bar{e}$. To this balance is attached a half-cell potential

$$Eh = E^\circ + \frac{RT}{nF} \text{Log} \frac{[\text{oxidized state}]}{[\text{reduced state}]}$$

which represents the voltage difference between an electrode (E_1) at which the above equilibrium is established and a standard



Splitting of redox reaction $R_1 + O_2 = O_1 + R_2$
(O_k and R_k are respectively oxidized and reduced states)

Figure 2.1 Duality of Oxidation and Reduction Processes at Electrodes.

hydrogen electrode (E_2) chosen as reference electrode (Ives and Janz, 1961). E° is the hypothetical half-cell potential when species in oxidized and reduced states have all unit activities; it is obtained from thermodynamic considerations regarding the free energy of formation of the species. More precisely, let

$$\sum_{\alpha} \nu_\alpha M_\alpha + n\bar{e} = \sum_{\beta} \nu_\beta M_\beta$$

where (ν_α, ν_β) are positive stochiometric coefficients relative to substances M_α and M_β respectively. The preceeding reaction (Pourbaix, 1973) can be written

$$\sum_{i} \nu_i M_i + n\bar{e} = 0$$

where ν_i is positive or negative depending on whether it represents ν_α or ν_β. Then, the half-cell voltage is

$$Eh = E° + \sum_{i} \frac{RT}{nF} \nu_i \, \mathrm{Log}[M_i]$$

where $E° = \Sigma \frac{\nu_i \mu_i^0}{nF}$ and $\mu_i^0 \equiv \Delta F_i^0$ is the standard chemical potential or free energy of formation of M_i.

A useful numerical value under normal room temperature (25°C) is the prefactor $2.3026 \frac{RT}{F} = .0591$ volt-mole for using decimal logarithms in the equations. F is the Faraday which is equivalent to 96500 coulombs or 23.060 kcal/volt. This gives the general equation for

$$\sum_{i} \nu_i M_i + n\bar{e} = 0$$

$$Eh = E^\circ + \frac{.0591}{n} \sum_i \nu_i \log[M_i]$$

$$E^\circ = \sum_i \frac{\nu_i \mu_i^0}{23.060n} \qquad \mu_i^0 \text{ in kcal/mole}$$

with voltages referenced to standard hydrogen electrode.

It is important to note that the above definition of Eh is in conformity with the so-called Stockholm Sign Convention recommended by The International Union of Pure and Applied Chemistry (IUPAC) according to which a positive Eh implies that H^+ is reduced to H_2 at the hydrogen reference ($\bar{e}$ sink) electrode, i.e. electrons are being produced at the working electrode ($\bar{e}$ source): the environment is therefore an oxidizing environment. If Eh is negative, the working electrode becomes an electron sink and the environment is reducing.

In practice, the oxidation potential Eh is measured with an electrode pair consisting of an inert electrode against a reference electrode providing a constant voltage. The inert electrode must be able to play the role of $\bar{e}$ source for the ions in solution of $\bar{e}$ sink accepting electrons liberated by reacting ionic species in solution depending on whether the potential of the half-cell involving the dissolved species is smaller or greater than the potential of the reference electrode which acts as a half-cell of constant potential.

The Eh electrode commonly used is a bright platinum wire probe. A good reference electrode used in place of the standard hydrogen electrode is the saturated calomel electrode

(Ives and Janz, 1961) which provides a constant voltage of 242 mv with respect to the standard hydrogen electrode at 25°C. Therefore, we have

$$E_h^{SCE} = E_h^{SHE} - 242 \text{ mV}$$

where E_h^{SCE} is the voltage difference between the platinum probe and the calomel electrode and E_h^{SHE} is the voltage that would exist between the platinum probe and a suitably positioned reference standard hydrogen electrode.

The pH of the solution is measured with a pH glass electrode coupled to a reference electrode (SCE). The pH electrode is essentially a sodium-calcium-silicate glass bulb containing a solution of fixed H^+ activity. The glass acts like a specific ion electrode sensitive to H^+. The electrode is readily used after calibration with standard test solutions of known pH.

2.2 Eh-pH Diagrams

The Eh-pH diagrams devised by M. Pourbaix (Pourbaix, 1945), and extensively used in corrosion literature (Pourbaix et al., 1966), (Uhlig, 1971), (West, 1971), as well as in geological references (Garrels and Christ, 1965) are convenient representations of stability fields of chemical species under specific environments. Each species assemblage has a characteristic range of chemical immunity whereby a given modification of an environment will not affect the species. Unfortunately, one

may at times be left hanging because, on kinetic grounds, reactions which are supposed to have occurred as a consequence of a specific environmental change cannot safely be ascertained to have reached their ultimate equilibrium states. This situation, however, plagues the whole field of chemistry, electrochemistry, and corrosion studies.

To illustrate the question of stability fields of chemical species relevant to our studies, we shall examine the diagrams for copper and iron, and their respective sulfides in some typical solutions. The choice of copper and iron is dictated by mining world interests where copper and iron sulfides happen to be major IP targets.

The Eh of natural environments covers approximately the range from -400 MV SHE in very reducing zones to +800 MV SHE in intensely oxidized settings, and the pH spans approximately the range from 2 in acidic zones to 10 in alkaline zones (Baas Becking et al., 1960).

2.2.1 Eh-pH Diagrams for Copper in Aqueous Solution

For the system Cu-H_2O, in the Eh-pH range prescribed above, the relevant chemical species involved are Cu, Cu_2O, CuO as solid substances, and Cu^+, Cu^{++}, $HCuO_2^-$ as dissolved substances (Pourbaix et al., 1966). Figure 2.2 summarizes the important stability fields adapted from Pourbaix et al. It is important to note that our Eh values are expressed in millivolts with the saturated calomel electrode as reference electrode.

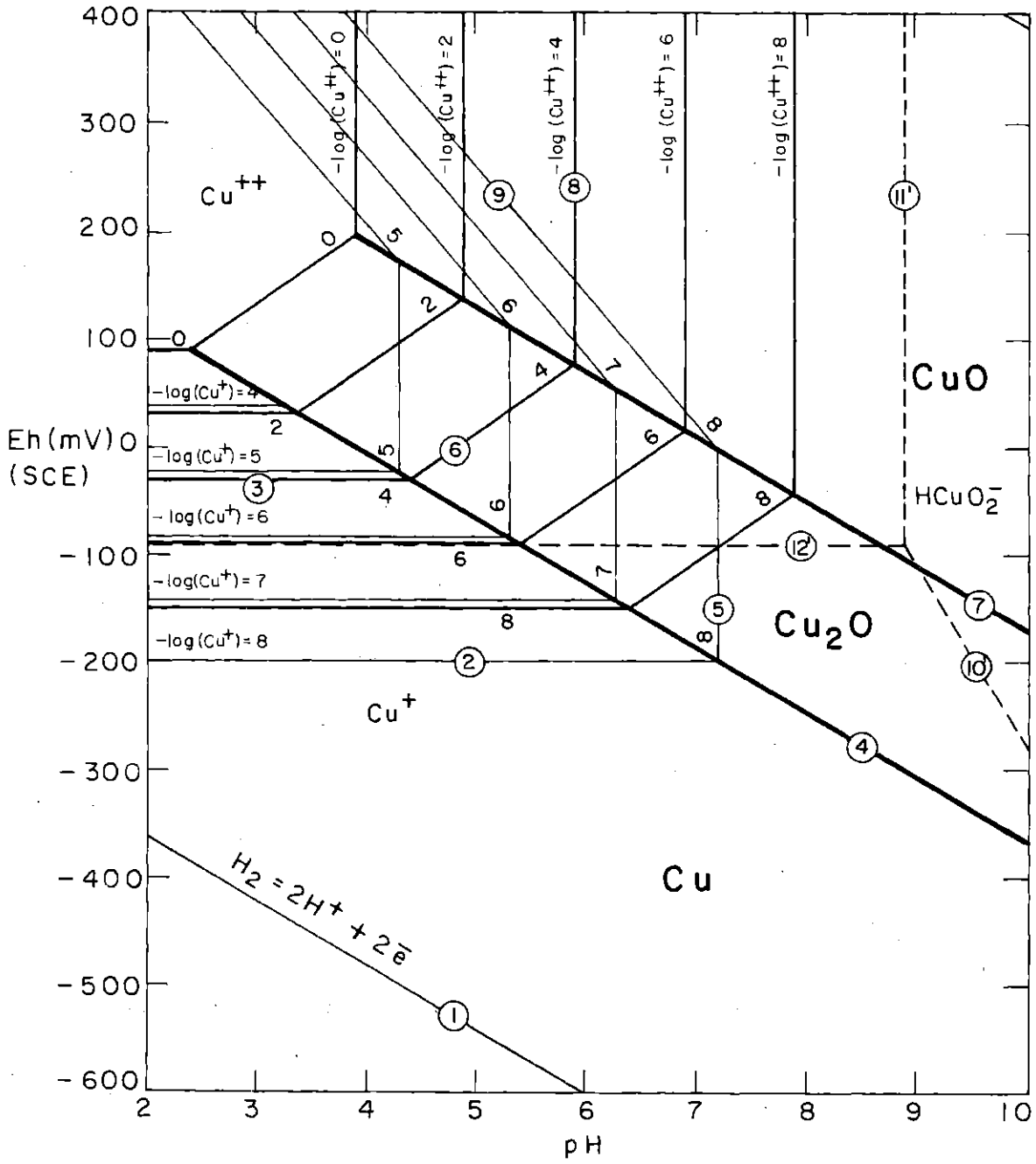


Figure 2.2 Eh-pH Diagram of Copper in Water (adapted from Pourbaix, 1966)

Cu is stable in a reducing environment close to the hydrogen ionization reaction which is the lower limit of stability of water:

1) $H_2 = 2H^+ + 2\bar{e}$ $\quad Eh = -242 - 59.1\ pH$

With increasing Eh, Cu gets oxidized to Cu^+ and/or Cu^{++}.

2) $Cu = Cu^+ + \bar{e}$ $\quad Eh - 278 + 59.1 \log [Cu^+]$

3) $Cu = Cu^{++} + 2\bar{e}$ $\quad Eh = 95 + 29.5 \log [Cu^{++}]$

Both reactions 2) and 3) do not involve any proton H^+ and are therefore represented on the diagram by horizontal lines indexed by $-\log[Cu^+]$ and $-\log[Cu^{++}]$, respectively. At moderately high Eh, copper forms Cu_2O.

4) $2Cu + H_2O = Cu_2O + 2H^+ + 2\bar{e}$ $\quad Eh = 229 - 59.1\ pH$

Cu_2O could as well be formed as a result of a chemical reaction involving Cu^+ and/or electrochemical reduction of Cu^{++}:

5) $2Cu^+ + H_2O = Cu_2O + 2H^+$ $\quad pH = -.84 - \log[Cu^+]$

6) $Cu_2O + 2H^+ = 2Cu^{++} + H_2O + 2\bar{e}$

$$Eh = -39 + 59.1\ pH + 59.1 \log[Cu^{++}]$$

Line 4) represents the lower limit of stability of Cu_2O. At sufficiently high Eh, Cu_2O forms CuO:

7) $Cu_2O + H_2O = 2CuO + 2H^+ + 2\bar{e}$

$$EH = (427\sim505) - 59.1\ pH$$

Line 7) represents the upper limit of stability of Cu_2O. CuO could as well be formed from a chemical reaction involving

Cu^{++} and/or electrochemical oxidation of Cu^{+}:

8) $Cu^{++} + H_2O = CuO + 2H^{+}$ $\quad pH = 3.94 - \frac{1}{2} \log [Cu^{++}]$

9) $Cu^{+} + H_2O = CuO + 2H^{+} + \bar{e}$ $\quad Eh = 378 - 118.2\ pH - 59.1 \log[Cu^{+}]$

At sufficiently high pH, the oxidation of Cu^{+} gives a dissolved species $HCuO_2^{-}$ through the electrochemical reaction:

10) $Cu^{+} + 2H_2O = HCuO_2^{-} + 3H^{+} + \bar{e}$

$$Eh = 1491 - 177.3\ pH + 59.1 \log \frac{[HCuO_2^{-}]}{[Cu^{+}]}$$

$HCuO_2^{-}$ could as well be the result of a chemical reaction involving Cu^{++}:

11) $Cu^{++} + 2H_2O = HCuO_2^{-} + 3H^{+}$ $\quad pH = 8.91 + \frac{1}{3} \cdot \log \frac{[HCuO_2^{-}]}{[Cu^{++}]}$

The lines 10' and 11' represent reactions 10 and 11 with, respectively $[Cu^{+}] = [HCuO_2^{-}]$ and $[Cu^{++}] = [HCuO_2^{-}]$. Lastly the oxidation of Cu^{+} into Cu^{++} according to

12) $Cu^{+} = Cu^{++} + \bar{e}$ $\quad Eh = -84 + 59.1 \log \frac{[Cu^{++}]}{[Cu^{+}]}$

is represented by the horizontal line 12' when $[Cu^{+}] = [Cu^{++}]$. This line joins with the point of intersection of lines 10' and 11' on 7.

The previous diagram could be extended to represent the ternary system Cu-Cl-H_2O where chlorine has been added. Cl^{-} is a common anion in natural waters and electrode impedances in

Cl^- solutions will be extensively studied below. The relevant additional species to be considered include two solid substances, nantokite, CuCl, and paratacamite, $3Cu(OH)_2 \cdot CuCl_2$, and two dissolved substances Cl^- and $CuCl_2^-$ (Pourbaix, 1973).

The resulting electrochemical reactions

13) $Cu + Cl^- = CuCl + \bar{e}$ $\quad Eh = -105 - 59.1 \log[Cl^-]$

14) $2Cu_2O + H_2O + 2Cl^- = 3Cu(OH)_2 \cdot CuCl_2 + 2H^+ + 4\bar{e}$

$$Eh = 209 - 29.5\ pH - 29.5 \log[Cl^-]$$

correspond to oxidation of Cu into CuCl and Cu_2O into paratacamite; in addition, two chemical reactions

15) $2CuCl + H_2O = Cu_2O + 2Cl^- + 2H^+$

$$pH = 5.66 + \log[Cl^-]$$

16) $3Cu(OH)_2 \cdot CuCl_2 = 4CuO + 2Cl^- + 2H^+ + 2H_2O$

$$pH = 7.40 + \log[Cl^-]$$

transform nantokite and paratacamite into cuprous and cupric oxides, respectively. Paratacamite could be the result of copper chloride reacting with water according to the electrochemical reaction:

17) $4\ CuCl + 6H_2O = 3Cu(OH)_2 \cdot CuCl_2 + 2Cl^- + 6H^+ + 4\bar{e}$

$$Eh = 542 - 88.65\ pH + 29.5 \log[Cl^-]$$

Figure 2.3(a) summarizes the results for the ternary system Cu-Cl-H_2O while Figure 2.3(b) depicts the stability fields of solids involved in the copper reactions for dilute (10^{-3}N)

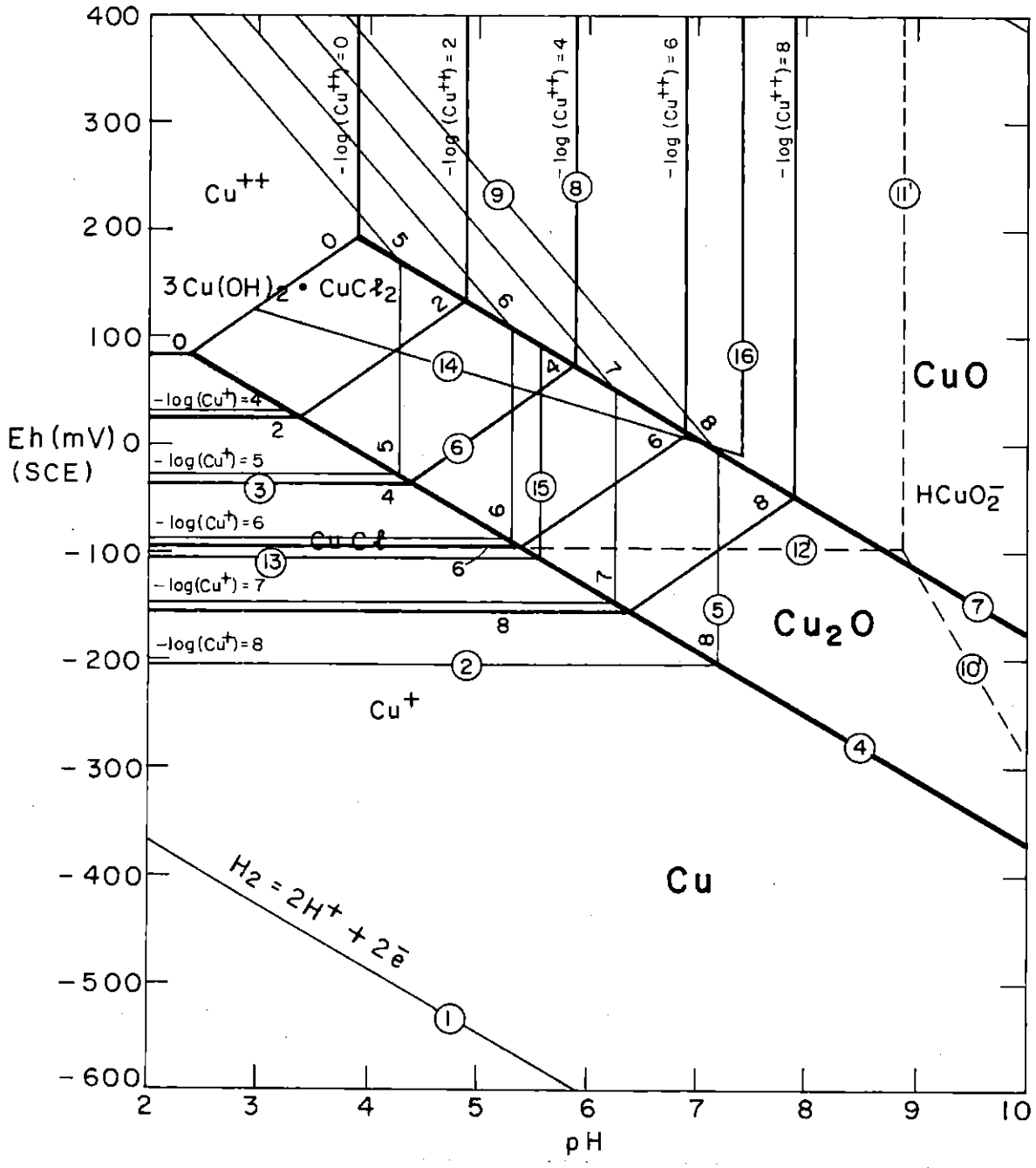


Figure 2.3(a) Eh-pH Diagram of Copper in Chloride Environment (adapted from Pourbaix, 1973)

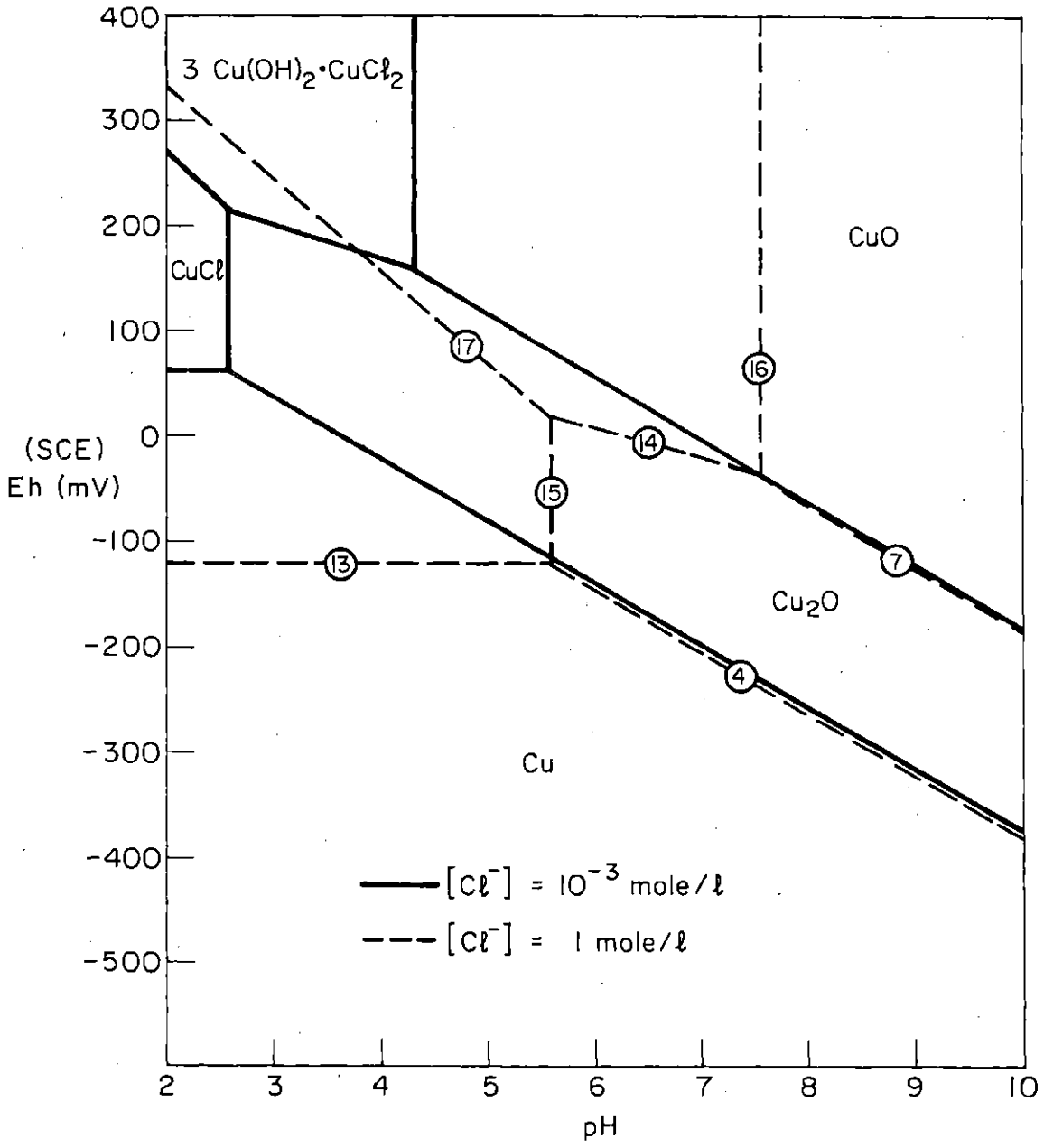


Figure 2.3(b) Stability fields of solids involved in copper reactions in chloride environments.

and concentrated (1 N) chloride solutions.

2.2.2 Eh-pH Diagrams for Iron in Aqueous Solutions

The same approach used in the preceeding paragraph can be used to delineate stability fields for species associated with iron. In our Eh-pH range prescribed above, the relevant chemical species involved are Fe, Fe_3O_4, and Fe_2O_3 as solids, and Fe^{++}, $Fe(OH)_2^+$, Fe^{+++}, and $FeOH^{++}$ as dissolved substances (Pourbaix et al., 1966). Figure 2.4 summarizes the results derived from the following equations:

1) $H_2 = 2H^+ + 2\bar{e}$ $\quad Eh = -242 - 59.1\ pH$

2) $Fe = Fe^{++} + 2\bar{e}$ $\quad Eh = -682 + 29.5 \log[Fe^{++}]$

3) $3Fe + 4H_2O = Fe_3O_4 + 8H^+ + 8\bar{e}$

$Eh = -327 - 59.1\ pH$

4) $2Fe_3O_4 + H_2O = 3Fe_2O_3 + 2H^+ + 2\bar{e}$

$Eh = -21 - 59.1\ pH$

5) $3Fe^{++} + 4H_2O = Fe_3O_4 + 8H^+ + 2\bar{e}$

$Eh = 738 - 236.4\ pH - 88.6 \log[Fe^{++}]$

6) $2Fe^{++} + 3H_2O = Fe_2O_3 + 6H^+ + 2\bar{e}$

$Eh = 486 - 177.3\ pH - 59.1 \log[Fe^{++}]$

7) $Fe^{++} + 2H_2O = Fe(OH)_2^+ + 2H^+ + \bar{e}$

$$Eh = 979 - 118.2\ pH + 59.1 \cdot \log \frac{[Fe(OH)_2^+]}{[Fe^{++}]}$$

8) $Fe^{++} + H_2O = FeOH^{++} + H^+ + \bar{e}$

$$Eh = 672 - 59.1\ pH + 59.1 \log \frac{[FeOH^{++}]}{[Fe^{++}]}$$

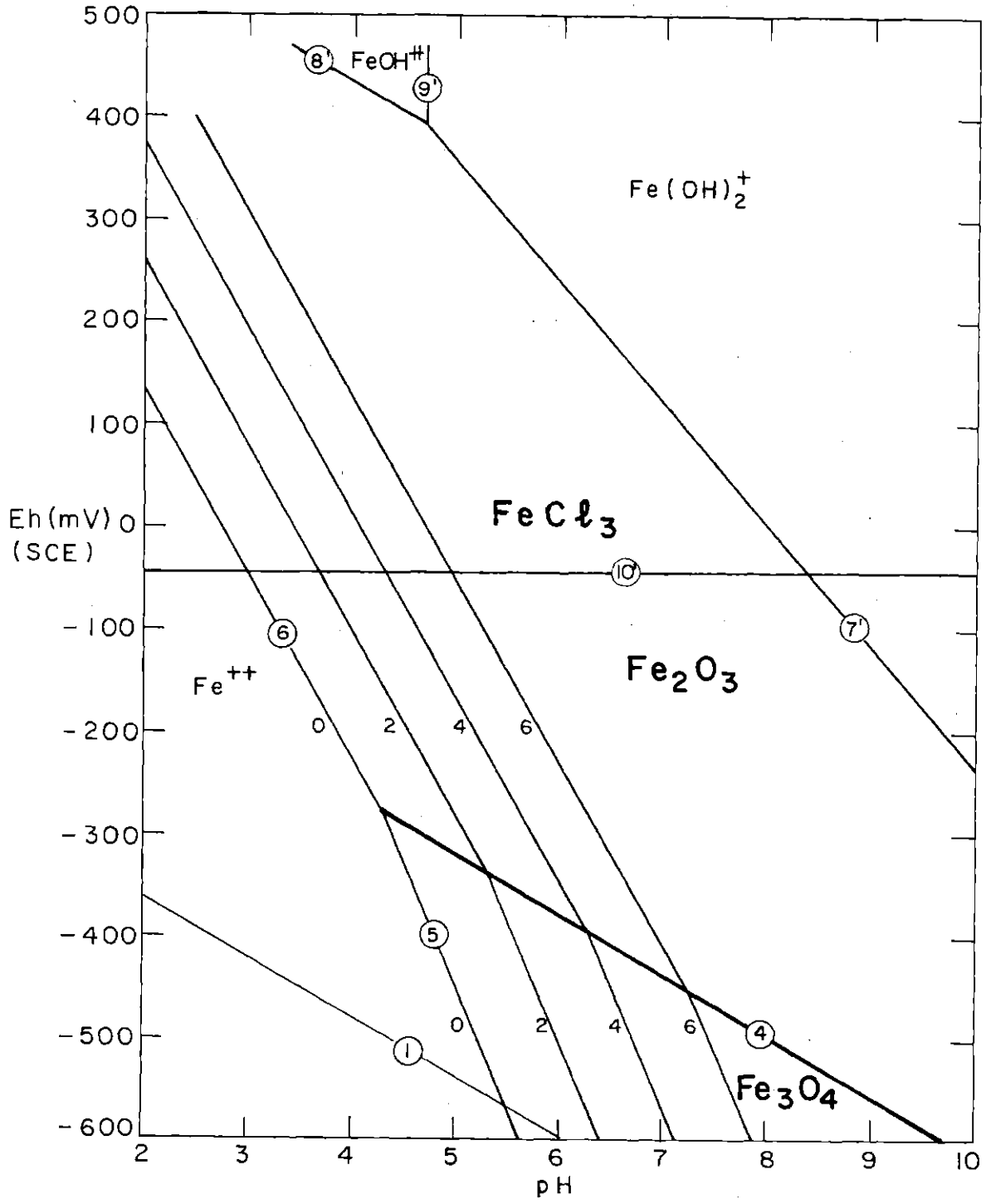


Figure 2.4 Eh-pH Diagram of Iron Chloride Environment (adapted from Pourbaix, 1973)

9) $FeOH^{++} + H_2O = Fe(OH)_2^+ + H^+$

$$pH = 4.69 + \log\frac{[Fe(OH)_2^+]}{[FeOH^{++}]}$$

In the presence of chloride ions, the following electrochemical reaction could occur:

10) $Fe + 3Cl^- = FeCl_3 + 3\bar{e}$

$$Eh = -45 - 59.1 \log[Cl^-]$$

However, $FeCl_3$ is unstable, and could dissociate to give either $3Cl^-$ and Fe^{3+} or Cl^- and $FeCl_2^+$, the respective equilibrium constant being of the order 10^{12} and 10. The line 10' represents the lower stability limit of $FeCl_3$.

2.2.3 Stability Fields of Copper Oxides and Sulfides

Copper is one of the rare metals to be present in nature at native state. This is due to its relatively well developed immunity zone straddling the domain of stability of water. Figure 2.5, adapted from Garrels and Christ (1965), exhibits various stability fields of copper sulfides and Oxides. It is important to note here that these fields corresponding to the system Cu-H_2O-S were established assuming a total concentration of dissolved sulfur of .1M. The effect of lowering the dissolved sulfur concentration will be to widen the stability field of native copper at the expense of the chalcocite and covellite stability fields.

2.2.4 Stability Fields of Iron Oxides and Sulfides

Iron forms two important oxides, magnetite and hema-

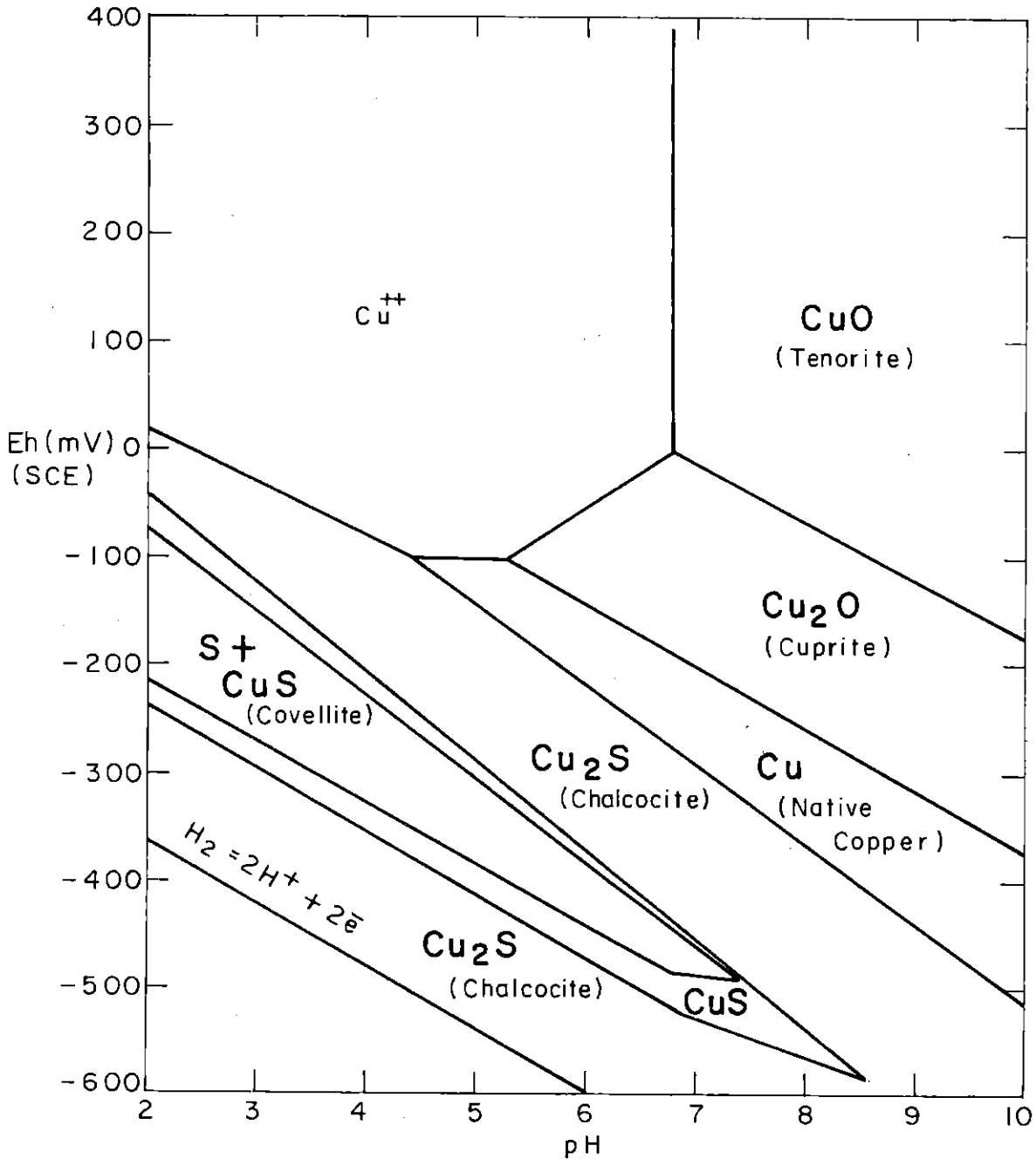


Figure 2.5 Eh-pH Diagram of Copper Sulfides (adapted from Garrels and Christ, 1965)

tite, stable, respectively, under reducing and oxidizing conditions. Similarly, it forms two important sulfides, pyrrhotite and pyrite, stable, respectively, under reducing conditions and mildly reducing conditions. Figure 2.6, adapted from Garrels and Christ (1965), shows the various fields of stability of the minerals. It is apparent that the pyrrhotite stability field requiring more stringent reducing conditions is out of sight in the diagram and would be near pH values ranging from 7 to 9, and Eh values near -750 mV SCE. Here the system $Fe-H_2O-S$ assumes a total dissolved sulfur concentration of only 10^{-6} m.

2.3 Experimental Set-Up

The set-up consists of an electrochemical cell, an impedance comparator, a storage scope and a low frequency oscillator. Several considerations determined the design of the electrochemical cell as well as in that of the impedance comparator. As outlined at the beginning of the chapter, we found it necessary to gather extensive experimental data under carefully controlled conditions to provide grounds for testing any theory of the electrode impedance. Furthermore, we believed the understanding of the influence of various factors on the electrode impedance would at least provide some empirical basis for the understanding of the IP mechanism as well as generate some information of general electrochemical interest.

It is necessary to have the following conditions under

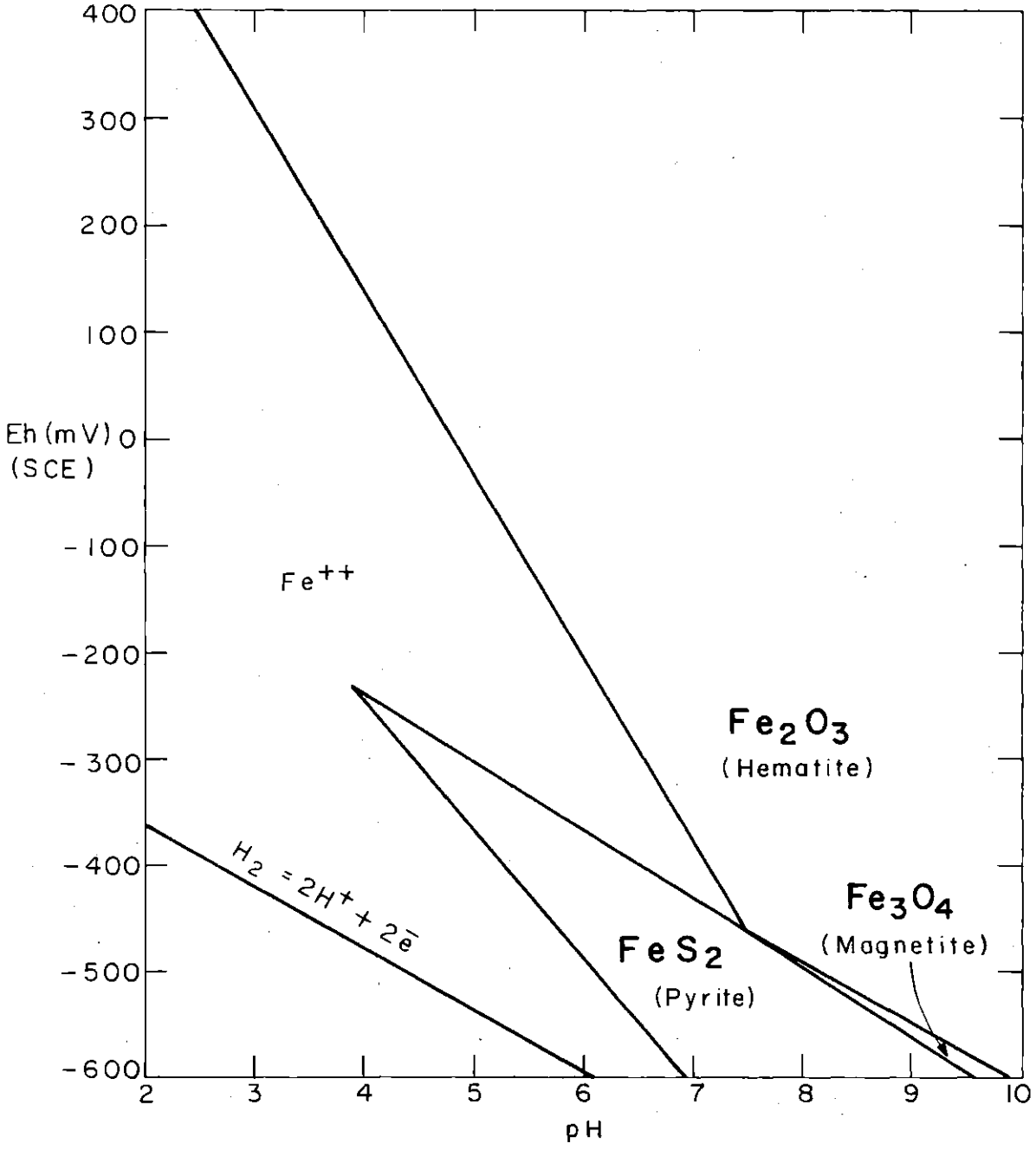


Figure 2.6 Eh-pH Diagram of Iron Sulfides (adapted from Garrels and Christ, 1965)

control: temperature and pressure in the electrochemical cell; geometry of the electrode configuration; nature and surface conditions of the electrodes; composition of the solution; and Eh and pH of the solution.

2.3.1 Geometry of the Cell and Electrode Configuration

The electrode system consists of two samples of the same metal or mineral contiguously disposed so that they are parallel and face each other at a distance of the order of 1 cm or less. The choice of the distance is mainly dictated by the magnitude of the solution resistance. If the solution resistance is relatively large, which is often the case for very dilute salt solutions, the electrode separation should be made very small so that the interfacial impedance is not drowned by the solution resistance. There is, however, a lower limit for the electrode separation dictated by the length of the diffusion zones at the electrodes set up by the lowest frequency used during a measurement. The separation should be at least a couple of diffusion lengths. Table 2.4 shows diffusion lengths at various frequencies for various diffusion coefficients. The values are in microns. Typical diffusion coefficients for ionic species are of the order of 2×10^{-5} cm^2/sec.

This electrode configuration is in keeping with the geometry adopted in the theory of Chapter I with the simple proviso that the impedance be halved because of the series disposition of the two interfacial impedances.

D cm^2/s / f_{CPS}	$.5x10^{-5}$	10^{-5}	$1.5x10^{-5}$	$2x10^{-5}$	$2.5x10^{-5}$	$5x10^{-5}$
1000	.28	.40	.49	.56	.63	.89
100	.89	1.26	1.55	1.78	1.99	2.82
10	2.82	3.99	4.89	5.64	6.31	8.92
1	8.92	12.62	15.45	17.84	19.95	28.21
.1	28.21	39.89	48.86	56.42	63.08	89.21
.01	89.21	126.16	154.51	178.41	199.47	282.09
.001	282.09	398.94	488.60	564.19	630.78	892.06

Table 2.4 Diffusion lengths (μm) as a function of frequency and diffusivities

The cell is a two liter plastic cylindrical container capped by a cover machined to provide an airtight seal with an O-ring squeezed between the cover and the container by three clamps symmetrically disposed. The access to the cell is

through the cover and all the necessary accessories are also attached to the cover.

Several orifices provide the access to the cell. An inlet with a burette and stopcock enables the introduction of necessary additives to the solution; two valves provide inlet and outlet of gas into the cell, the inlet orifice being extended to the bottom of the cell by a tube so that the bubbling does affect the solution. Three other orifices are equipped with a standard calomel electrode, a pH-glass electrode and a platinum electrode for the Eh measurement, all well sealed with tight fitting O-rings. One orifice accommodates a thermometer.

The working electrodes are positioned on two supporting frames attached to the cover of the container from within. These two frames provide a fixed geometry with the option of adjusting the spacing of the electrodes to desired values.

The electrodes are imbedded in a cold setting resin in a molding system so designed as to allow one face of the electrode to be exposed to the solution (working area), and the other face of the electrode to be exposed at the bottom of a threaded hole in the resin so that a threaded piece of teflon equipped with a spring and O-ring provide a spring-loaded electrical contact well protected from leakage into the solution. These contacts are connected with two well insulated wires to electrical plugs on the cover of the cell.

Figure 2.7 shows the schematic of the cell with its accessories. The solution could be stirred with a magnetic stirrer at the bottom of the cell. The motor of the magnetic stirrer, which tends to heat up slowly during its run, is separated from the cell by some insulating material to shield the cell from that extraneous heat.

2.3.2 Experimental Conditions and their Control

The first factors to adequately control are the pH and Eh of the solution, for, as outlined in Section 2.1, these two parameters provide a convenient framework to interpret electrochemical reactions. The pH is controlled by on-line addition of hydrochloric acid, HCl, or potassium hydroxide, KOH, depending on whether a shift towards the acidic or alkaline region, respectively, is desired. The Eh control is somewhat trickier. The method adopted after a number of various tests is the circulation of hydrogen gas through the solution. The passage of hydrogen gas not only flushed out the air initially dissolved in the system, but it provided a reducing environment which turned out to be an important condition in the experiments.

In order for the measured Eh and pH of the solution to approximate as closely as possible the prevailing conditions at the electrodes, the solution is stirred with the magnetic stirrer set up at the bottom of the cell.

The preparation of the solutions themselves requires

Figure 2.7 Schematic of the experimental set-up.

IC = impedance comparator

SC = memory scope (Tektronix)

OS = low frequency oscillator (Wavetek)

ME = pH meter (Orion)

LC = line converter

H = electrode holders

M = molds in which electrodes are imbedded

E = working electrodes

C = spring loaded contacts

IG = inlet gas

OG = outlet gas

IV = inlet valve

OV = outlet valve

B = burette

R = calomel reference electrode

Pt = platinum probe Eh electrode

pH = pH glass electrode

ST = magnetic bar

C = cell

MS = magnetic stirrer

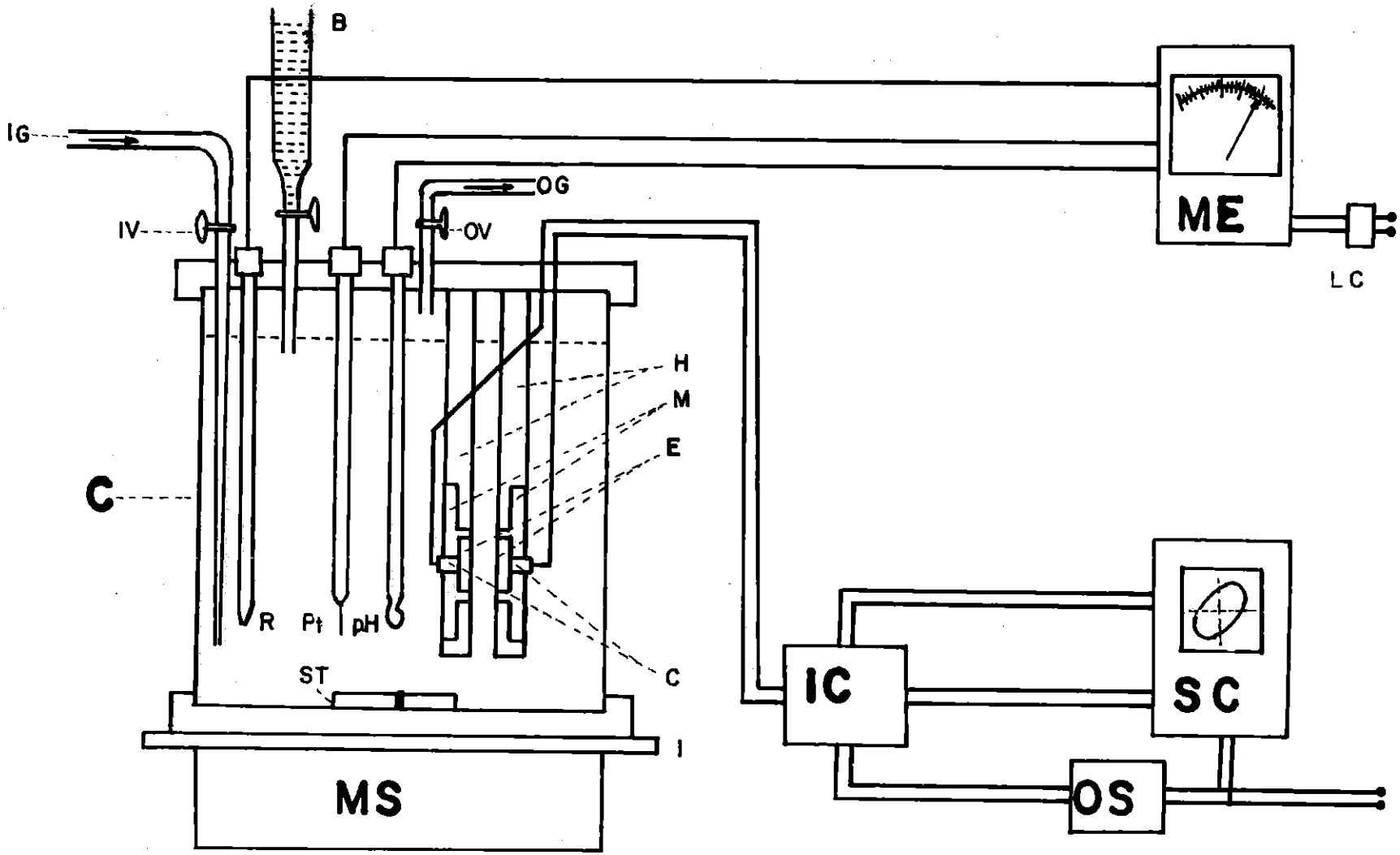


Figure 2.7

reagent grade compounds and distilled water. We did not stretch the care so far as to use multiply-distilled water in the preparation of our solutions. In addition, we analyzed some samples of the distilled water for Cu and Fe using the atomic absorption spectrophotometer of the MIT Department of Earth and Planetary Sciences. We could detect only very small concentrations of Cu and Fe, usually much less than 10^{-6} m which, for all practical purposes, could be considered satisfactory blank tests.

The electrodes were carefully polished, generally to the standard size 600 of polishing paper. There were some cases where we used diamond polish or iron thinning techniques for the sake of comparing the influence of surface conditions.

2.3.3 The Impedance Comparator

The circuit of the impedance comparator is shown in Figure 2.8. It is essentially a bridge feeding across the working electrodes a very small sinusoidal voltage of 4 mv in amplitude and very small current densities to stay within the limits of linearity. A set of current gains enables measurement of a wide range of impedances. The sinusoidal voltage is provided by a Wavetek low frequency oscillator. The response of the electrode is amplified by a series of operational amplifiers set up to provide a gain of 100. This output is fed into the Y component of an oscilloscope while the input voltage is tapped into the X component of the oscilloscope. The electrode and amplifier bias essentially provide a bucking of any

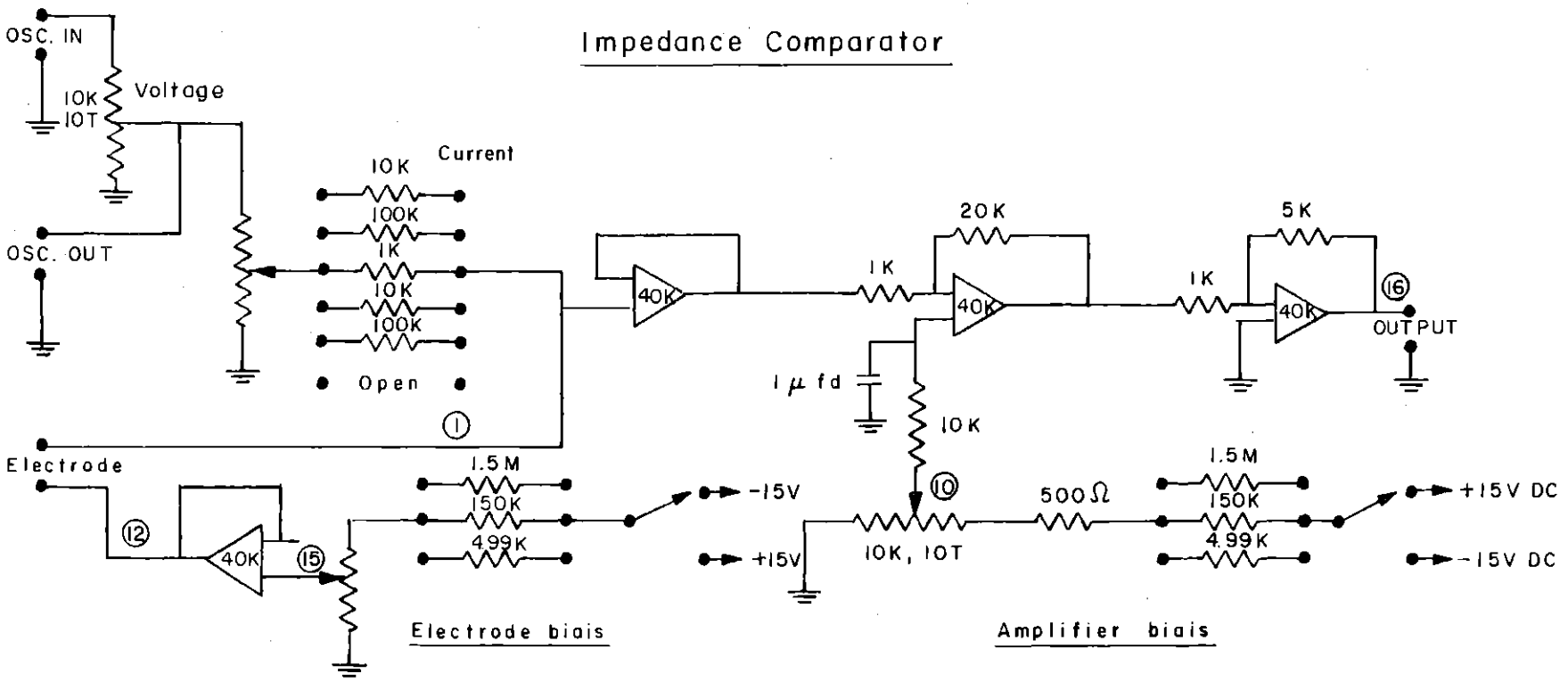


Figure 2.8 Schematic of the Impedance Comparator

DC imbalance preventing proper display of the Lissajous pattern on the oscilloscope.

2.3.4 Methods of Measurement

A given experimental run consists in measuring the electrode impedance spectrum at 1000 cps and lower frequencies in decade steps. At each frequency, the phase angle is computed from the Lissajous ellipse displayed on the oscilloscope; the amplitude of the impedance is obtained by substituting a variable decade resistor to the electrode input and while feeding in it the same current, by adjusting the resistor so as to obtain the same voltage level as the one given by the electrode output.

The pH and Eh of the solution are measured respectively with a pH-glass electrode and a platinum probe against a standard calomel reference electrode. We use an Orion pH-meter which is essentially a voltmeter with very high input impedance. We also measure the electrode potential against the calomel electrode because some information of electrochemical interest could be contained in the variations of these potentials with various conditions.

2.4 Typical Results of Measurements

We display in Tables 2.5 through 2.11 typical results in raw form obtained for various electrodes under specified conditions. Most often, the two working electrodes A_1 and A_2 facing each other do not have the same area. It is therefore necessary to define an equivalent area, A, corresponding to a working electrode which would give equal impedance. Since

both interfacial impedances are in series, the equivalent area, A, will be defined by

$$\frac{1}{A} = \frac{1}{A_1} + \frac{1}{A_2}$$

where A_1 and A_2 are the areas of each working electrode, respectively.

A wide variety of electrolyte solutions were used, among which were chloride, sulfate, nitrate, and sulfide solutions. Electrodes used comprised metals like copper and iron, and metallic sulfides like covellite, chalcocite, chalcopyrite, pyrite, and pyrrhotite.

It should also be noted that each spectrum in Tables 2.5 through 2.11 often represents only the starting point of a whole series of experiments which investigate the effects of the various parameters mentioned in the previous paragraph on electrode impedance. The interpretation of such measurements requires first the inversion of the data, i.e. the resolution of the elements of the equivalent circuit model adopted for fitting the spectra. From the values of these elements, appropriate electrochemical parameters like active ionic species concentrations and exchange current densities will be estimated

2.5 Equivalent Circuit Fitting

The existence of an equivalent circuit simulating the electrode impedance is a consequence of the linear regime set for the electrode processes. The nature of the circuit is dictated by these processes. As outlined in Section 1.5, our fitting

procedure provides a resolution matrix which points out the important elements contributing to the impedance. This feature helped us greatly in simplifying the original circuits which were conceived to represent a wide combination of processes like Madden's basic equivalent circuit (Madden, 1961). After some 200 or so electrode impedance fittings, first using Madden's basic equivalent circuit; and later, the circuit shown in Figure 1.4, we came to the inexorable conclusion that only very few elements in the above circuits were really necessary, namely, the solution resistance in series with a parallel combination of the fixed layer capacitance, and a Warburg impedance in series with a reaction resistance.

This final circuit is similar to the one derived in Section 1.2 (Figure 1.1). Such a result seems quite surprising, in view, as we shall see later, of the variety of electrodes and environments investigated during this study. It essentially underlines the fundamental similarity of the impedance determining electrode reactions in apparently diverse electrode processes.

For the sake of clarity, we reprocessed all of our measured spectra using this simple equivalent circuit in the inversion scheme. We display in Tables 2.12 through 2.18 the fits corresponding to the raw data of Tables 2.5 through 2.11. The typical % error of the circuit fit was about 5%.

Conditions / Frequencies	A Solution: .001 N KCl .001 N $CuSO_4$ pH = 5.9 Eh = 218mv A = .633cm^2		B Solution: .001 N KCl pH = 6.2 Eh = 140mv E = -32mv A = .633cm^2		C Solution: .001 N $CuSO_4$ pH = 5.4 Eh = 278mv A = .633cm^2	
	Z	ϕ	Z	ϕ	Z	ϕ
1000	2830	1.43	1630	7.18	1800	2.87
100	2870	1.43	2320	25.15	2030	4.30
10	3060	2.87	6350	33.37	2215	2.87
1	3534	11.54	14000	30.00	2400	.72
.1	5684	22.02	34300	30.00	2400	.72

Table 2.5 Copper Electrode Impedance

Conditions / Frequencies	A Solution: .001 N $FeCl_2$ pH = 5.0 Eh = 150mv E = -265mv A = .708cm^2		B Solution: .001 N KCl pH = 6.2 Eh = 140mv E = -270mv A = .755cm^2		C Solution: .00005 N KCl pH = 6.1 Eh = 150mv E = -180mv A = .671cm^2	
	Z	ϕ	Z	ϕ	Z	ϕ
1000	1500	1.43	1480	.14	3200	1.43
100	1500	2.15	1480	2.15	3375	4.30
10	1615	4.30	1600	8.63	4130	17.46
1	2010	10.08	2510	30.00	9350	42.45
.1	2400	2.87	6500	22.02	37000	42.45

Table 2.6 Iron Electrode Impedance

Conditions / Frequencies	A Solution: .001 N $CuSO_4$ pH = 5.2 Eh = 220mv E = 160mv A = .337cm^2		B Solution: .001 N Na_2SO_4 pH = 5.8 Eh = 100mv E = 130mv A = .417cm^2		C Solution: .001 N KCl pH = 6.0 Eh = 180mv E = 100mv A = .499cm^2	
	Z	ϕ	Z	ϕ	Z	ϕ
1000	5715	.72	4120	.14	3100	.14
100	5715	.72	4215	2.15	3200	.14
10	6200	1.43	4450	4.30	3400	.72
1	6460	1.43	5350	14.48	4400	14.48
.1	6500	2.87	10400	35.10	8000	30.00

Table 2.7 Covellite Electrode Impedance

Conditions / Frequencies	A Solution: .001 N $CuSO_4$ pH = 5.6 Eh = 160mv E = 140mv A = .581cm^2		B Solution: .001 N KCl pH = 6.2 Eh = 110mv E = 70mv A = .353cm^2		C Solution: .001 N Na_2S pH = 10.4 Eh = -400mv E = -620mv A = .487cm^2	
	Z	ϕ	Z	ϕ	Z	ϕ
1000	3380	.72	3435	1.43	2830	.01
100	3530	.72	3505	3.58	2890	2.15
10	3600	.72	4120	14.48	3170	2.87
1	3600	.14	8100	38.68	3325	.14
.1	3700	.14	26000	38.68	3400	.01

Table 2.8 Chalcocite Electrode Impedance

Conditions	A Solution: .001 N $CuSO_4$ pH = 5.50 Eh = 350mv E = 205mv		B Solution: .001N $Ca(NO_3)_2$ pH = 5.8 Eh = 185mv E = 75mv		C Solution: .001 N NH_4Cl pH = 6 Eh = 160mv E = 67mv	
Frequencies	A = .718cm^2		A = .613cm^2		A = .484cm^2	
	Z	ϕ	Z	ϕ	Z	ϕ
1000	3000	.01	2180	2.15	2180	1.43
100	3000	.01	2260	2.87	2270	4.30
10	3050	.07	2560	13.00	2770	18.97
1	3250	4.30	4670	38.68	6590	48.59
.1	4000	14.48	20000	61.04	32500	55.59

Table 2.9 Chalcopyrite Electrode Impedance

Conditions	A Solution: .001 N KCl pH = 6 Eh = 160mv E = 87mv		B Solution: .001 N NaCl pH = 6.0 Eh = 220 E = 87mv		C Solution: .001 N $FeCl_2$ pH = 5.5 Eh = 130mv E = 100mv	
Frequencies	A = .442cm^2		A = .586cm^2		A = .586cm^2	
	Z	ϕ	Z	ϕ	Z	ϕ
1000	3745	.72	3300	.01	2320	1.43
100	3850	2.87	3475	1.43	2360	2.87
10	4350	13.00	3860	10.08	2660	10.08
1	8100	38.68	5950	23.58	4430	28.36
.1	27000	36.87	11200	22.02	10000	25.15

Table 2.10 Pyrrhotite Electrode Impedance

Conditions Frequencies	A Solution: .001 N KCl pH = 6.2 Eh - 130 mv E = 132 mv A = .675 cm^2		Solution: .001 N NaCl pH = 6.0 Eh = 170 mv E = 165 mv A = .629 cm^2		Solution: .001N $FeCl_2$ pH = 5.2 Eh = 80 mv E = 177 mv A = .548 cm^2	
	Z	ϕ	Z	ϕ	Z	ϕ
1000	1660	2.87	1840	1.43	2020	1.43
100	1820	3.58	1875	2.87	2030	1.43
10	1930	11.54	2140	14.48	2160	8.63
1	3600	40.54	4420	46.47	3399	35.10
.1	14500	46.47	22000	50.81	13600	48.59

Table 2.11 Pyrite Electrode Impedance

R_s stands for the solution resistance in $\Omega \cdot cm^2$, C the fixed layer capacity in F/cm^2, R_1 the reaction resistance in $\Omega \cdot cm^2$, W the Warburg impedance at unit angular frequency per cm^2 ($\omega = 1$), C_i, the equivalent active species concentration and i_0 the exchange current density. In each case, the resolution matrix which testifies to the relevance of each element of the circuit is displayed.

Close examination of the equivalent circuit parameters shows two outstanding results. First, the Warburg element in the circuit dominates the electrode impedance. Second, the reaction resistance component is very small in most instances. The importance of the Warburg impedance is of special significance since it provides us with a means to estimate the active ionic species concentrations. The values of the capacitive component vary from a couple of microfarads to hundreds of microfarads. It appears that the derived exchange current densities are of the order of 10^{-5} A/cm^2 or greater by several orders of magnitude in various instances. Such wide variations of exchange current densities

	A				B				C			
Freq	Zobs	Zmod	ϕobs	ϕmod	Zobs	Zmod	ϕobs	ϕmod	Zobs	Zmod	ϕobs	ϕmod
1000	1791	1767	1.43	.97	1032	1089	7.18	3.78	1139	1159	2.87	1.13
100	1817	1834	1.43	1.85	1468	1396	25.15	28.72	1285	1276	4.30	6.40
10	1937	1946	2.87	4.28	4019	4200	33.37	33.45	1402	1449	2.87	1.72
1	2237	2292	11.54	11.25	8862	8630	30.00	31.60	1519	1467	.72	.88
.1	3598	3510	22.02	23.70	21711	21250	30.00	38.68	1519	1508	.72	2.22
	Rms error=2.33%				Rms error=7.91%				Rms error=3.47%			
	Resolution Matrix				Resolution Matrix				Resolution Matrix			
Rs(Ω)	1753	1.00	.01	.02	.00	1085	.99	.00	.00	.00	1157	.99	.03	.02	.00
C(μF)	4	.01	.01	.00	.00	2	.00	.96	-.02	.00	7	.03	.46	.08	.02
R_1(Ω)	60	.02	.00	.08	.01	2906	.00	-.02	.94	.01	292	.02	.08	.86	.05
W(Ω)	1581	.00	.00	.01	.97	14770	.00	.00	.01	.99	65	.00	.02	.05	.19
Ci	$.40\times10^{-4}$ mole/l				$.42\times10^{-5}$ mole/l				$.97\times10^{-3}$ mole/l			
i_0	$.41\times10^{-3}$ A/cm^2				$.86\times10^{-5}$ A/cm^2				$.86\times10^{-4}$ A/cm^2			

Table 2.12 Equivalent Circuit Fitting of Electrode Impedance Normalized to 1cm^2 of Area for COPPER

	A				B				C			
Freq	Zobs	Zmod	ϕobs	ϕmod	Zobs	Zmod	ϕobs	ϕmod	Zobs	Zmod	ϕobs	ϕmod
1000	1062	1083	1.43	.04	1117	1156	.14	.06	2147	2252	1.43	.31
100	1062	1083	2.15	.40	1117	1156	2.15	.64	2265	2265	4.30	2.93
10	1143	1096	4.30	3.86	1208	1168	8.63	6.29	2771	2651	17.46	19.85
1	1423	1452	10.08	10.56	1895	1901	30.00	35.03	6274	6699	42.45	44.14
.1	1699	1672	2.87	4.12	4907	4729	22.02	23.13	24827	23181	42.45	47.17
	Rms error=3.19%				Rms error=5.18%				Rms error=6.28%			
	Resolution Matrix				Resolution Matrix				Resolution Matrix			
Rs (Ω)	1083	1.00	-.01	.00 .00	1156	1.00	.00	.00 .00	2251	1.00	.00	.00 .00
C (ΩF)	211	-.01	.74	.00 .06	124	.00	.97	-.02 .04	13	.00	.93	-.07 -.01
R_1 (Ω)	525	.00	.00	.92 .08	3023	.00	-.02	.94 .09	462	.00	-.07	.00 .00
W (Ω)	84	.00	.06	.08 .18	1122	.00	.04	.09 .72	19560	.00	-.01	.00 .99
Ci	$.75\times10^{-3}$ mole/l				$.56\times10^{-4}$ mole/l				$.32\times10^{-5}$ mole/l			
i_0	$.48\times10^{-4}$ A/cm^2				$.83\times10^{-5}$ A/cm^2				$.54\times10^{-4}$ A/cm^2			

Table 2.13 Equivalent Circuit Fitting of Electrode Impedance Normalized to 1cm^2 of Area for IRON

	A				B				C			
Freq	Zobs	Zmod	ϕobs	ϕmod	Zobs	Zmod	ϕobs	ϕmod	Zobs	Zmod	ϕobs	ϕmod
1000	1924	1914	.72	.22	1719	1778	.14	.04	1548	1618	.14	.06
100	1924	1939	.72	1.91	1759	1778	2.15	.42	1598	1619	.14	.59
10	2087	2097	1.43	1.62	1857	1805	4.30	3.61	1698	1661	.72	4.97
1	2174	2136	1.43	1.07	2232	2193	14.48	16.99	2198	2150	14.48	17.05
.1	2188	2212	2.87	2.78	4340	4350	35.10	33.55	3996	3944	30.00	29.77
	Rms error=1.37%				Rms error=3.42%				Rms error=4.00%			
	Resolution Matrix				Resolution Matrix				Resolution Matrix			
Rs(Ω)	1913	1.00	-.01	.02	.00	1778	1.00	-.01	.00	.00	1618	1.00	-.01	.00	.00
C(μF)	21	-.01	.11	.05	.02	119	-.01	.76	-.12	-.04	94	-.01	.67	-.24	-.01
R_1(Ω)	191	.02	.05	.53	.10	185	.00	-.12	.02	.02	336	.00	-.24	.18	.05
W´(Ω)	119	.00	.02	.10	.28	2782	.00	-.04	.02	.96	2175	.00	-.01	.05	.96
Ci	$.53\times10^{-3}$ mole/l					$.22\times10^{-4}$ mole/l					$.29\times10^{-4}$ mole/l				
i_0	$.13\times10^{-3}$ A/cm^2					$.13\times10^{-3}$ A/cm^2					$.74\times10^{-4}$ A/cm^2				

Table 2.14 Equivalent Circuit Fitting of Electrode Impedance Normalized to 1cm^2 of Area for COVELLITE

	A				B				C			
Freq	Zobs	Zmod	ϕobs	ϕmod	Zobs	Zmod	ϕobs	ϕmod	Zobs	Zmod	ϕobs	ϕmod
1000	1964	1968	.72	.89	1214	1237	1.43	.25	1378	1377	.01	.32
100	2051	2083	.72	1.56	1239	1243	3.58	2.39	1407	1402	2.15	2.80
10	2092	2110	.72	.26	1456	1416	14.48	16.06	1544	1579	2.87	2.25
1	2092	2116	.14	.26	2863	2972	38.68	37.19	1619	1607	.14	.79
.1	2150	2135	.14	.74	9191	8913	38.68	43.60	1656	1641	.01	1.73
	Rms error=1.82%				Rms error=4.48%				Rms error=1.75%			
	Resolution Matrix				Resolution Matrix				Resolution Matrix			
Rs(Ω)	1961	1.00	.00	.03	.00	1237	1.00	.00	.00	.00	1377	1.00	-.01	.02	.00
C(μF)	5	.00	.07	.07	.01	29	.00	.89	-.15	-.01	20	-.01	.22	.06	.02
R_1(Ω)	146	.03	.07	.39	.05	345	.00	-.15	.05	.01	215	.02	.06	.73	.07
W (Ω)	308	.00	.01	.05	.23	6974	.00	-.01	.01	.98	54	.00	.02	.07	.12
Ci	$.20\times10^{-2}$ mole/l					$.90\times10^{-5}$ mole/l					$.11\times10^{-2}$ mole/l				
i_0	$.17\times10^{-3}$ A/cm^2					$.72\times10^{-4}$ A/cm^2					$.11\times10^{-3}$ A/cm^2				

Table 2.15 Equivalent Circuit Fitting of Electrode Impedance Normalized to 1cm^2 of Area for CHALCOCITE

	A				B				C			
Freq	Zobs	Zmod	ϕobs	ϕmod	Zobs	Zmod	ϕobs	ϕmod	Zobs	Zmod	ϕobs	ϕmod
1000	2136	2156	.01	.01	1336	1425	2.15	.11	1055	1117	1.43	.23
100	2136	2156	.01	.11	1385	1426	2.87	1.11	1099	1120	4.30	2.20
10	2172	2163	.07	1.00	1569	1474	13.00	9.96	1341	1232	18.97	18.07
1	2314	2283	4.30	5.32	2863	2764	38.68	44.89	3189	3352	48.59	52.60
.1	2848	2844	14.48	14.29	12260	12318	61.04	55.64	15730	15095	55.59	54.40
	Rms error=1.24%				Rms error=8.09%				Rms error=6.39%			
	Resolution Matrix				Resolution Matrix				Resolution Matrix			
Rs(Ω)	2156	1.00	.01	.00	.00	1425	1.00	.00	.00	.00	1117	1.00	.00	.00	.00
C(μF)	388	.01	.34	.13	.07	56	.00	.96	.00	-.02	35	.00	.97	.00	-.01
R_1(Ω)	149	.00	.13	.06	.07	87	.00	.00	.00	.00	80	.00	.00	.00	.00
W (Ω)	782	.00	.07	.07	.84	13580	.00	-.02	.00	.97	15310	.00	-.01	.00	.99
Ci	$.80\times10^{-4}$ mole/l				$.46\times10^{-5}$ mole/l				$.41\times10^{-5}$ mole/l			
i_0	$.17\times10^{-3}$ A/cm^2				$.29\times10^{-3}$ A/cm^2				$.31\times10^{-3}$ A/cm^2			

Table 2.16 Equivalent Circuit Fitting of Electrode Impedance Normalized to 1cm^2 Area for CHALCOPYRITE

	A				B				C			
Freq	Zobs	Zmod	ϕobs	ϕmod	Zobs	Zmod	ϕobs	ϕmod	Zobs	Zmod	ϕobs	ϕmod
1000	1657	1685	.72	.28	1933	2038	.01	.09	1359	1417	1.43	.09
100	1703	1693	2.87	2.16	2036	2039	1.43	.96	1383	1418	2.87	.96
10	1924	1888	13.00	14.29	2261	2112	10.08	8.96	1559	1459	10.08	9.19
1	3583	3768	38.68	36.73	3486	3642	23.58	23.77	2596	2712	28.36	30.68
.1	11945	11451	36.87	44.06	6562	6369	22.02	24.37	5860	5605	25.15	27.81
	Rms error=5.07%				Rms error=4.53%				Rms error=5.61%			
	Resolution Matrix				Resolution Matrix				Resolution Matrix			
Rs(Ω)	1685	1.00	.00	.00 .00	2038	1.00	.00	.00 .00	1417	1.00	.00	.00 .00
C(μF)	22	.00	.87	-.05-.02	47	.00	.88	-.06 .03	67	.00	.93	-.05 .03
R_1(Ω)	108	.00	-.02	.00 .00	2074	.00	-.06	.85 .07	2137	.00	-.05	.86 .07
W (Ω)	9099	.00	-.02	.00 .98	2609	.00	.03	.07 .92	2478	.00	.03	.07 .92
Ci	$.69\times10^{-5}$ mole/l				$.24\times10^{-4}$ mole/l				$.25\times10^{-4}$ mole/l			
i_0	$.23\times10^{-3}$ A/cm^2				$.12\times10^{-4}$ A/cm^2				$.12\times10^{-4}$ A/cm^2			

Table 2.17 Equivalent Circuit Fitting of Electrode Impedance Normalized to 1cm^2 of Area for PYRRHOTITE

	A				B				C			
Freq	Zobs	Zmod	ϕobs	ϕmod	Zobs	Zmod	ϕobs	ϕmod	Zobs	Zmod	ϕobs	ϕmod
1000	1120	1190	2.87	.15	1157	1197	1.43	.17	1107	1126	1.43	.09
100	1228	1192	3.58	1.50	1179	1199	2.87	1.67	1112	1127	1.43	.94
10	1303	1265	11.54	12.15	1346	1278	14.48	14.20	1184	1160	8.63	8.22
1	2430	2534	40.54	41.99	2780	2953	46.47	49.16	1858	1920	35.10	37.85
.1	9787	9380	46.47	49.51	13838	13033	50.81	54.22	7453	7146	48.59	50.84
	Rms error=5.45%				Rms error=5.60%				Rms error=3.62%			
	Resolution Matrix				Resolution Matrix				Resolution Matrix			
Rs(Ω)	1190	1.00	.00	.00	1197	1.00	.00	.00	1126	1.00	.00	.00
C(μF)	49	.00	.94	-.02	44	.00	.96	-.01	84	.00	.95	-.03
R_1(Ω)	89	.00	-.02	.00	102	.00	-.01	.00	131	.00	-.03	.00
W (Ω)	8567	.00	-.02	.00	13360	.00	-.01	.00	6977	.00	-.02	.00
Ci	$.73 \times 10^{-5}$ mole/l				$.47 \times 10^{-5}$ mole/l				$.90 \times 10^{-5}$ mole/l			
i_0	$.28 \times 10^{-3}$ A/cm^2				$.24 \times 10^{-3}$ A/cm^2				$.19 \times 10^{-3}$ A/cm^2			

Table 2.18 Equivalent Circuit Fitting of Electrode Impedance Normalized to $1cm^2$ of Area for PYRITE

are not surprising, however, after cursory excursion in listed values from the literature (Tibor Erdey-Grúz, 1972).

The underlined values of the circuit elements and reaction parameters indicate that these values are well resolved. In general, when elements are unresolved the values given can be considered limiting values, as shown below.

True value		Indicated value
C	$\leq$	C
R_1	$\leq$	R_1
W	$\leq$	W
C_i	$\geq$	C_i
i_0	$\geq$	i_0

C_i must be considered a lower limit even when it is well resolved since any surface diffusion process will be included in the W estimate and acts essentially in series with the solution diffusion process. Also if several species are involved in the reaction their diffusion effects also act as in series. Such results are the basic input into the investigation of ionic species involved in the impedance determining reactions which we will undertake in the next chapter.

CHAPTER III

Empirical Classification of Ionic Species and Electrode Reactions

From the "geoelectrochemical" point of view, natural IP environments are aqueous solutions populated by a variety of ionic species which contribute to the characterization of the environment. Since our approach to the IP mechanism is, in essence, electrochemical, it is important to understand the contribution of each ionic species (or a combination of them) to the electrode processes, i.e. to separate ionic species into "active" and "inactive" ones. It is easy to see that this could become a life-time hobby. Thus, our investigation is necessarily limited to a few ionic species selected with some degree of arbitrariness on the basis of analysis of various natural environments.

The methodology which is followed relies essentially on the results of the equivalent circuit fitting. As outlined in Section 1.3, the magnitude of the Warburg impedance depends prominently on the concentration of the active ionic species. The procedure is therefore to find in the environment of a given experiment, an ionic species whose concentration C_i tracks reasonably with the concentration derived from the electrode impedance. Table 3.1 shows the Warburg impedances at various frequencies associated with a given active ionic species concentrations. As mentioned before, C_i determined from the Warburg impedance can be considered a lower limit

since if several diffusion processes are involved their impedance contributions act in series. C_i does also depend on the true area of the electrodes involved in supporting the reactions as seen through the filtering of a diffusion process. The Warburg impedance is mainly determined from the lowest frequencies which have diffusion lengths of 17 and 56 μm, respectively, so that we can reasonably ignore the surface area increase due to the very fine scale topography of the electrode surfaces. The identification of any active ionic species will, of course, hinge on reasonable knowledge of the environment. This is the stage where the Eh-pH diagrams presented in the previous chapter could be put to some use.

3.1 Excursion in the Eh-pH Diagrams

We have shown in Chapter II how the stability fields of ionic species could be defined in terms of Eh and pH. It is convenient to represent concisely the results of each experiment in the Eh-pH reference system by reporting on each experimental point, the equivalent concentration derived. Thus, as the environment is modified in a systematic way according to the methods described in Section 2.3.2, we can generate a curve describing the evolution of the environment in terms of Eh and pH and use as a third dimension the impedance level in terms of an equivalent active ionic species concentration.

We find it convenient to use as a parameter the logarithm of the reciprocal of the concentrations by analogy to the definition of pH. Typical experimental results are displayed in Figures 3.1 through 3.19.

fcps / Ci mole/l	1	.1	.01
10^{-6}	62 666	198 166	626 657
$5x10^{-6}$	12 533	39 633	125 331
10^{-5}	6 267	19 817	62 666
$5x10^{-5}$	1 253	3 963	12 533
10^{-4}	627	1 982	6 267
$5x10^{-4}$	125	396	1 253
10^{-3}	63	198	627
$2x10^{-3}$	31	99	313
$4x10^{-3}$	16	49	157
$6x10^{-3}$	10	33	104
$3x10^{-3}$	8	25	78
10^{-2}	6	20	63

Table 3.1 Warburg Impedance ($\Omega x cm^2$) Associated to Active Ionic Species at 1, .1 and .01 cps

3.2 Active and Inactive Ionic Species

Our attempt to perform an empirical classification of ionic species covered a relatively narrow range of anions and cations commonly encountered in

natural media. Chlorides (Cl^-), sulfates ($SO_4^=$), sulfides ($S^=$), carbonates ($CO_3^=$), nitrates (NO_3^-), were the main anions used, while the cations included potassium (K^+), sodium (Na^+), copper (Cu^{++}), iron (Fe^{++}), calcium (Ca^{++}) and of course hydronium (H^+) and (OH^-).

Four results emerge from this investigation:

1. Cupric ions may be active at the electrodes;

2. $S^=$ may be active at the electrodes

3. Only in one instance was H^+ identified as active.

In most cases, the electrode impedance appears remarkably independent of pH. We shall analyze this singular behavior in the fourth chapter.

4. All the other ionic species appear inactive under the conditions of our experiments.

The above conclusions can be ascertained by a close look at the series of experiments summarized in Figures 3.1 through 3.19.

3.2.1 Active Behavior of Cupric Ions and Associated Reactions

We have approached the behavior of cupric ions using copper electrodes as well as copper sulfide electrodes in solutions of KCl "doped" with Cu^{++} or in solutions of $CuSO_4$. This doping is to provide cupric ions in sufficient amount to make up the equilibrium concentration of Cu^{++} at given Eh and pH. Close scrutiny of Figure 3.1 shows that the equivalent concentration, C_i, is very close to the equilibrium con-

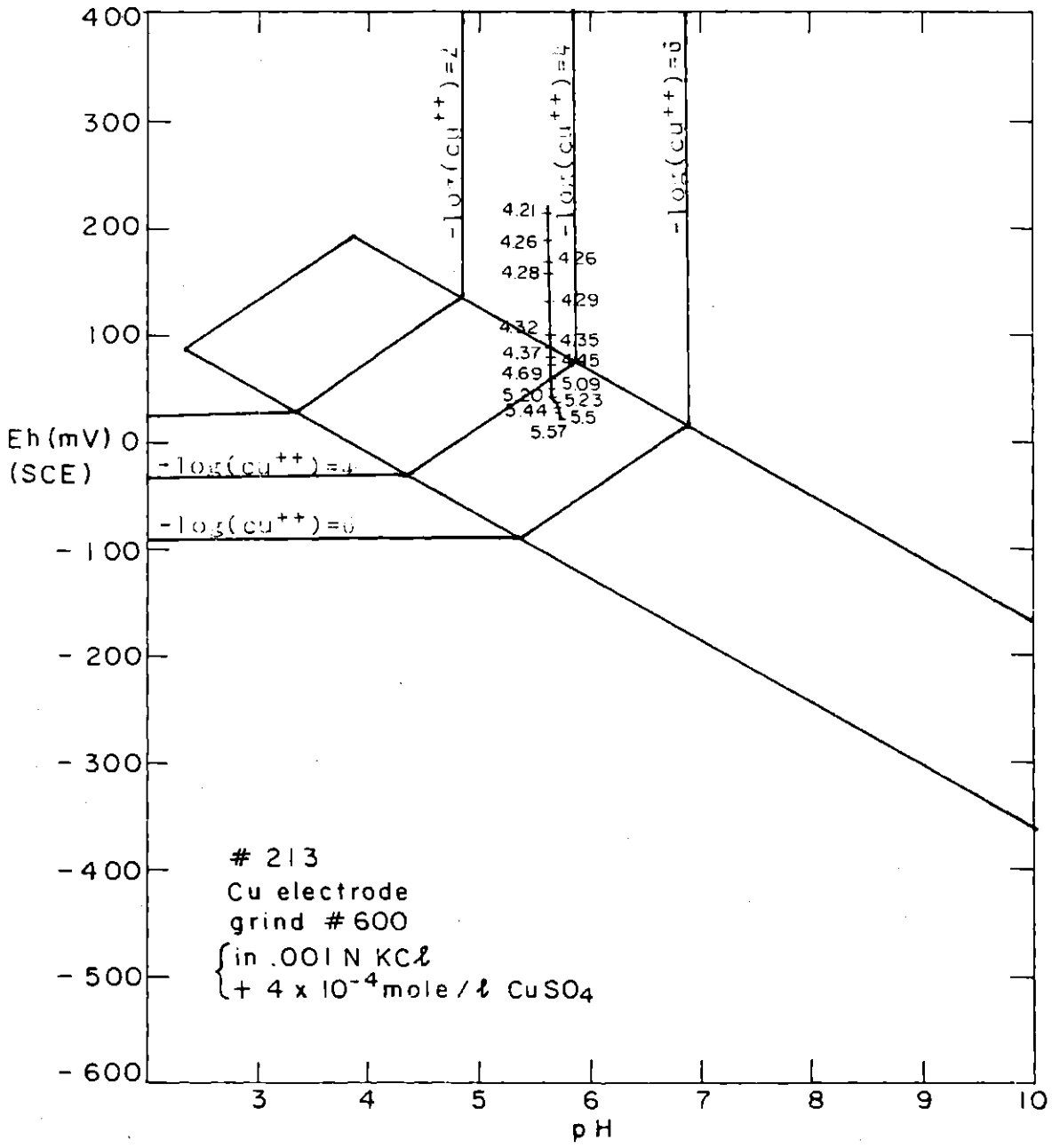


Figure 3.1 Warburg Impedance as a Function of Eh-pH (expressed as -log C, C = apparent concentration).

centration of Cu^{++}. Lowering the Eh, i.e. making the environment more reducing, will tend to deplete the solution in cupric ions: it is observed that the equivalent concentration decreases in keeping with the level of concentration of cupric ions. Such matching implies that cupric ions are involved in copper electrode processes.

A typical electrochemical process at a copper electrode involving Cu^{++} is the corrosion process

$$Cu = Cu^{++} + 2\bar{e}$$

which may control the copper electrode impedance under the above experimental conditions. As we shall see later, such electrode processes are complicated by the state of the electrode surfaces.

Cupric ions are also active at the copper sulfide electrodes, chalcocite and covellite. Figure 3.2 shows a series of experiments dealing with chalcocite electrodes in dilute $CuSO_4$. The equivalent concentration matches cupric ion concentration from pH = 6 to pH = 4 on the acidification path of the environment. Beyond this range and on the alkalinization path (dashed line), the equivalent concentration drops, testimony that surface phenomena, as we shall see in Section 3.3, became important. The same conclusion applies to experiments reported in Figure 3.3 where the chalcocite electrodes were used in KCl solution doped with $CuSO_4$ at various levels of concentration.

Since the electrode impedances are independent of pH, the

electrode reactions should not involve H^+ or OH^-. Thus the only plausible electrochemical reactions involving Cu^{++} and chalcocite are the oxidation of chalcocite which may lead to formation of covellite and/or digenite with departure of copper from the chalcocite crystal lattice. Typical reactions would be

$$\underset{\text{(chalcocite)}}{Cu_2S} = \underset{\text{(covellite)}}{CuS} + Cu^{++} + 2\bar{e} \qquad Eh = 288 + 29.5 \log[Cu^{++}]$$

$$5Cu_2S = \underset{\text{(digenite)}}{Cu_9S_5} + Cu^{++} + 2\bar{e} \quad | Eh?$$

$$5Cu_2S = \underset{\text{(anilite)}}{Cu_7S_5} + 3Cu^{++} + 6\bar{e} \quad | Eh?$$

Each of these reactions is plausible insofar as thermochemical data on digenite and anilite are not sufficiently determined to make quantitative discrimination. It is, however, known that digenite and anilite are low temperature phases ($< 80°C$) of copper sulfides which are transformed into chalcocite and covellite, respectively, at higher tempuratures (Craig and Scott, 1974).

The active behavior of cupric ions at covellite electrodes is demonstrated in Figures 3.4 through 3.6. Here the plausible reaction would be the oxidation of covellite according to the reaction

$$CuS = Cu^{++} + S + 2\bar{e} \quad | Eh = 349 + 29.5 \log[Cu^{++}]$$

Here again, surface phenomena become predimonant at the end of the acidification line (pH below 3, approximately) and on the alkalinization line.

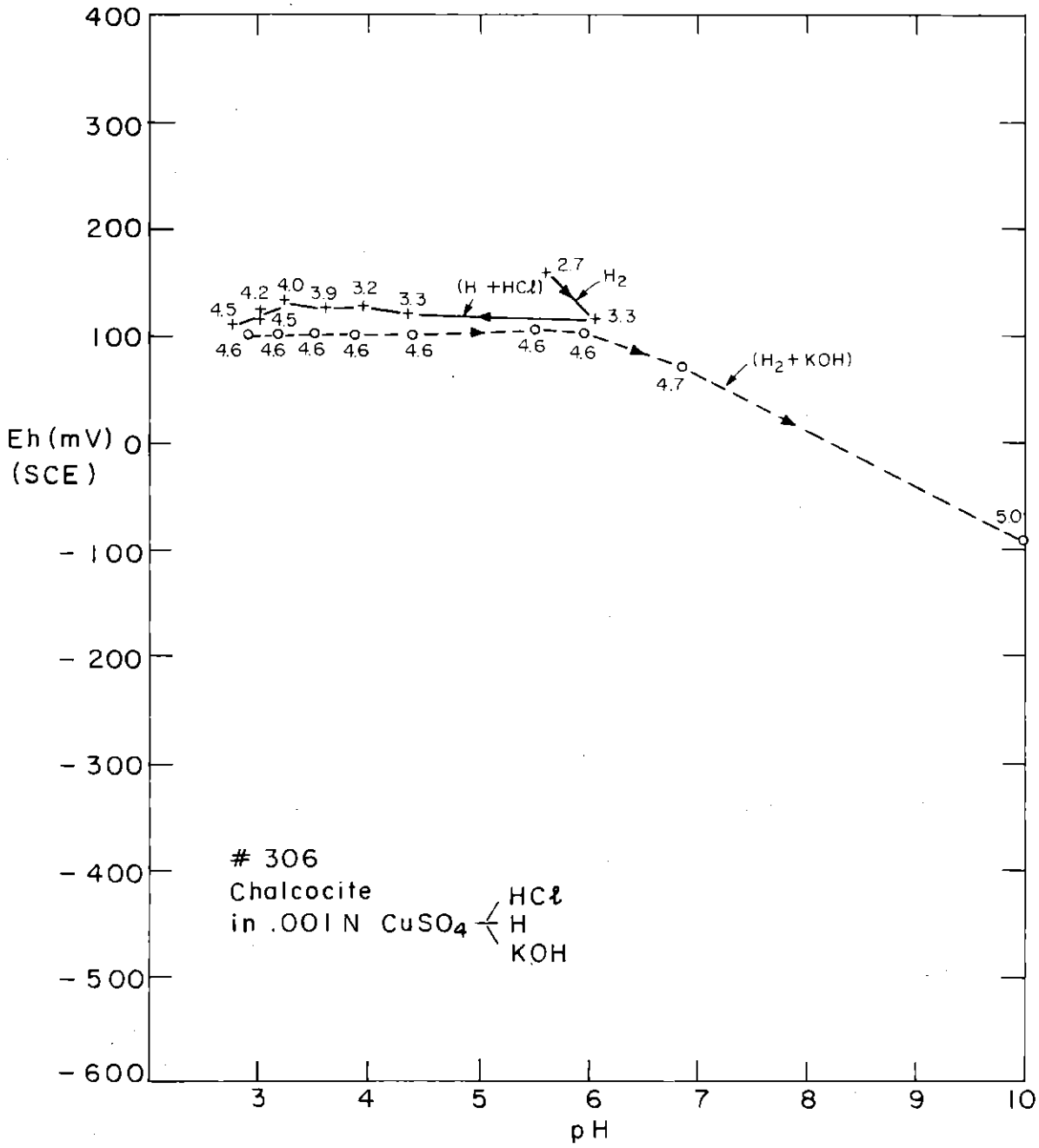


Figure 3.2 Warburg Impedance as a Function of Eh-pH (expressed as -log C, C = apparent concentration)

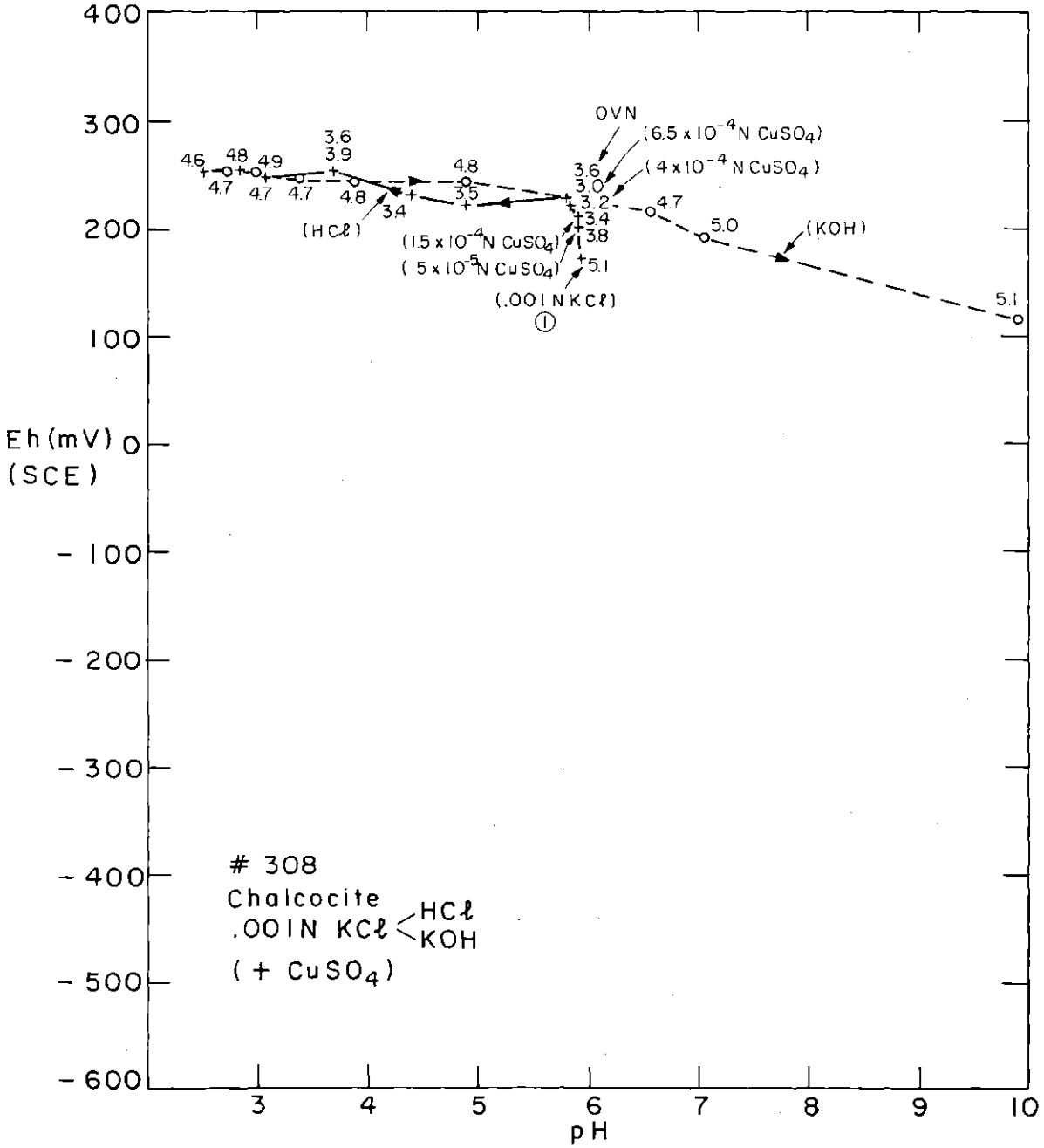


Figure 3.3 Warburg Impedance as a Function of Eh-pH (expressed as -log C, C = apparent concentration)

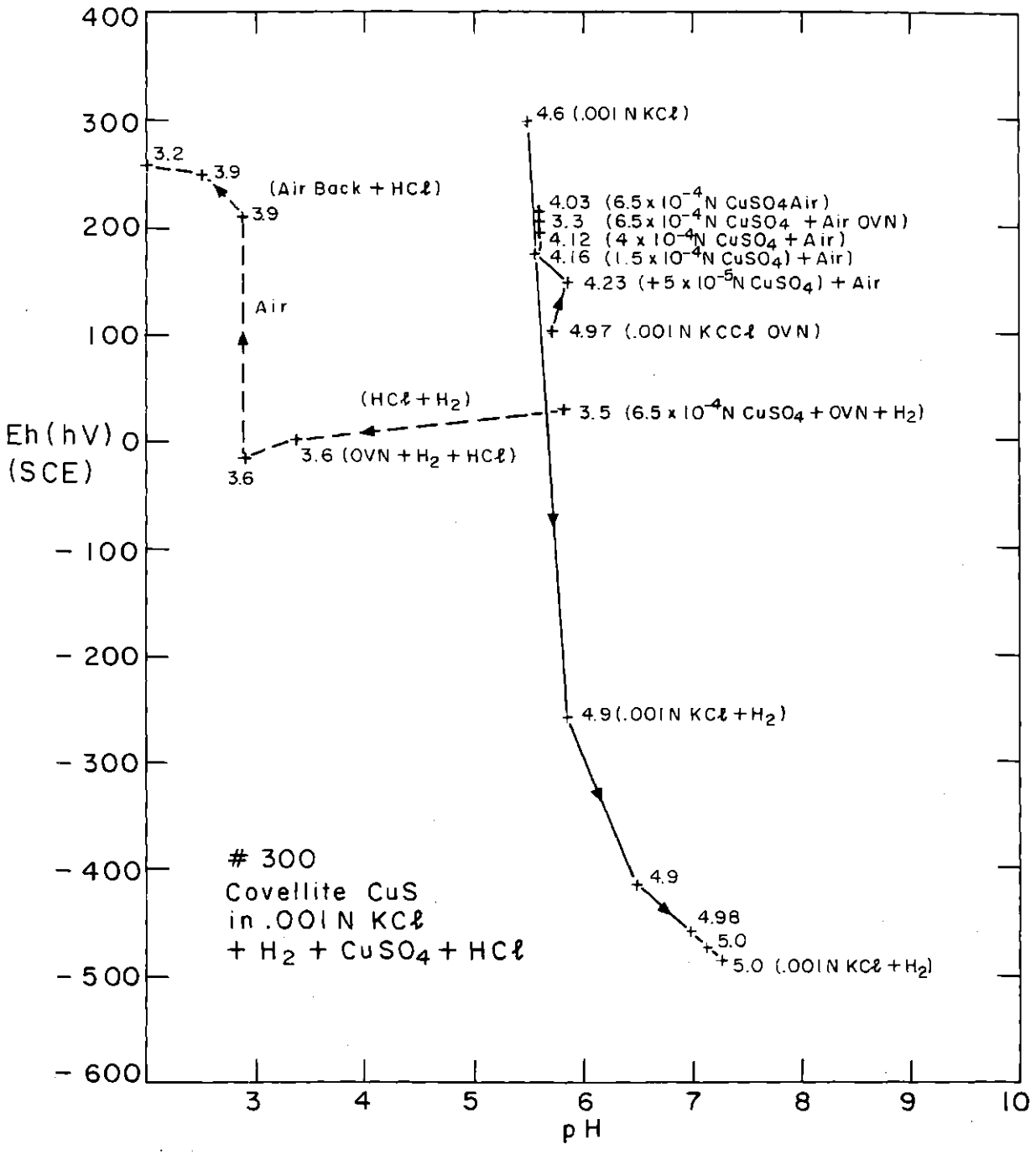


Figure 3.4 Warburg Impedance as a Function of Eh-pH (expressed as -log C, C = apparent concentration).

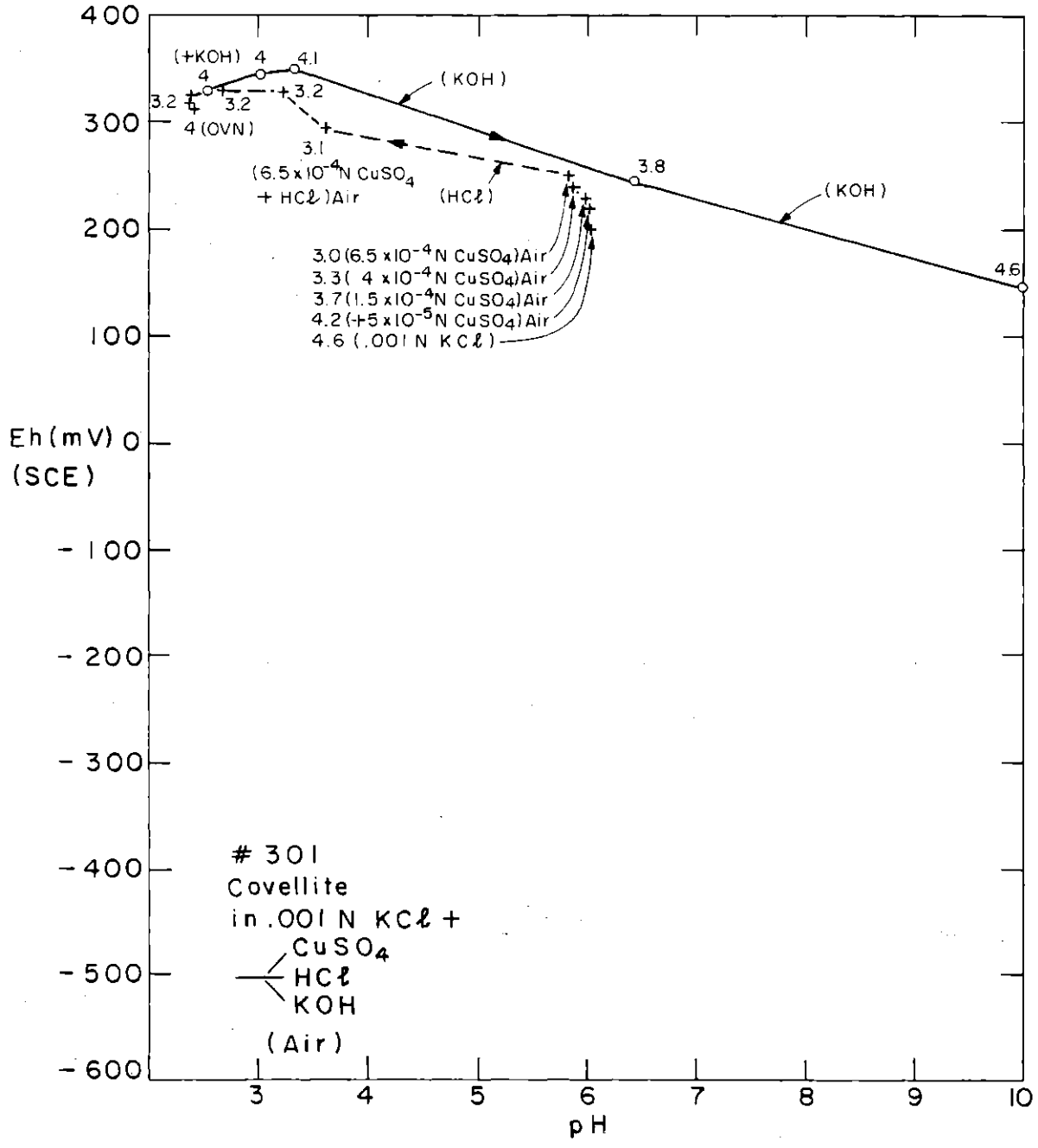


Figure 3.5 Warburg Impedance as a Function of Eh-pH (expressed as -log C, C = apparent concentration)

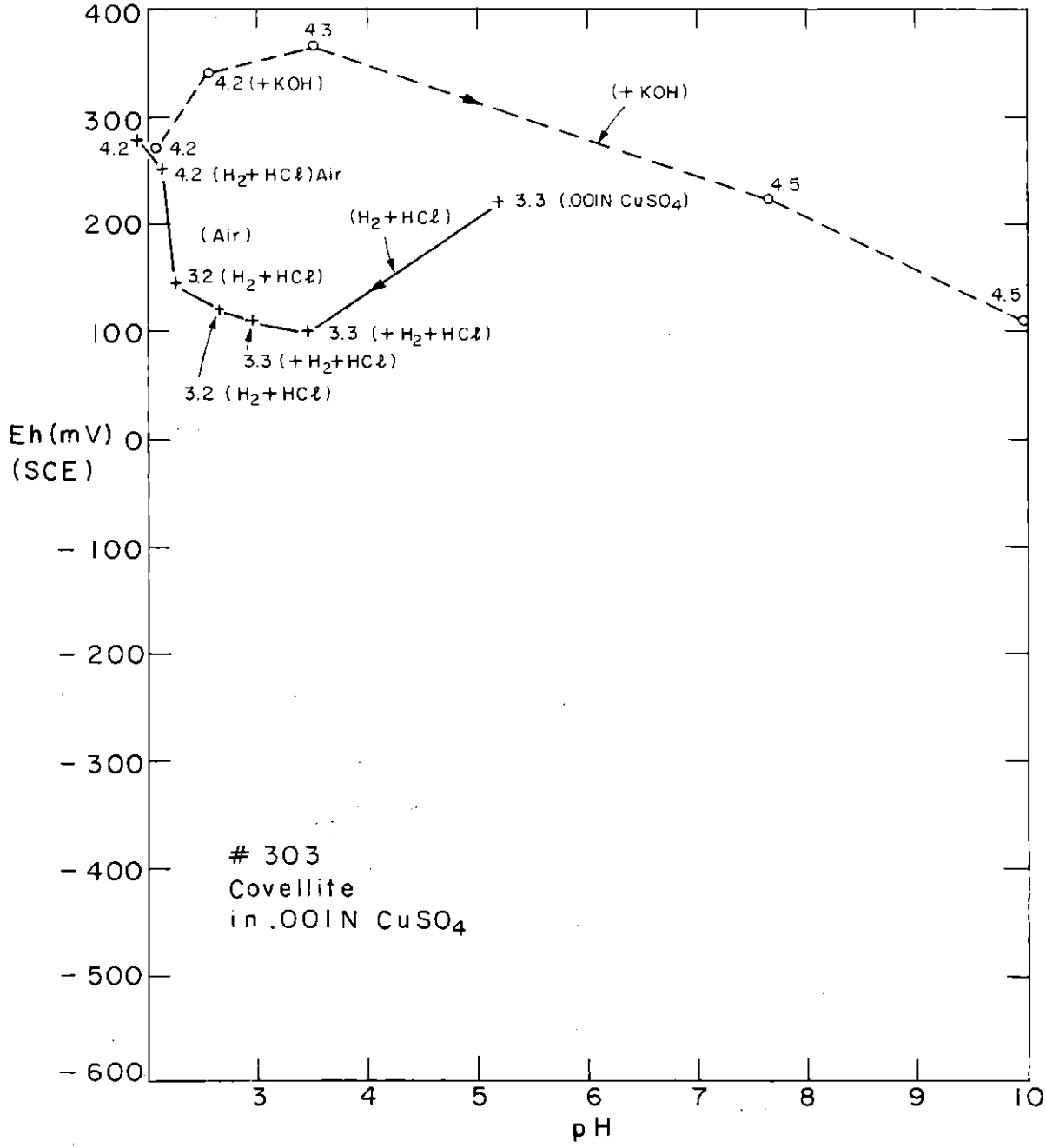


Figure 3.6 Warburg Impedance as a Function of Eh-pH (expressed as -log C, C = apparent concentration)

3.2.2 Active Behavior of Sulfide Ions and Associated Reactions

Measurement of electrode impedance spectra of chalcocite in sodium sulfide solutions shows that the impedance level depends on the concentration of sulfide ions. In Figure 3.7, a 10^{-2}N solution of Na_2S with pH and Eh, respectively 11.5 and -550 mv, got progressively acidified (HCl) to pH of about 2.5, and thereafter alkalinized. The acidification path shows a level of equivalent concentration close to the concentration of sulfide ions. The alkalinization path departs slightly from the concentration, presumably due to the instability of sulfide ions in acid solutions giving a cloud of H_2S. Similarly, Figure 3.8 shows spectral measurement in more dilute sodium sulfides. The impedance level is higher with the equivalent concentration again matching approximately the sulfide ions' concentration. However, on the basis of the Eh-pH diagram for sulfur (Pourbaix, 1966), at the conditions of the experiments, sulfide ions should not be stable but rather form HS^-. We suspect that the formation of HS^- is a relatively slow reaction so that we still have sulfide ions present for the electrode reactions. The progressive increase of the electrode impedance, as witnessed by the gradual decrease in concentration brings some support to this conclusion.

A plausible electrochemical reaction involving the sulfide ions would be the oxidation of chalcocite to covellite

$$Cu_2S + S^{=} = 2CuS + 2\bar{e} \quad | \quad Eh = -779 - 29.51 \log[S^{=}]$$

This active behavior of sulfide ions is to be sharply

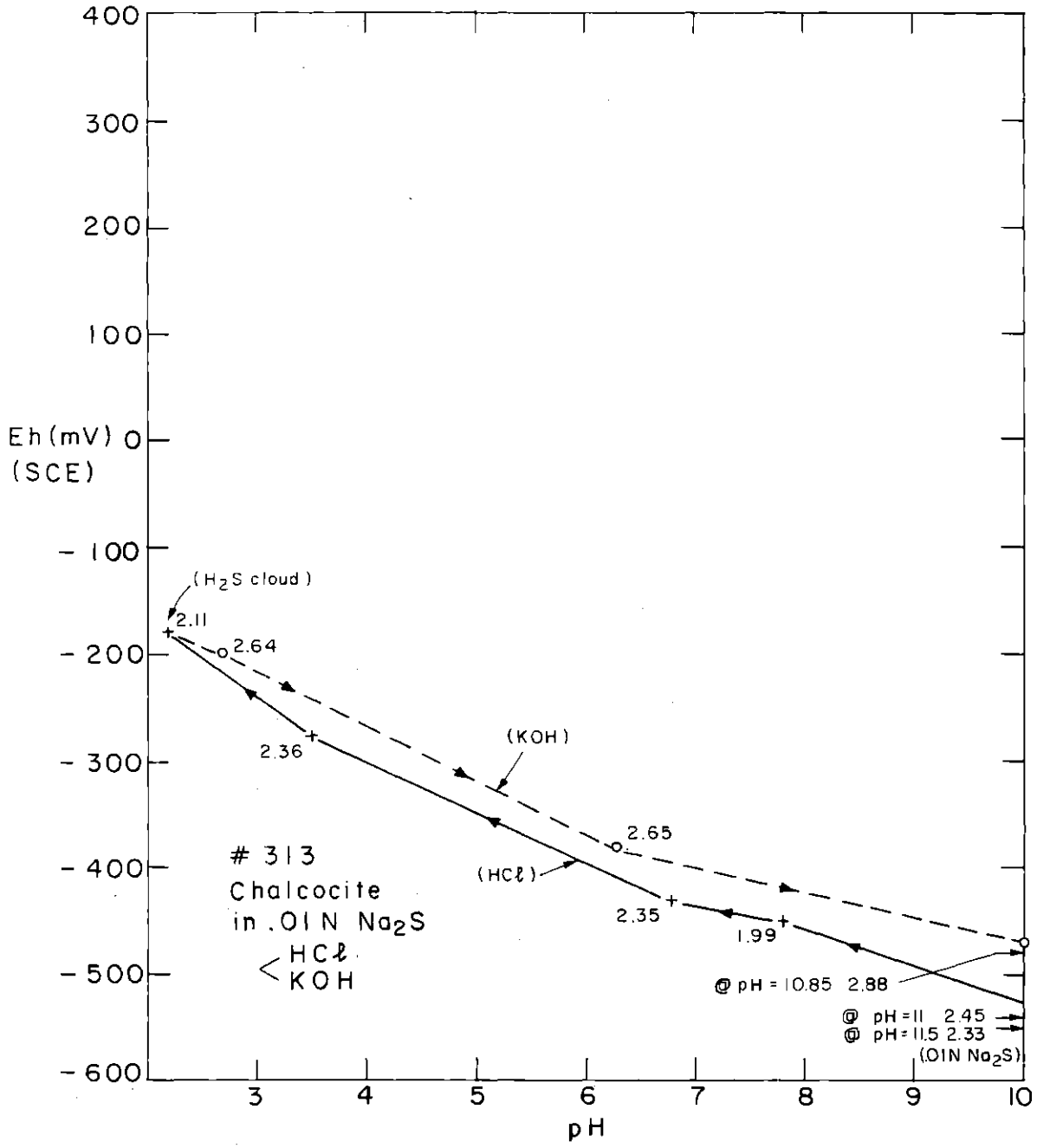


Figure 3.7 Warburg Impedance as a Function of Eh-pH (expressed as -log C, C = apparent concentration)

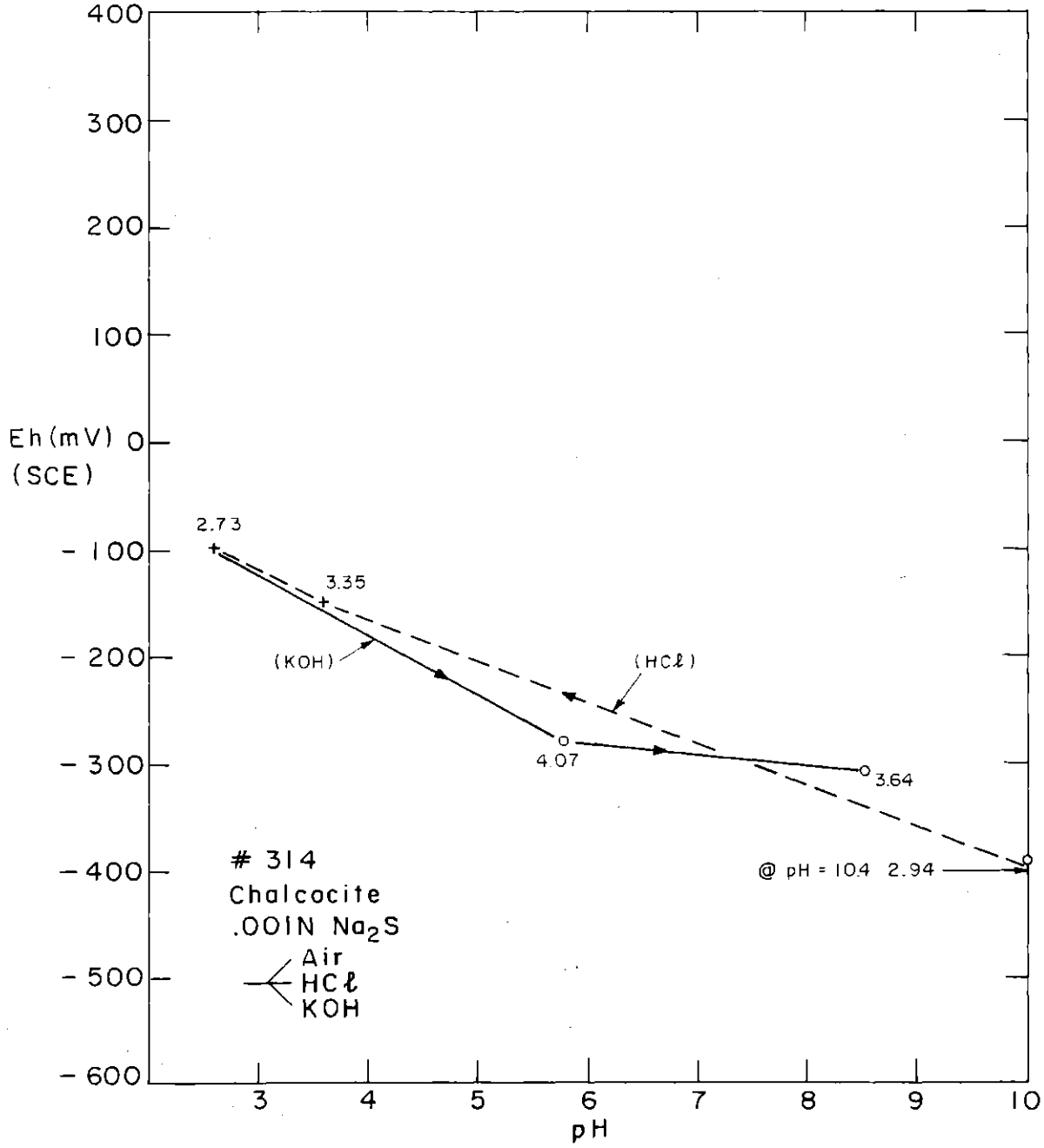


Figure 3.8 Warburg Impedance as a Function of Eh-pH (expressed as -log C, C = apparent concentration)

contrasted to sulfate ions which appear remarkably inert as we shall see later.

3.2.3. The Exceptional Case of Active Behavior of H^+ Ions

Figure 3.9 depicts the single case in all our measurements where H^+ appeared to be active, i.e. the electrode impedance was presumably controlled by H^+ ions. This singular case occurred with a 1μ diamond polished copper electrode. The solution was 10^{-3} N KCl and the environment was progressively reduced with a pH varying from about 6 to 7. In no other situation were the impedances high enough to expose the effect of such a dilute ionic concentration. This case is testimony to the important role of the surface condition as we shall see in Chapter IV.

3.3 Ionic Diffusion from Electrodes: The Wagner Analogy

In the absence of the active species described in the previous section, a different mechanism must operate for the electrochemical step determining the electrode impedance. This conclusion is essentially based on experimental evidence. Indeed, we display in Figures 3.10 through 3.19 a series of experiments where copper electrodes, as well as chalcocite, covellite, and pyrrhotite electrodes have been studied in solutions of potassium chloride, sodium sulfate, sodium carbonate, calcium nitrate.

The striking feature of all the results shown is the remarkable uniformity of the equivalent concentration for a given series of experiments in various environments. The corresponding uniformity of Warburg impedances of various electrode impedance spectra corroborates the results obtained by Madden (Madden,

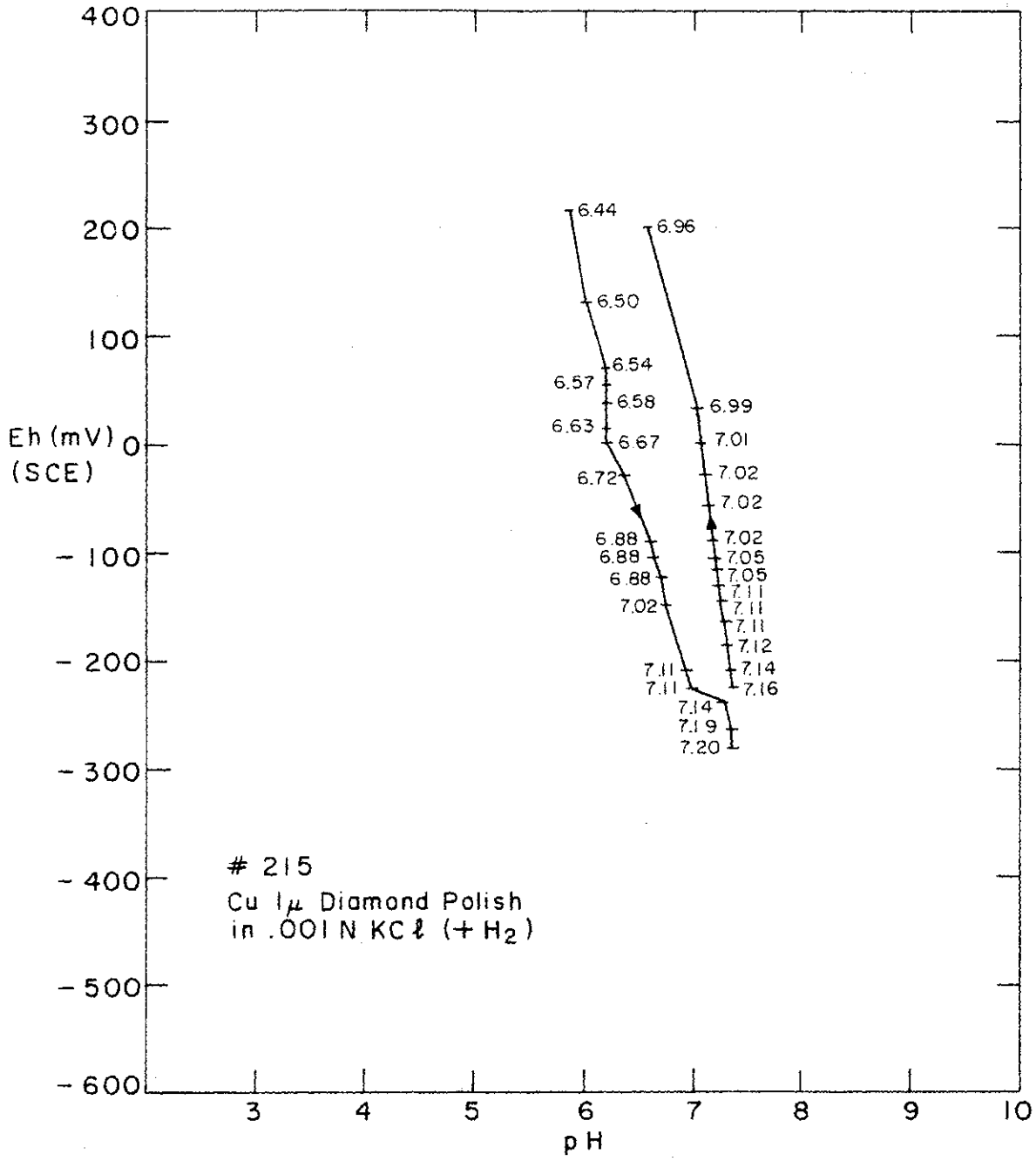


Figure 3.9 Warburg Impedance as a Function of Eh-pH (expressed as -log C, C = apparent concentration)

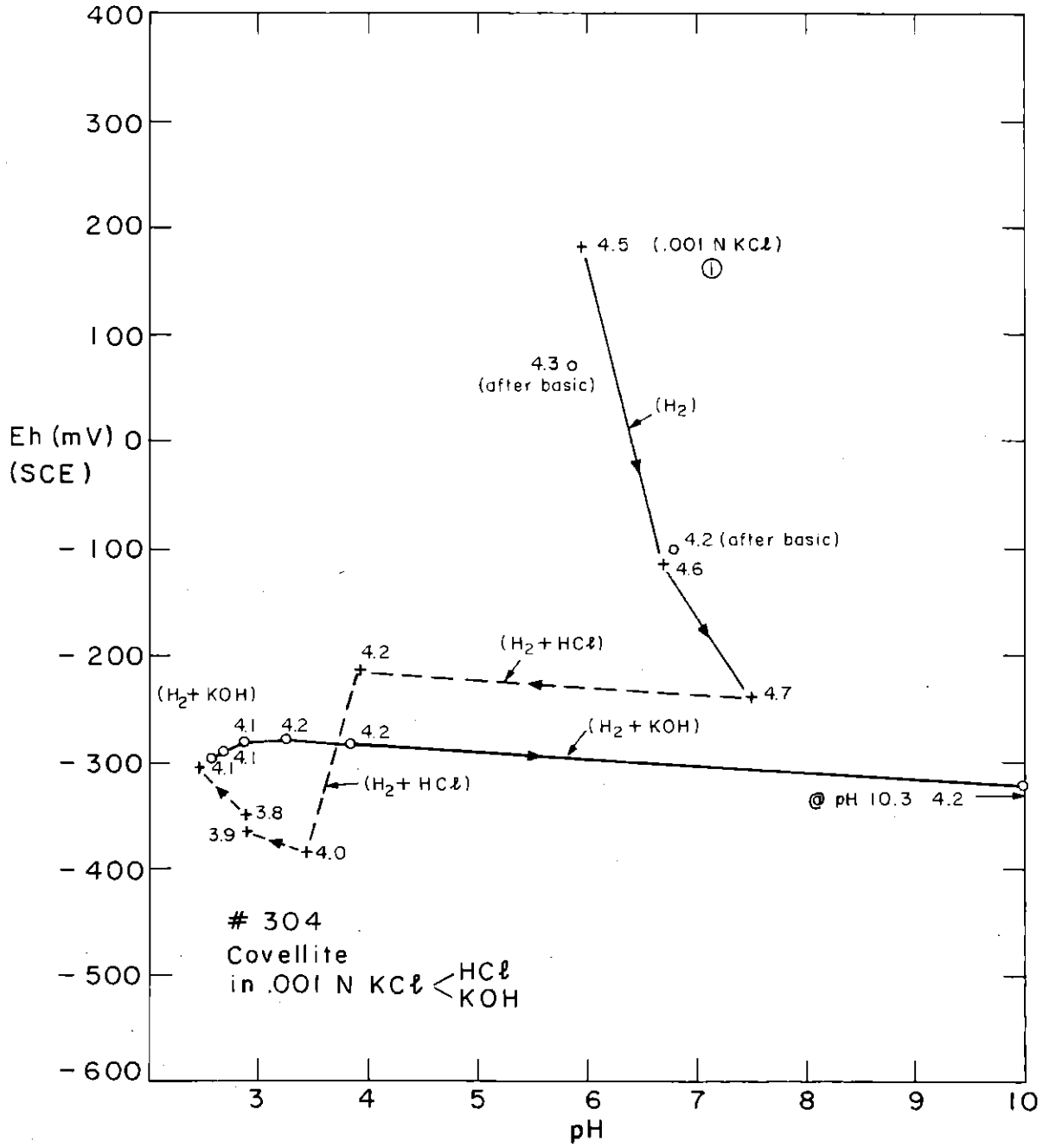


Figure 3.10 Warburg Impedance as a Function of Eh-pH (expressed as -log C, C = apparent concentration)

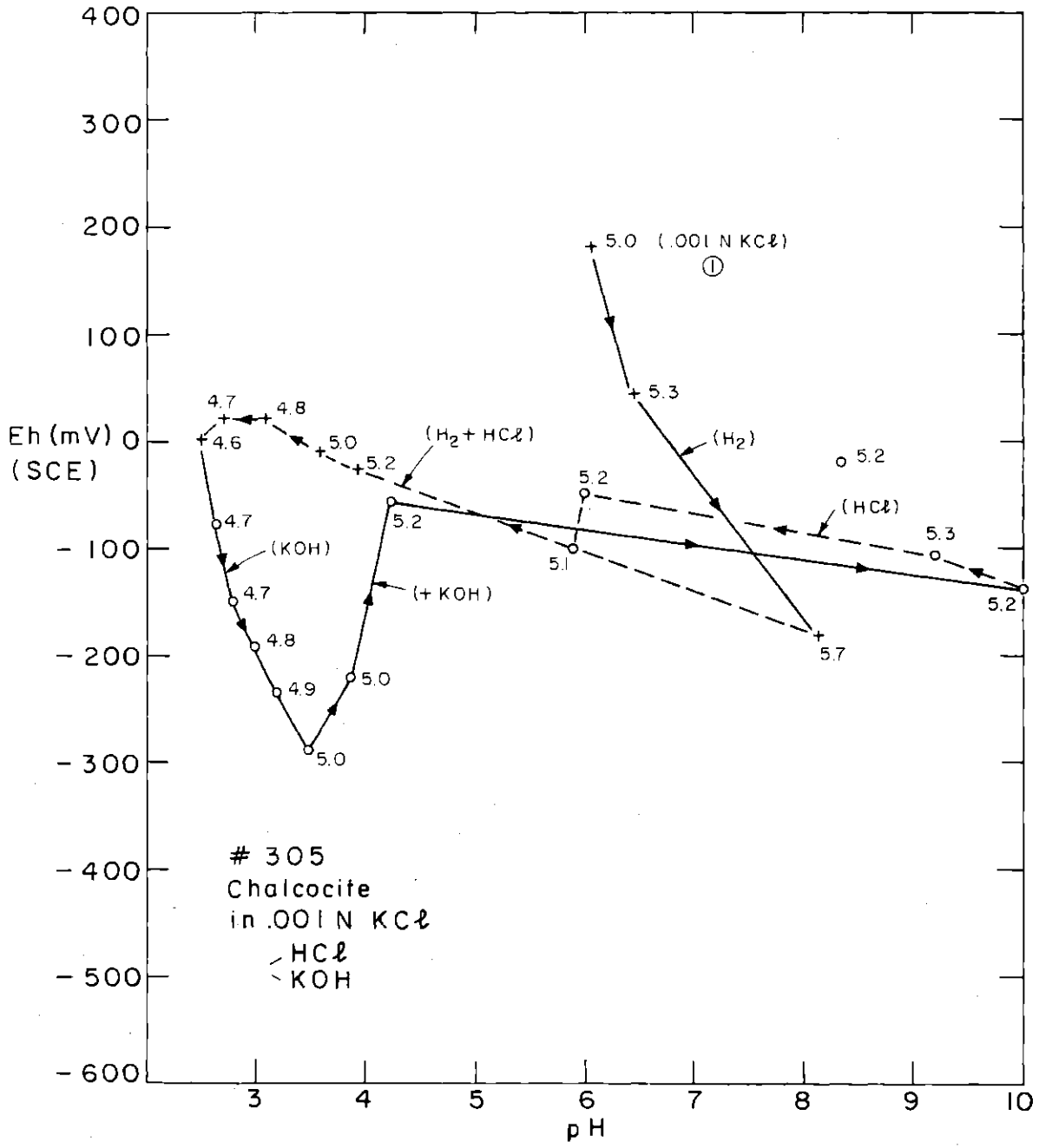


Figure 3.11 Warburg Impedance as a Function of Eh-pH (expressed as -log C, C = apparent concentration)

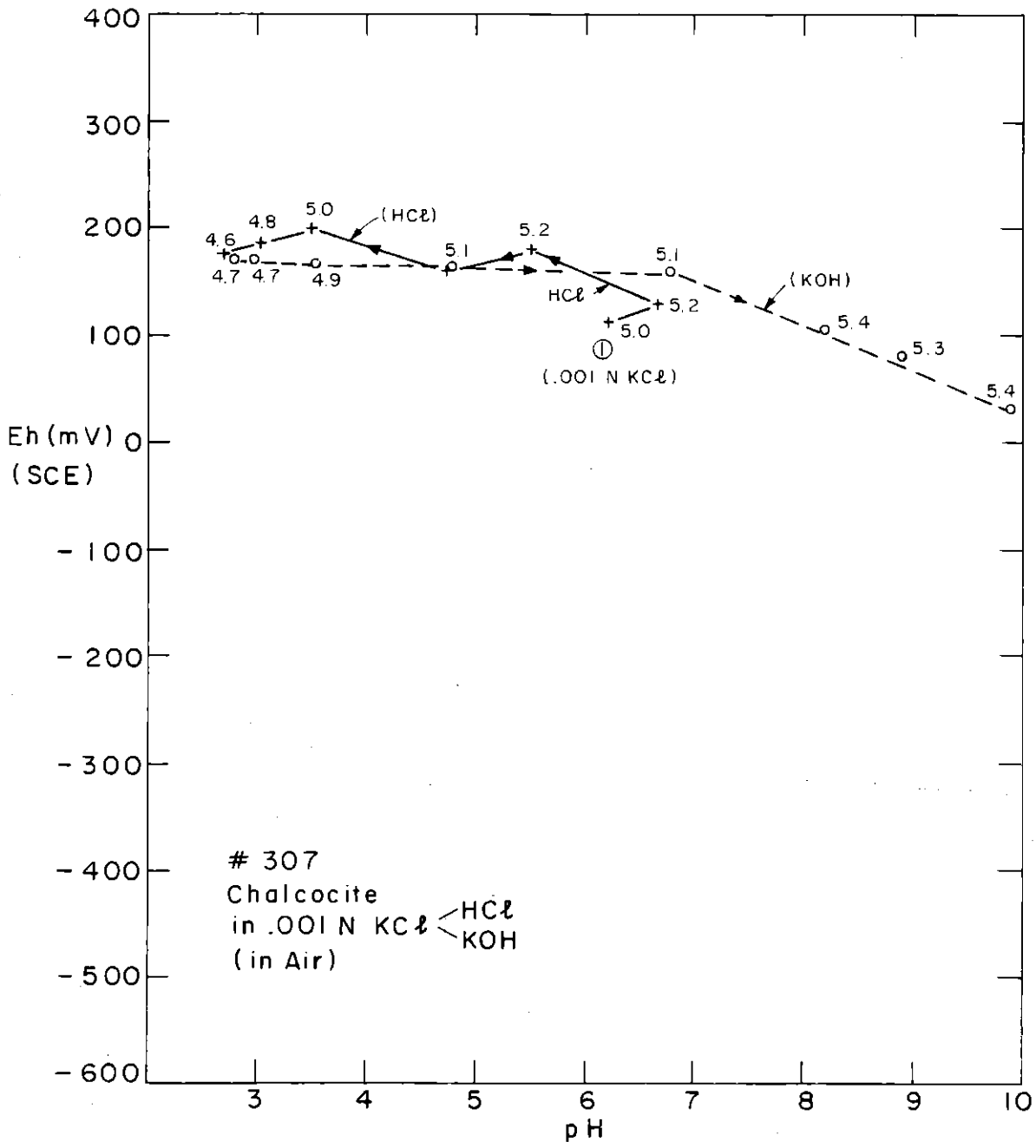


Figure 3.12 Warburg Impedance as a Function of Eh-pH (expressed as -log C, C = apparent concentration)

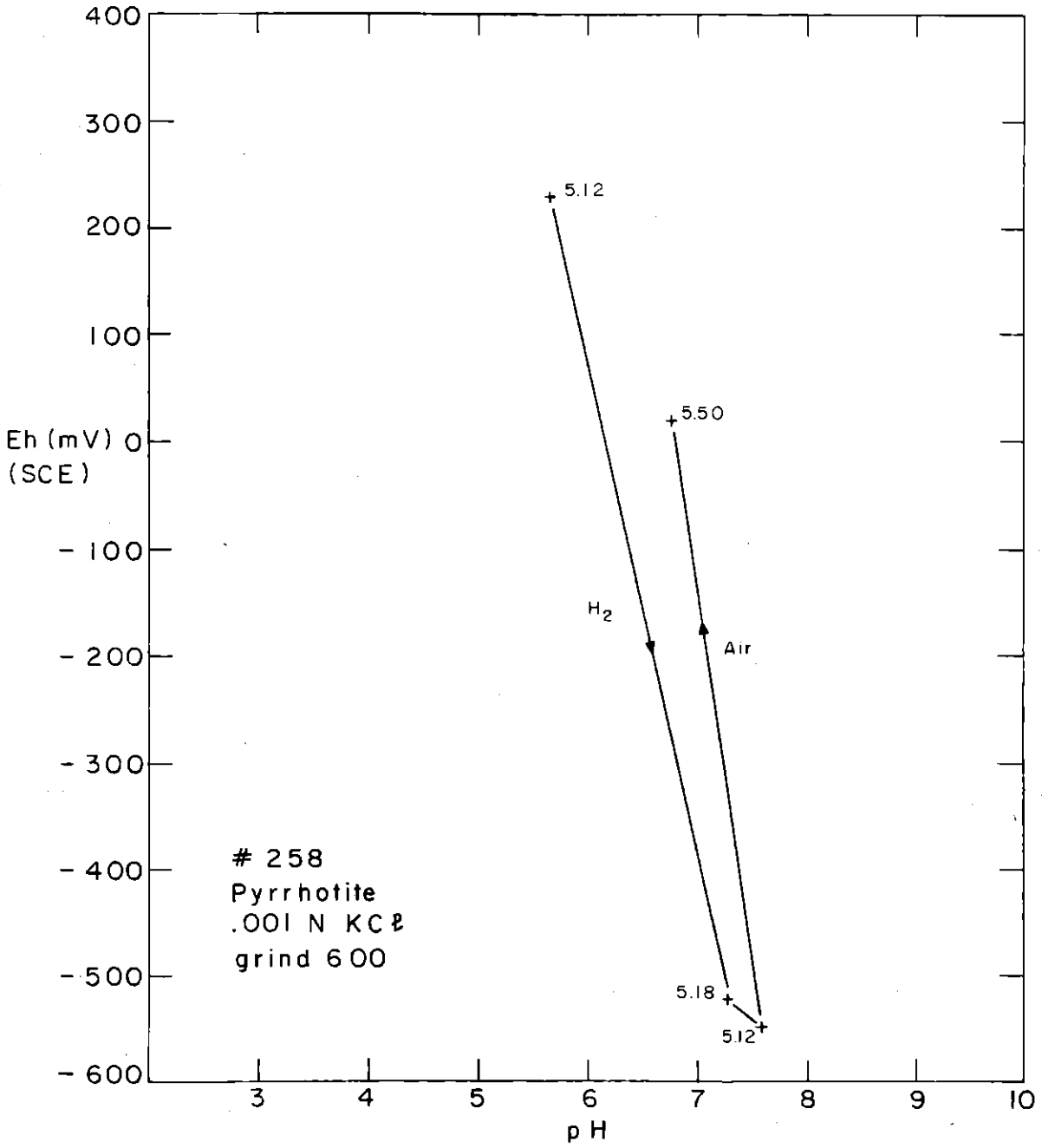


Figure 3.13 Warburg Impedance as a Function of Eh-pH (expressed as -log C, C = apparent concentration)

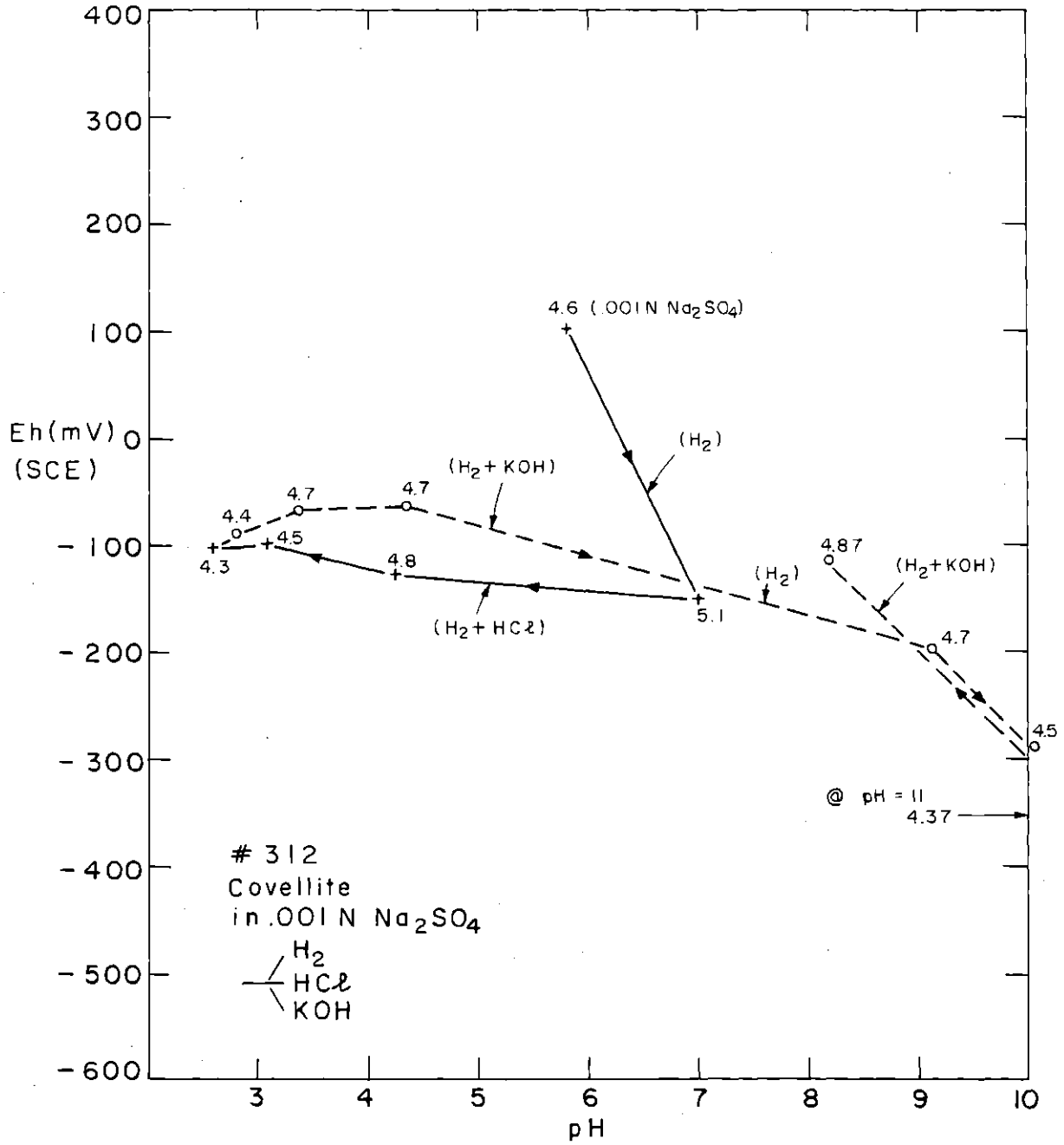


Figure 3.14 Warburg Impedance as a Function of Eh-pH (expressed as -log C, C = apparent concentration)

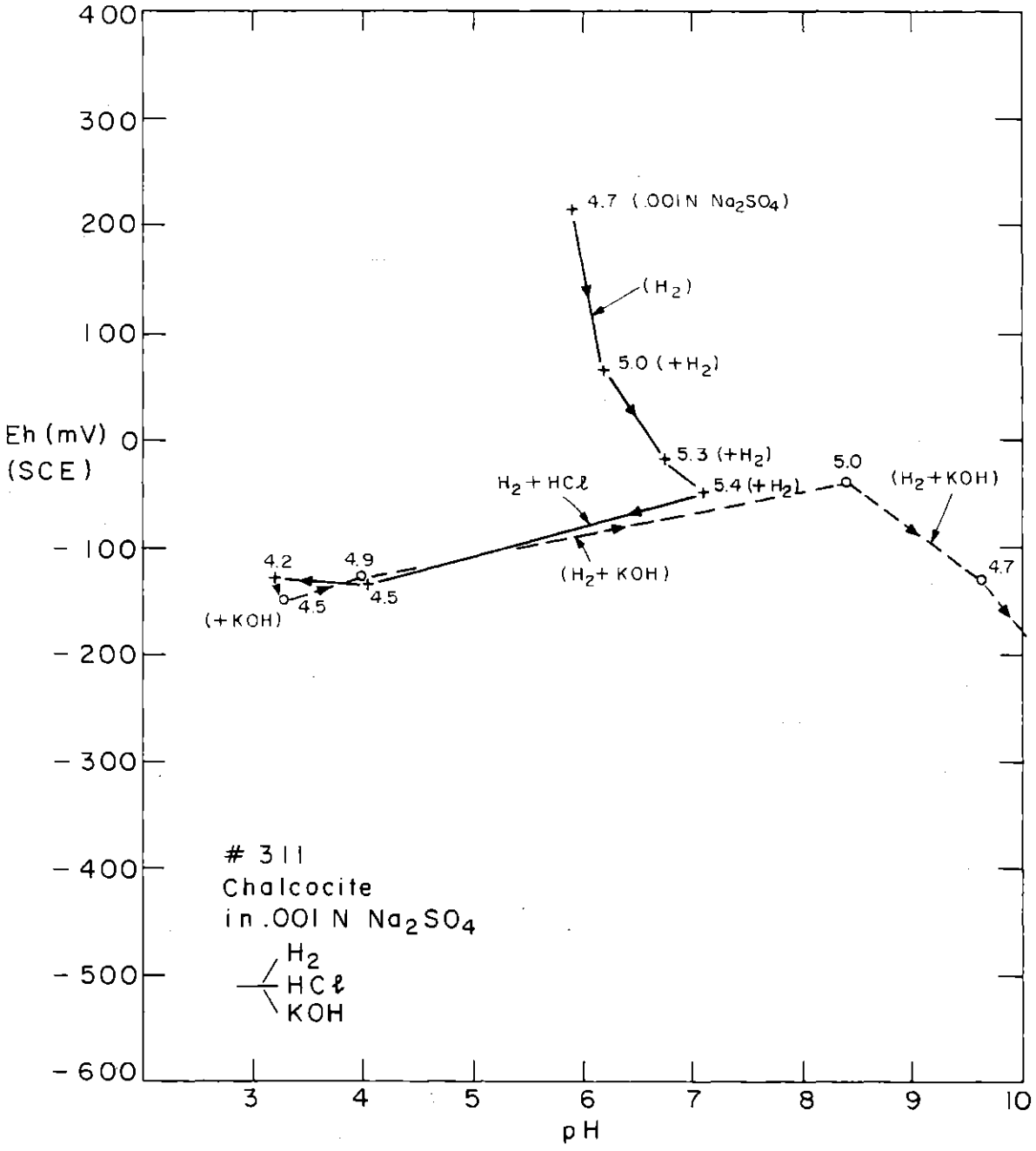


Figure 3.15 Warburg Impedance as a Function of Eh-pH (expressed as -log C, C = apparent concentration)

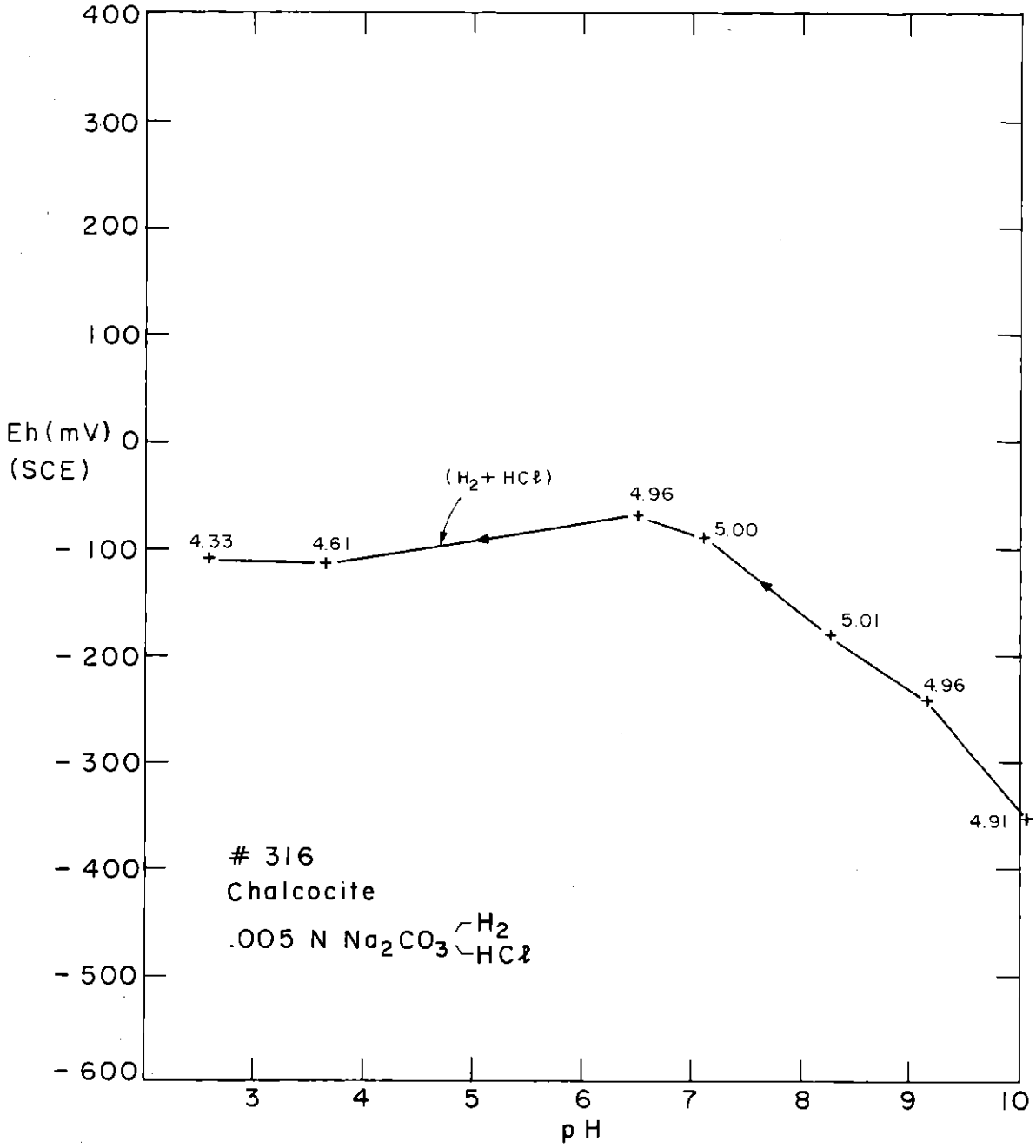


Figure 3.16 Warburg Impedance as a Function of Eh-pH (expressed as -log C, C = apparent concentration)

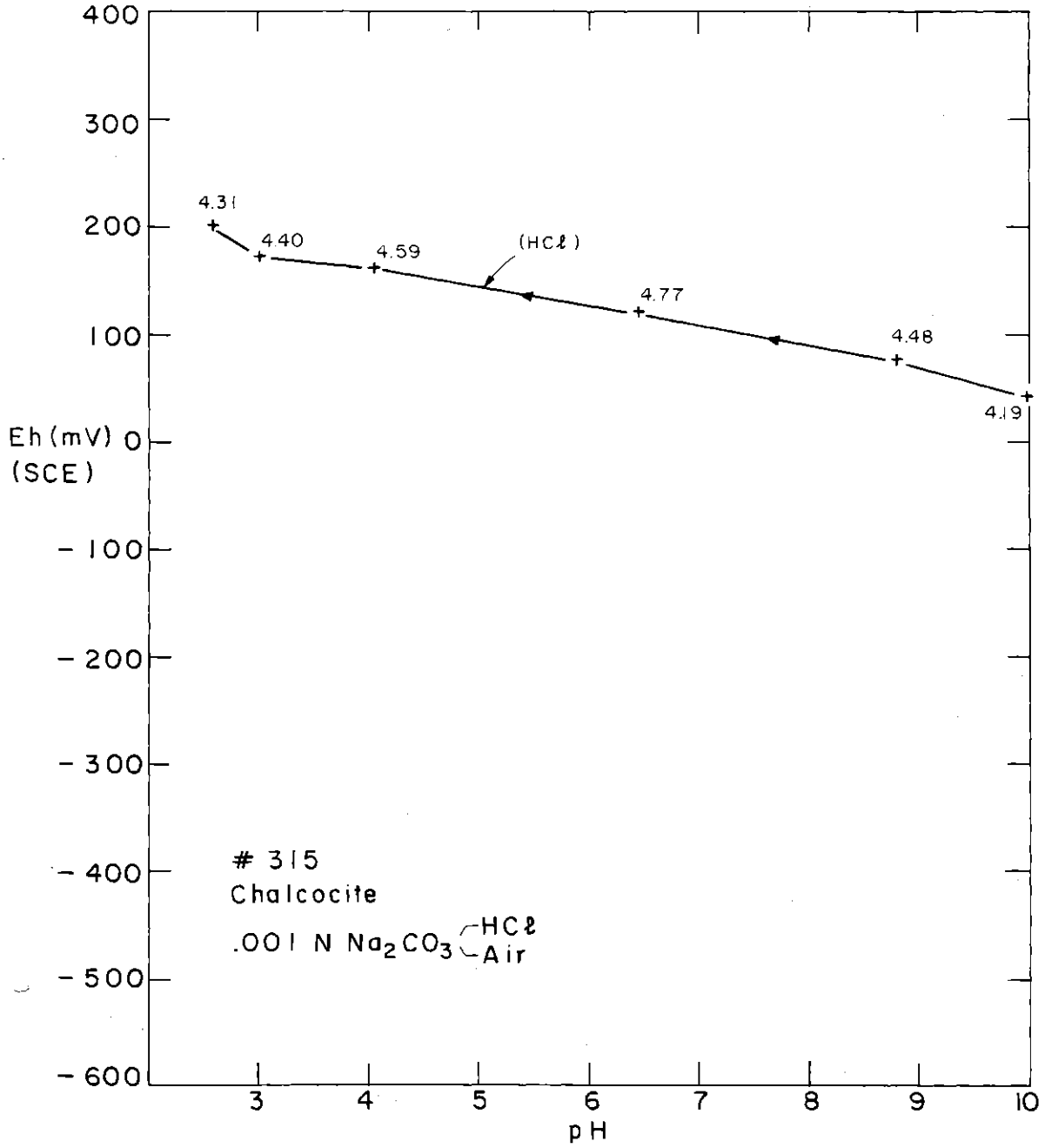


Figure 3.17 Warburg Impedance as a Function of Eh-pH (expressed as -log C, C = apparent concentration)

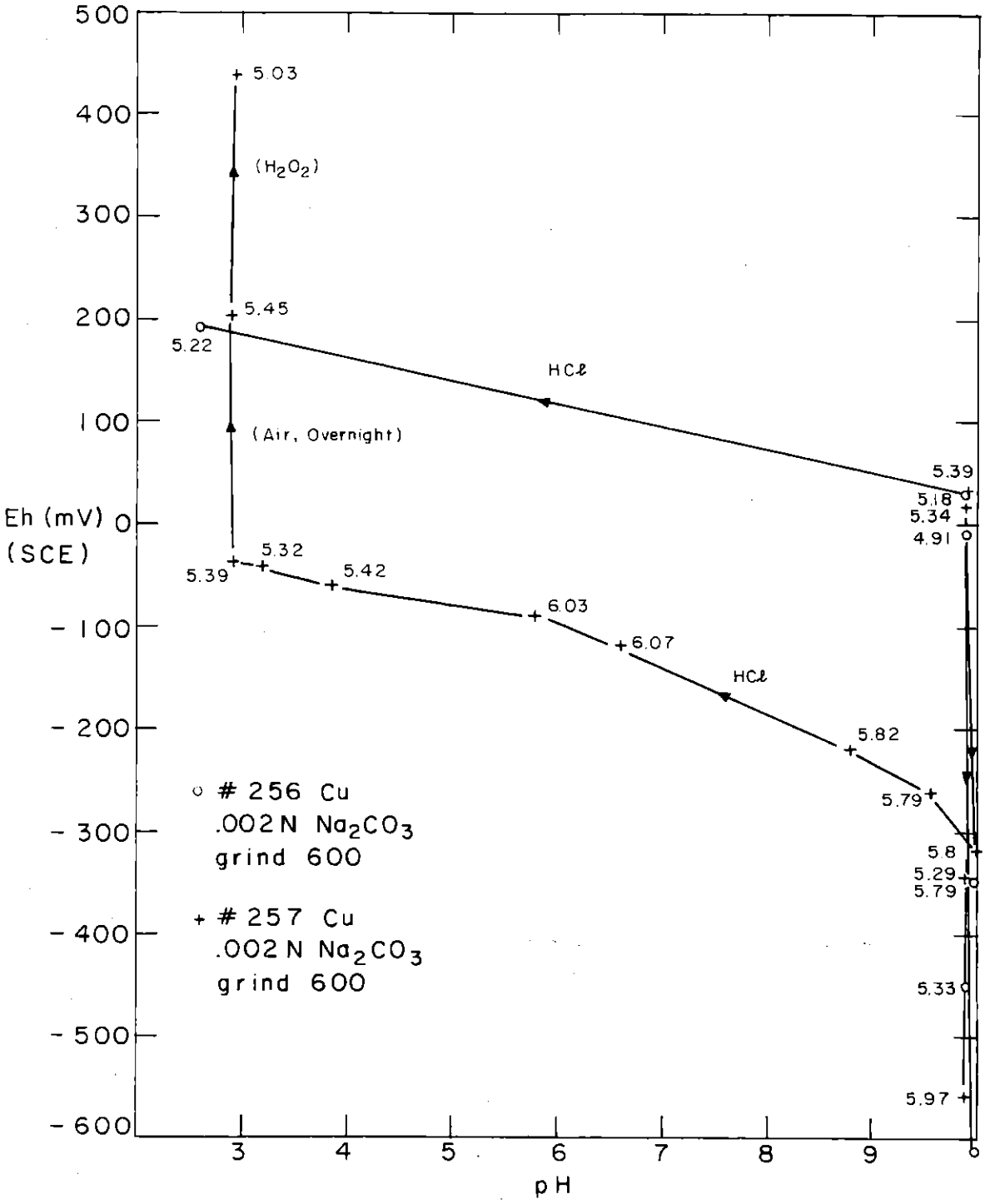


Figure 3.18 Warburg Impedance as a Function of Eh-pH (expressed as -log C, C = apparent concentration)

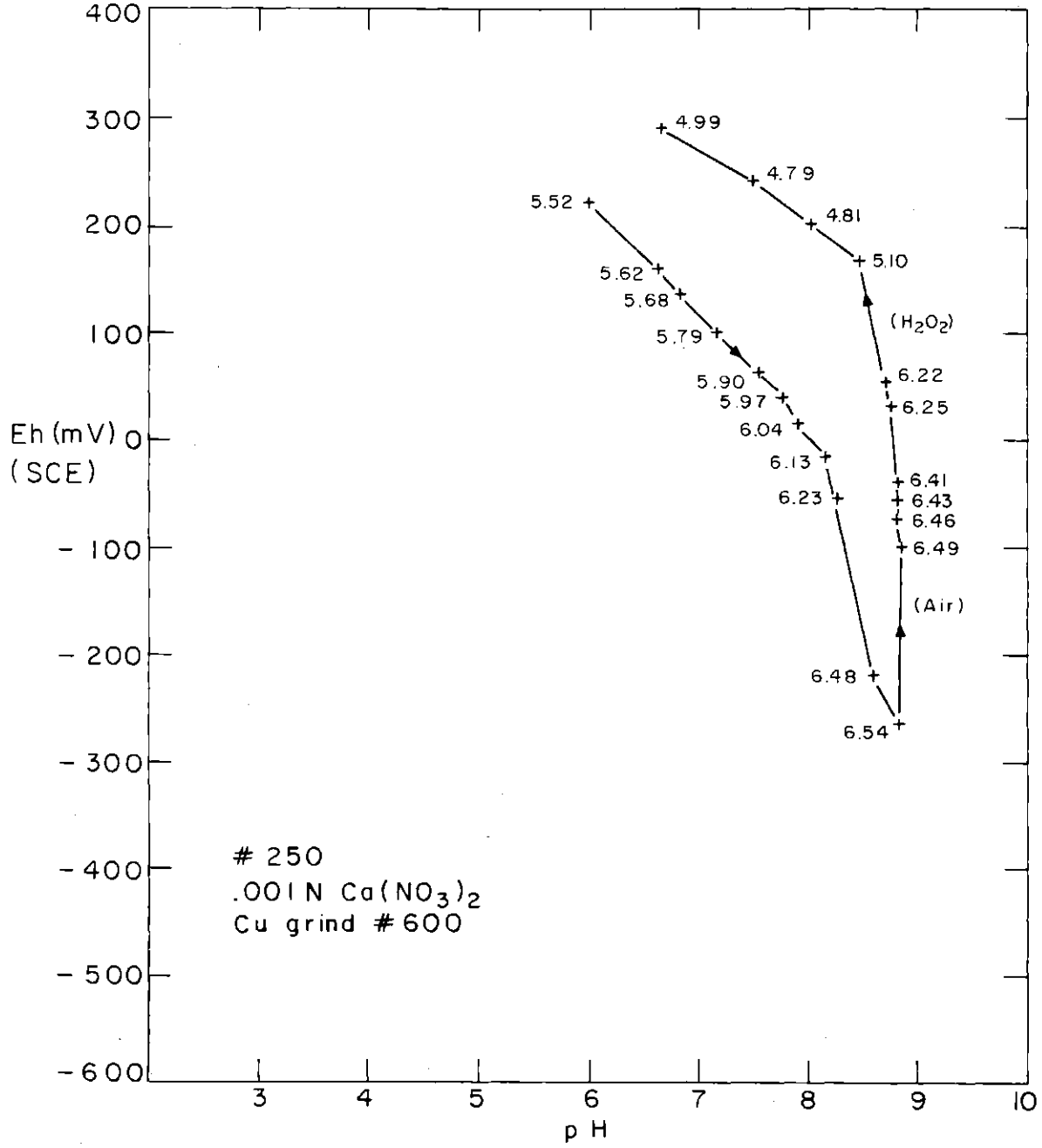


Figure 3.19 Warburg Impedance as a Function of Eh-pH (expressed as -log C, C = apparent concentration)

1961). It follows that in the absence of active ionic species, the electrode impedance is remarkably independent of the chemistry of the solution. The only remaining factors susceptible to control the impedance are processes inherent in the electrode itself and the condition of the electrode surface in conjunction with some process that allows a common ionic species to carry the Faradaic current into the electrode from the solution.

3.3.1 The Warburg Series

We showed in Section 1.2 that if several ionic species take part in the impedance determining electrochemical reaction, the electrode impedance is dominated by a Warburg component which is a series of Warburg impedances associated to each ionic species. We call this impedance due to diffusion of species from the solution "solution Warburg".

Where surface phenomena become important, any resulting impedance must be in series with this solution Warburg. Thus if the impedance due to the electrode surface looks like a Warburg impedance, it is still possible to represent the electrode impedance with one Warburg which is in reality a sum of surface and solution Warburg. We shall later propose ways to separate those Warburgs. For the moment, we want to formulate a plausible hypothesis which could explain the insensitivity of the electrode impedance to the solution chemistry in absence of active species providing thereby a new basis for the interpretation of the electrode impedance in such environments.

3.3.2 The Wagner Analogy of Ionic Diffusion in Electrodes

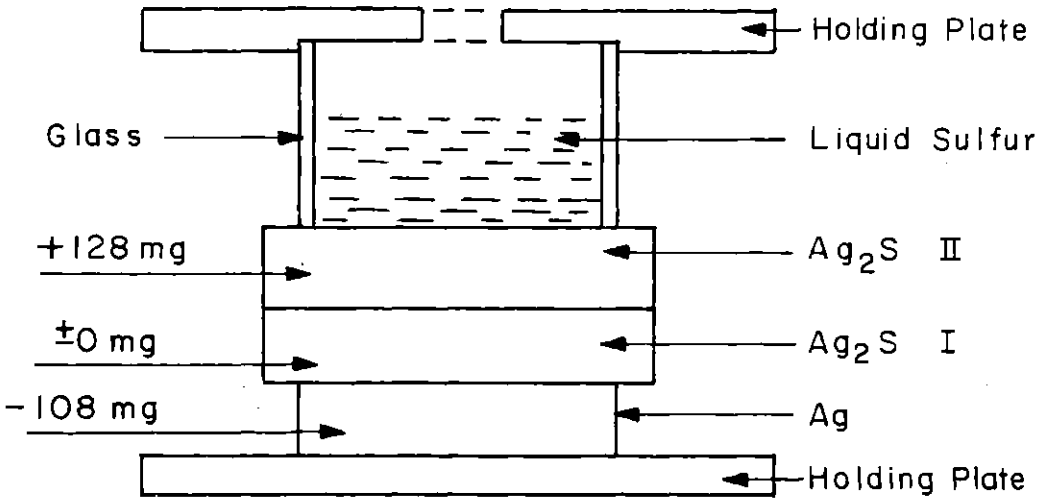
In a series of three fundamental articles entitled "Beitrag Zur Theorie des Anlaufvorgangs"* written between 1933 and 1938, Carl Wagner set forth a theory of the mechanism of oxidation (Wagner, 1933), (Wagner, 1936), Wagner and Grunewald, 1938), demonstrating the preeminence of the diffusion of metallic ions to the reaction sites. The basis of Wagner's argument hinges on an experiment devised to understand the mechanism of formation of silver sulfide. The experimental set-up is shown in Figure 3.20. It is observed after heating the system at 220°C for 1 hour that the silver sulfide Tablet I does not change its weight, whereas the silver sulfide Tabler II increases its weight commensurately with the decrease in weight of the silver cylinder. The implication of this result is that silver has to diffuse through the sulfide tablets to the reaction zone either inside the Ag_2S II or at the boundary between the liquid sulfur and the sulfide tablet. In fact, Wagner's theory postulates

1. Diffusion of cations outwards (toward O, S, or halogen);
2. Diffusion of anions inwards (toward the metal); and
3. Diffusion of electrons outwards,

processes which depend prominently on the electrical conduc-

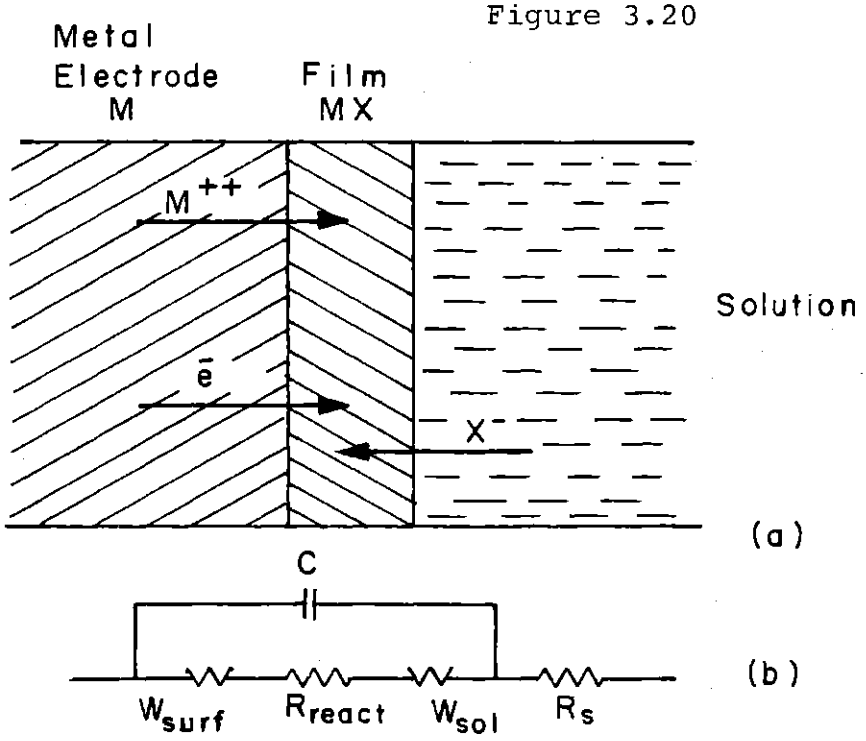
---

*Introduction to the Theory of Tarnishing



Wagner's experiment exhibiting the diffusion of silver towards the reaction sites for formation of silver sulfide

Figure 3.20



Equivalent circuit of the electrochemical analog of Wagner's oxidation mechanism

Figure 3.21

tivity of the film formed and the transference number of each species.

An electrochemical analogy can be set up to describe electrode processes where surface diffusion processes cannot be ignored. If the surface diffusion consists essentially in transporting metallic ions towards reaction sites between the metal and the solution, Figure 3.21(a) describes the various elements involved as well as the geometry of the system. It is convenient to describe the system in terms of electrical equivalent circuits.

The motion of anions X^- contributes to a diffusion impedance which can be represented by a Warburg impedance W_{sol}, while the motion of metallic ions contributes to a Warburg impedance term W_{surf}. As outlined in Section 3.3.1, these two Warburgs act in series with a resistance representing the reaction step. To these elements must be added the double layer capacitance and the solution resistance. Figure 3.21(b) shows the final equivalent circuit. It is seen that if the solution Warburg is small compared to the surface Warburg, the electrode impedance will be controlled by the electrode surface, and will be relatively independent of the chemistry of the solution. This appears to be the case in the series of experiments displayed in Figure 3.10 through Figure 3.19 in absence of active species.

The series of experiments represented in Figure 3.10 deal with a covellite electrode initially in potassium chloride

10^{-3}N. The initial impedance spectrum gave an equivalent concentration of $10^{-4.5}$. Thereafter, the environment was reduced to an Eh of the order of -300 mv while the pH was scanned towards acidic and alkaline regions. The Warburg impedance is of the order of 600 $\Omega \cdot cm^2$ at 1 cps and is relatively independent of the environment. Similar experiments conducted with chalcocite electrodes (Figure 3.11) show a much higher level of Warburg impedance of the order of 6000 $\Omega \cdot cm^2$ at 1 cps and remarkably independent of the environment. The same level of impedance is exhibited by chalcocite in a non-reduced solution of KCl in the whole pH range (Figure 3.12). Similarly, pyrrhotite electrodes in KCl show the same level of Warburg impedance even under reduced conditions (Figure 3.13).

Covellite and chalcocite electrodes in sodium sulfate solution show also a level of impedance independent of the environment, demonstrating thereby the inactive behavior of sulfate ions (Figures 3.14 and 3.15). Similarly, the inactive behavior of carbonate ions and the insensitivity of copper and chalcocite electrodes to the chemistry of carbonate environments is shown in Figures 3.16 through 3.18. Copper electrodes in calcium nitrate show an equally high level of Warburg impedance, testimony of not only the inactive behavior of nitrates and calcium ions, but of the predominance of surface diffusion phenomena associated with the copper electrode in such environments.

In summary, the classification of ionic species into

"active" and "inactive" ones can be complicated by the state of the electrode surface. In the presence of the active species Cu^{++} or $S^{=}$, the electrode impedance can be predicted on the basis of the concentration of these active species which is related to the Warburg impedance as presented in Table 3.1. Outside such cases, surface phenomena relatively independent of the solution chemistry must be the controlling factors on the electrode impedance. This hypothesis has been strengthened further by a series of experiments where, by affecting the state of the electrode surface, a dramatic change of the electrode impedance follows. These experiments and their implications are the subject of the next chapter. In all these cases, in order that the solution Warburg not affect the electrode impedance, we require that only ions of high concentration be involved in the reactions.

CHAPTER IV

Depolarization Experiments

In the previous chapters, we attempted to induce significant changes of the electrode impedance by systematic modification of the chemistry of the solution. This attempt was often unsuccessful, and we put forth the hypothesis that in the absence of active species, the electrode impedance must be controlled by phenomena occurring along the electrode surface. We therefore conducted a series of experiments under various surface conditions in order to appraise empirically the extent of the influence of the state of the surface.

4.1 Critical Role of the Surface Condition

An initial hint of the influence of the state of the electrode surface came from experiments on diamond-polished copper electrodes in potassium chloride. As mentioned in Section 3.2.3, such condition gave one instance where the electrode impedance appeared to be controlled by H^+ in the pH range from about 5.8 to 7.2. In any case, however, the impedance of diamond-polished copper electrode in KCl was of the order of 600,000 $\Omega \cdot cm^2$ which is about the highest level of impedance obtained during the course of this whole study.

The results of two experiments with copper electrodes treated with polishing paper of grain-size #600 are compared to a case of diamond-polished copper in similar environments in Figure 4.1. It appears that the diamond-polished electrode

impedances are more than one order of magnitude larger than the electrodes treated with polishing paper. Similarly, chalcocite and covellite electrodes, when diamond-polished, show a higher level of impedance: Figures 4.2 and 4.3, which could be contrasted, respectively, to Figures 3.10 and 3.11, demonstrate this induced higher level of impedance and the continued insensitivity of these impedances to the solution chemistry. Measurements conducted on electrodes polished by ion-thinning techniques gave results similar to the electrodes treated with polishing paper. The explanation of this seemingly paradoxical result became apparent after close examination of the polished samples with reflecting microscope. It appeared that only the diamond-polished samples were relatively "smooth". The ion-thinned samples, as well as the samples treated with polishing paper had about the same degree of complexity in surface microstructure. We shall see in Section 4.3 that it is possible to achieve large decreases in the electrode impedance by electrical treatment of the electrode surface. For the moment, the continued insensitivity of the electrode impedance to the solution chemistry requires that we take a closer look at the surface diffusion impedance. Indeed, our previous surface diffusion impedance model in Section 1.4 was somewhat simplistic since it assumed essentially one active center. The situation becomes more complex, however, with the presence of several active centers.

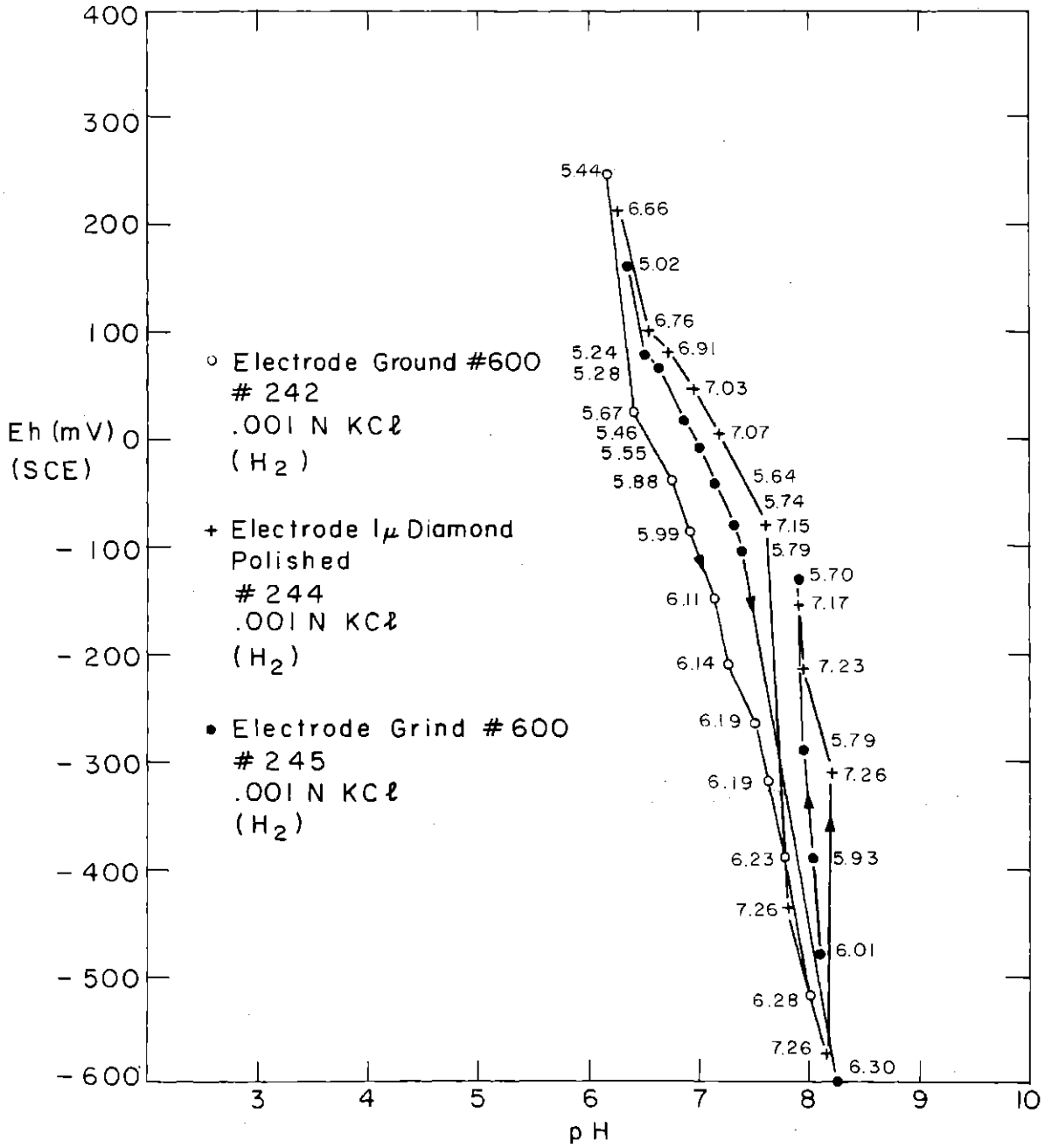


Figure 4.1 Warburg Impedance as a Function of Eh-pH (expressed as -log C, C = apparent concentration) for copper electrodes.

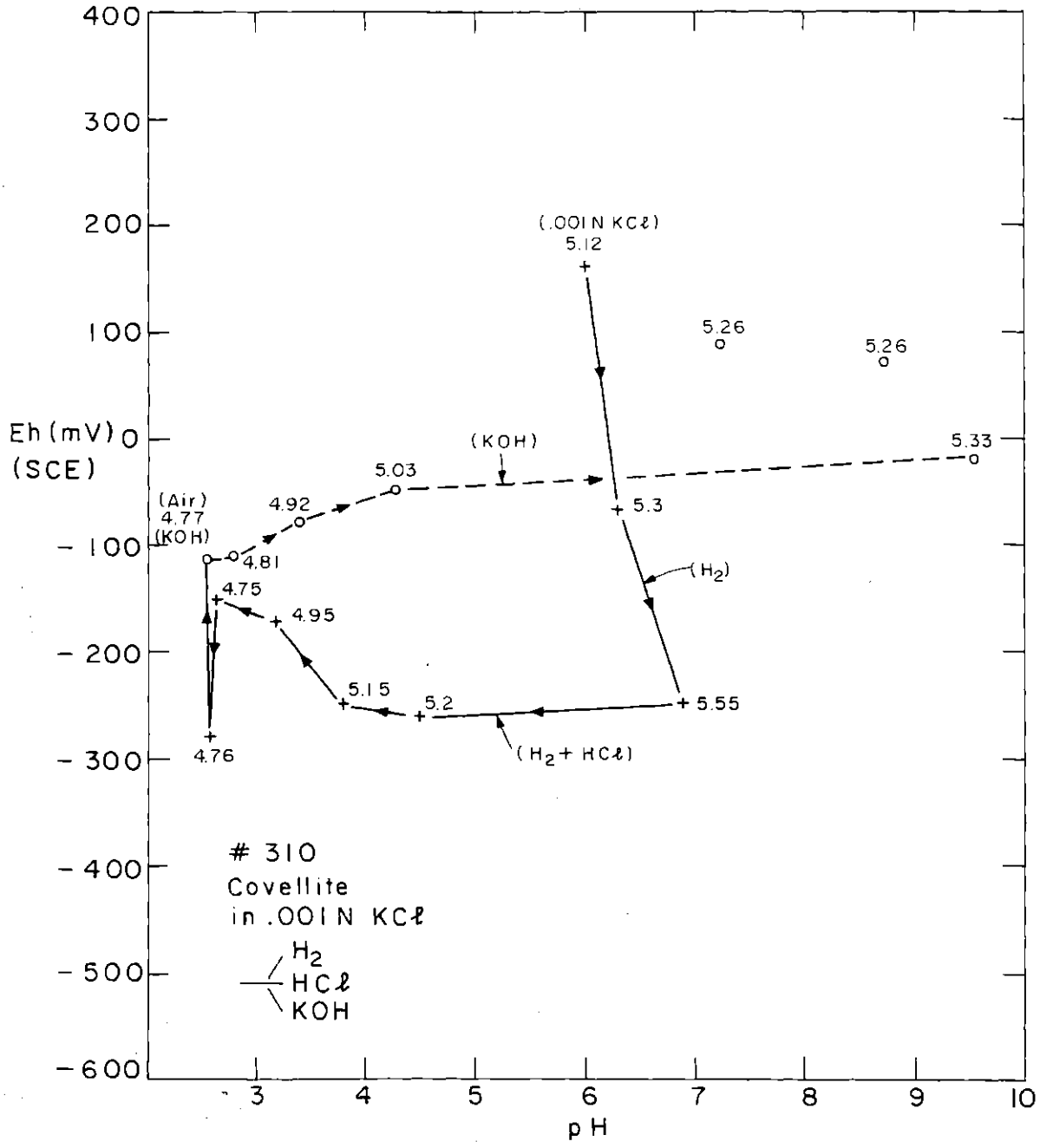


Figure 4.2 Warburg Impedance as a Function of Eh-pH (expressed as -log C, C = apparent concentration) for Diamond-Polished Covellite in KCl Solution.

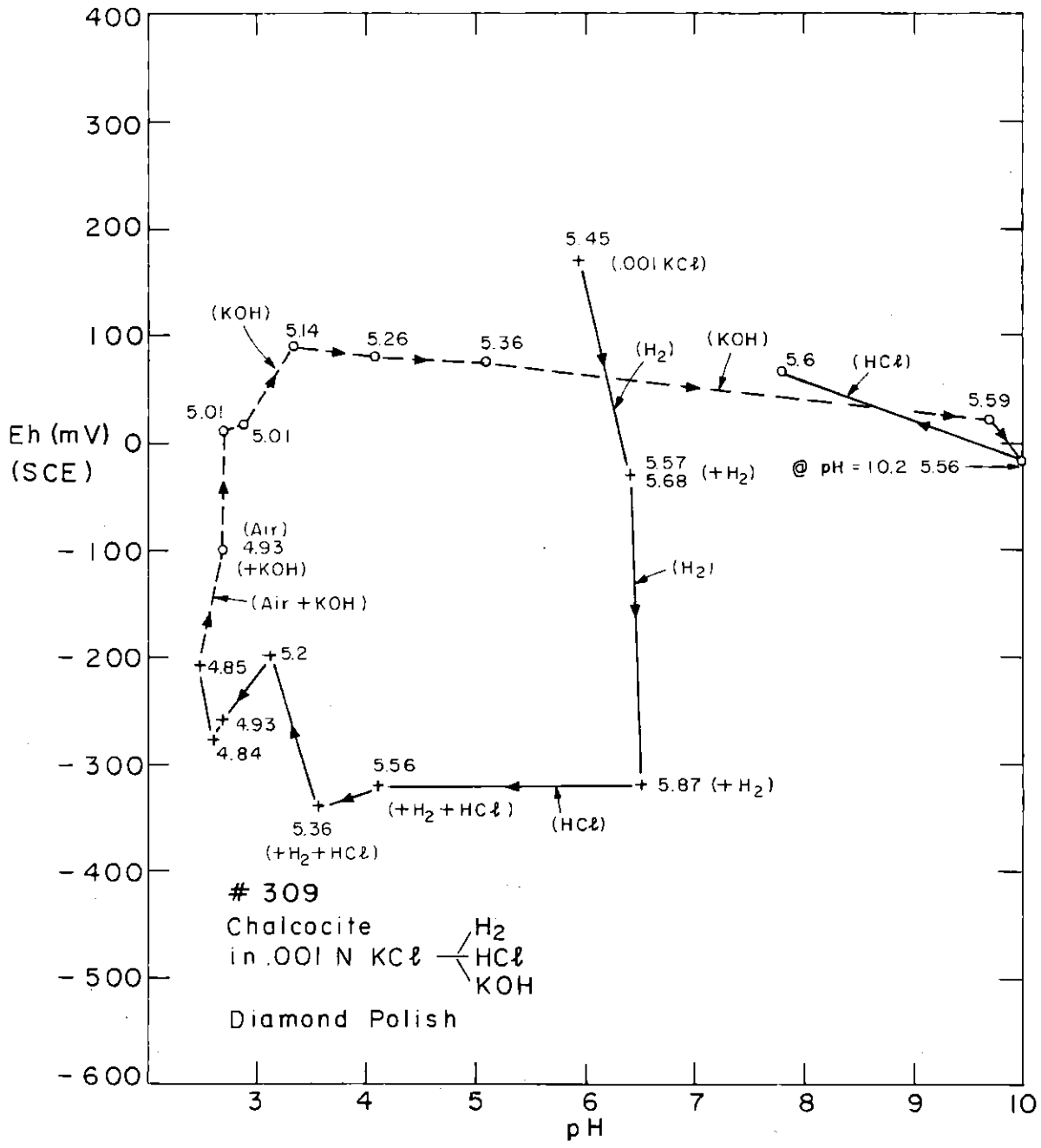


Figure 4.3 Warburg Impedance as a Function of Eh-pH (expressed as -log C, C = apparent concentration)

4.2 A Closer Look into the Surface Diffusion Contribution to the Electrode Impedance

For a simple illustration of the influence of several active centers, let us consider the one-dimensional surface diffusion impedance due to two line sources on the surface. The corresponding diffusion equations are

$$\frac{\partial C}{\partial \tau} = D_s \frac{\partial^2 C}{\partial x^2}$$

$$\text{Flow} = I_o e^{j\omega\tau} \quad \text{at } x = \pm x_o$$

Assuming sinusoidal time dependence, we get the solution for the concentration change

$$C = a \cosh \left(x\sqrt{\frac{j\omega}{D_s}}\right.$$

and the flow

$$D_s \frac{\partial C}{\partial x} = A \sqrt{j\omega D_s} \sinh \left(x\sqrt{\frac{j\omega}{D_s}}\right)$$

The surface diffusion impedance factor is

$$Z^F_{chem} \equiv \frac{C}{D_s \frac{\partial C}{\partial x}}\Bigg|_{x=x_o} = \frac{1}{\sqrt{j\omega D_s}} \frac{1}{\tanh x_o\sqrt{\frac{j\omega}{D_s}}}$$

The flow is related to the reaction current i_α by

$D \frac{\partial C}{\partial x} = i_\alpha/F\nu \div$ appropriate source geometry G factor. In analogy to Equation (1.1-3), using surface reaction rate parameters, we have

$$i_\alpha = \frac{Fi_o}{RT} V_f - i_o \frac{\Delta C_s \nu}{C_s} - \text{similar terms for other components of the reaction}$$

where i_o is the surface exchange current density, V_f the voltage drop across the fixed layer, C_s the surface concentration, ν a stochiometric coefficient. We have, in addition,

$$\Delta C_s = \frac{i_\alpha}{F\nu} Z^F_{chem}/G,$$

so that we get

$$i_\alpha = \frac{Fi_o}{RT} V_f - i_o \frac{i_\alpha}{C_s F} Z^F_{chem}/G - \text{other similar terms}$$

and

$$Z = \frac{V_f}{i_\alpha} = \frac{RT}{Fi_o} + \frac{RT}{F^2 C_s} Z_{chem}/G + \text{other similar terms}$$

Thus the surface diffusion impedance per unit length is

$$Z_{surf} = \frac{RT}{GF^2 C_s} \frac{1}{\sqrt{j\omega D_s}} \frac{1}{\tanh\left(x_o \sqrt{\frac{j\omega}{D_s}}\right)} \qquad (4.3\text{-}1)$$

At high frequency, this impedance is

$$Z_{surf} = \frac{RT}{GF^2 C_s} \frac{1}{\sqrt{j\omega D_s}}$$

which is a Warburg impedance depending on the surface concentration and diffusivity. From statistical mechanics considerations, surface diffusivities and volume diffusivities are identical if one assumes identical energy of activation for surface and volume diffusion, and both have units of cm^2/sec. Therefore the above one-dimensional surface Warburg impedance is similar to the three-dimensional one except for the concentration which is expressed in moles/cm^2 and the source geometry term, G, expressed in source length per unit area.

Hence the surface Warburg can be expressed as

$$Z_{W_s} = \frac{RT}{[nr_1]C_s F^2 \sqrt{j\omega D_s}}$$

where n is the number of sources per unit area and r_1 the source length or circumference. The magnitude W_s of this Warburg impedance is

$$W_s = \frac{RT}{[nr_1]C_s F^2 \sqrt{\omega D_s}}$$

Thus

$$W_s \equiv \frac{1.22 \times 10^{-4}}{nr_1 C_x \sqrt{\omega}} \ \Omega \cdot cm^2, \text{ assuming } D_s = 2.5 \times 10^{-5} \ cm^2/sec$$

At low frequency, however,

$$Z_{surf} = \frac{RT}{nr_1 F^2 C_s j\, x_o}$$

which is a chemical capacitance with the capacity

$$C = \frac{F^2}{RT} C_s x_o n r_1 \text{ per unit area.}$$

This chemical capacity results from the continued accumulation of reaction products between the active zones.

For a two-dimensional diffusion, assuming a distribution of active centers with cylindrical symmetry, the surface diffusion impedance factor will be a complex function involving Hankel functions of order zero and one, which must satisfy various flow conditions at the sources. If the source radius and separation between centers are much greater than some diffusion lengths, the surface diffusion impedance behaves like a Warburg impedance. If the separation of the active disks are less than some diffusion lengths, the impedance will behave like a capacitance. However, if the source separation is greater than, and the source radius less than, some diffusion lengths, the impedance will behave asymptotically like a resistor.

It is useful to investigate the limits bestowed on the magnitude of the capacity and Warburg impedance by the finite source spacings and surface concentrations existing on the electrode surface:

If the impedance appears Warburg-like, the minimum spacing is equal to the diffusion length

which at .1 cps is about 56 μm, assuming a surface diffusivity of 2.5×10^{-5} cm^2/sec. Since nr_1x_o can at most be 1 cm^2, assuming no surface area increase, the source geometry

$$nr_1 < \frac{1}{x_{o_{crit}}} = \frac{1}{54 \times 10^{-4}} \simeq 180/cm.$$

Since

$$W_s = \frac{RT}{nr_1C_sF^2\sqrt{\omega D_s}} = \frac{1.22 \times 10^{-4}}{nr_1C_s\sqrt{\omega}} \ \Omega \cdot cm^2$$

we can set a minimum observable Warburg impedance due to surface diffusion by allowing for the highest surface concentration possible over the entire surface of the electrode ($nr_1x_o = 1$). Assuming atomic spacing of 2Å, we get a maximum surface concentration of 2.5×10^{15} molecules/cm^2 which gives $C_{s_{max}} = 4.15 \times 10^{-9}$ mole/cm^2. Hence, the minimum surface diffusion Warburg which can be seen at a frequency $\omega = 1$ is about

$$W_{s_{min}} = 163 \ \Omega \cdot cm^2$$

This minimum is an underestimate since the activity coefficient of such a saturated condition would be considerably less than 1. This lower bound of Warburg impedance means essentially that inasmuch as electrodes processes require surface diffusion, the effective ionic species concentration as computed from electrode impedance spectra will appear to have an approximate upper bound of about $c_{i_{max}} = 10^{-3.4}$ mole/l

leading thereby to systematic underestimation of the concentration of possible active ionic species in solution.

Similarly, since the accumulation of products may create a chemical capacity $C = \frac{F^2}{RT} C_s n r_1 x_o = 1.63 \times 10^6 C_s n r_1 x_o$ Farad, we can set an upper limit for the chemical capacity using the same atomic spacing constraints for the surface population of species. We get, therefore,

$$C_{max} = 6640 \ \mu F$$

Thus, any surface diffusion impedance has a lower bound of the order of about 200 $\Omega \cdot cm^2$ at a frequency of $\omega = 1$.

The existence of these bounds for surface Warburg and chemical capacity would have interesting implications for the surface diffusion processes as they could be inferred from electrode impedance spectra. More specifically, if an equivalent circuit fit requires high capacity value and low Warburg term, this may be the result of substantial coating of the electrode by active centers.

Such a decrease in electrode impedance can also be an indication of an increased effective surface area. It is thus of interest to examine the effects on the electrode impedance of an increase in the effective surface area of the electrode which is a result of some topography or surface roughness induced on the electrode. Analytical solutions for the electrode impedance could be found for very simple geometries of the topography either by the use of electrical images, a method employed by Charles Kasper (1940, 1942)

to investigate the current distribution at electrodes during electrodeposition, or by the use of conformal mapping, a method employed by Carl Wagner (1951, 1961) to derive the current distribution in electrodes with one-dimensional V-shaped or U-shaped grooves. Such models and their extensions by the addition of several identical grooves would simulate the microstructure of mechanically polished electrode surfaces, and the solution will involve elliptic and hyper-elliptic functions with boundary conditions almost analytically intractable. An excellent review of these methods has been published in a report by Fleck, Hanson and Tobias (1964) with the purpose of providing the means for the numerical evaluation of the current distribution in electrochemical systems. Similar problems have been investigated extensively with special reference to porous electrodes. A good coverage of these works is to be found in a series of papers published by Robert de Levie (1963, 1964, 1965, 1967).

To avoid a cumbersome mathematical treatment for even so simplistic profiles, we shall examine the influence of surface roughness through our familiar electrical equivalent circuit approach. Let us look first at the solution Warburg. It depends essentially on the ratio of the change in concentration of the Faradaic current carriers to their flow. Therefore it is necessary to see whether the level of concentration within the crevices of the surface asperities mirror the outside concentration. If the diffusion lengths are

greater than the topography, the critical parameter to consider is the ratio of the diffusion layer volume to the volume associated with the surface roughness. If this diffusion layer volume is much greater than the integrated volume of the crevices, the solution concentrations within the crevices should follow closely the solution concentration just outside the surface and the surface will appear flat as far as the solution Warburg is concerned. The Warburg terms are mostly derived from the low frequency end of the impedance spectrum where the diffusion lengths are of the order of 20-60 μm, and it is unlikely that the induced topography, typically of the order of a couple of microns, will affect the solution Warburg.

The effect of an increased surface area on the fixed layer capacity is different, however. The non-Faradaic current flow across the fixed layer can be coupled to the non-Faradaic flow associated with the diffuse layer capacity by all the ionic components in the solution associated with the surface roughness. If the resistance of this coupling is small compared to the fixed layer capacitive impedance, then all of the excess surface area can participate in the non-Faradaic current flow, and the fixed layer capacity will increase with the effective surface area.

Surface diffusion processes, of course, are involved with the actual surface and thus, if we can assume the same surface concentrations and density of active centers, the impedances resulting from surface diffusion will decrease proportionately to the increase of effective surface area.

The equivalent circuit representing the surface diffusion impedance will tend to be capacitive at low frequency if the distance between active centers is of the order or less than the diffusion lengths for the lowest frequencies. This implies the addition of a chemical capacitance in series with the Warburg impedance of the basic equivalent circuit. Figure 4.4 displays a comparison between the amplitude behavior of the one-dimensional surface diffusion impedance [Equation (4.3.1)] and a series combination of a capacitance and a Warburg. In Figure 4.5 are compared their respective phases. It appears that both amplitudes and phases have asymptotically the same behavior. At intermediate frequencies, however, the surface diffusion impedance model has a steeper gradient compared to the relatively slow variation of the impedance of the CW* series combination. To obtain a more

---

*Capacity-Warburg in series.

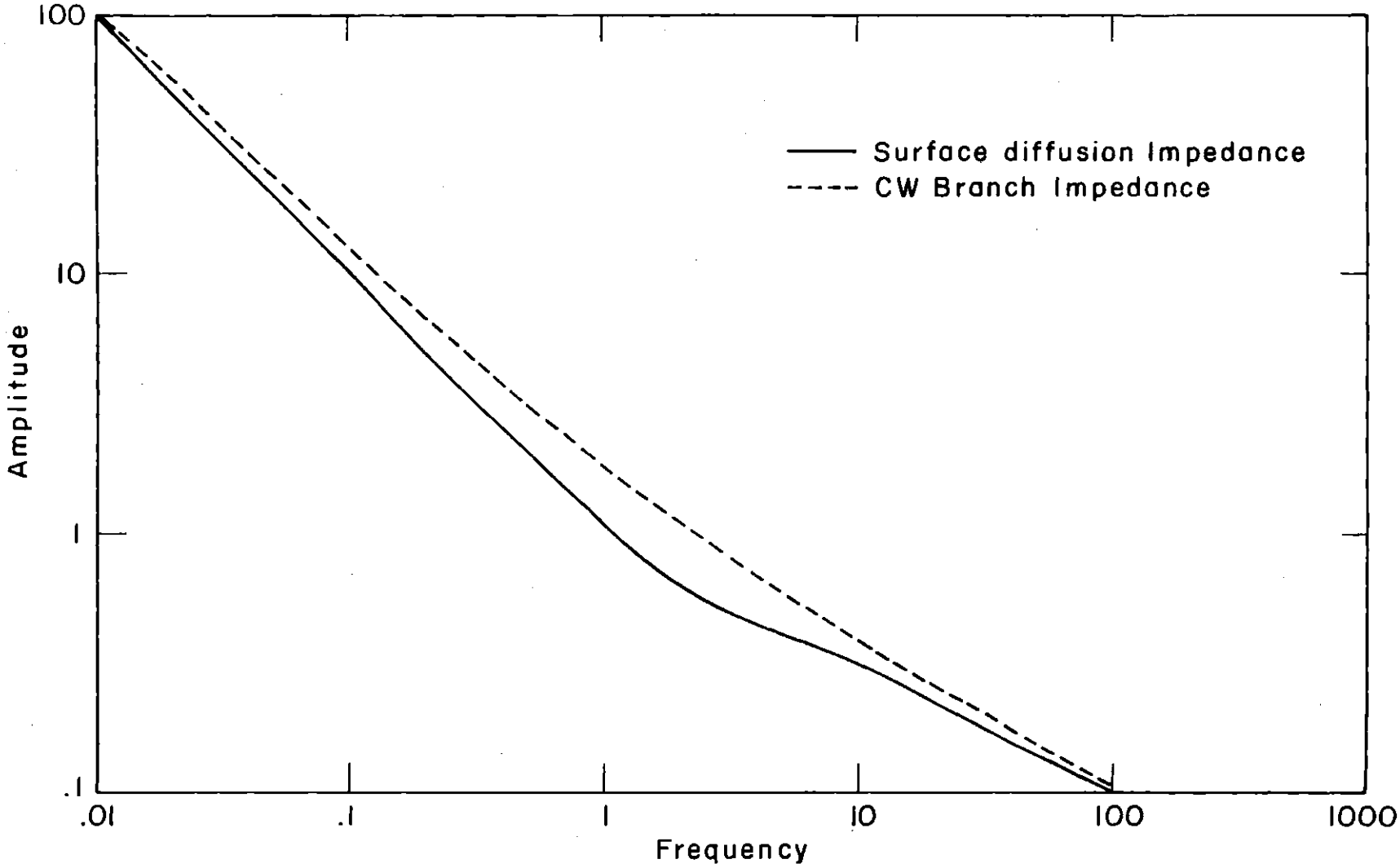

100
10
1
.1
Amplitude
.01
.1
1
10
100
1000
Frequency
Surface diffusion Impedance
CW Branch Impedance

Figure 4.4

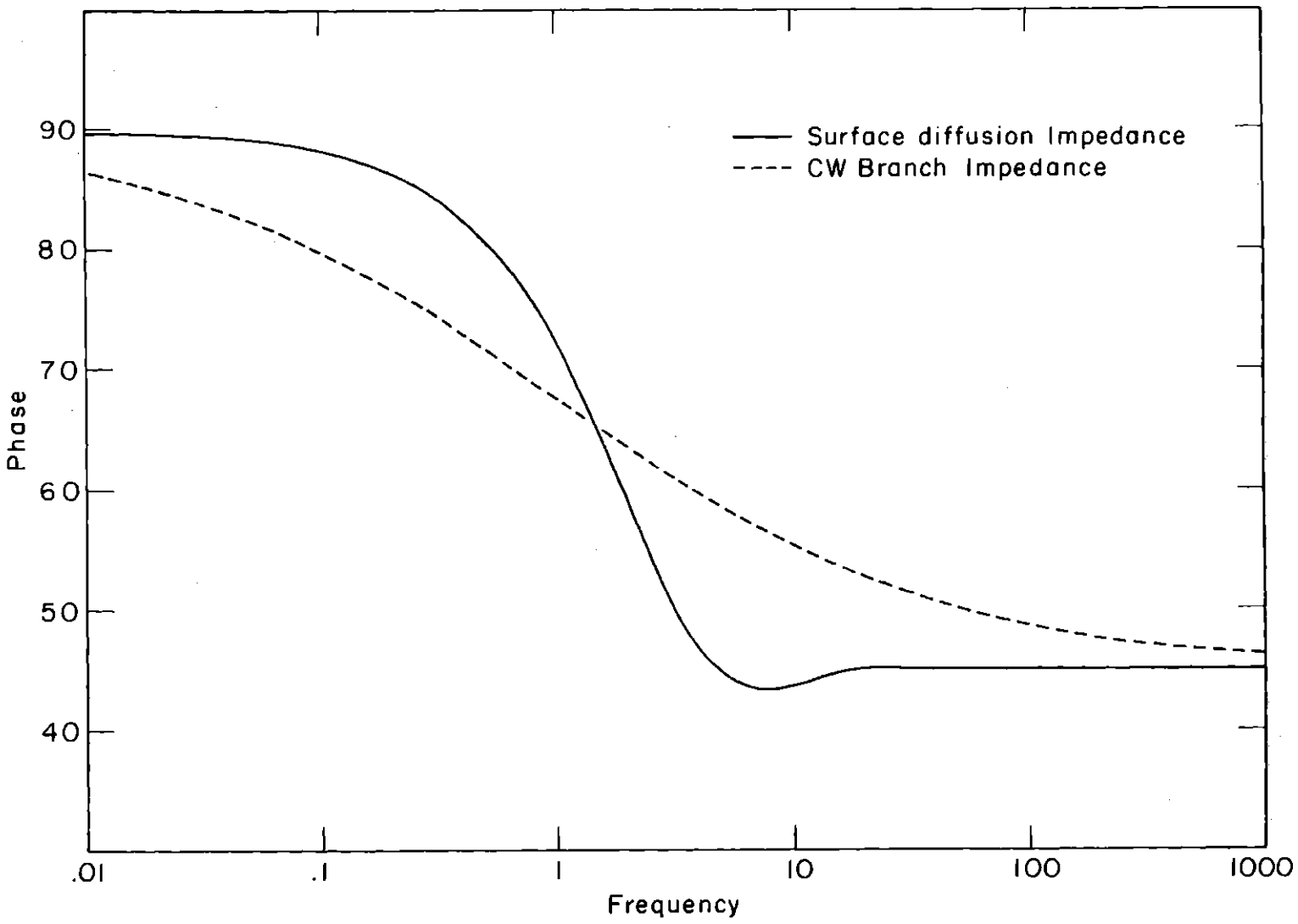

Surface diffusion Impedance
CW Branch Impedance
90
80
70
60
50
40
Phase
.01
.1
1
10
100
1000
Frequency

Figure 4.5

spread-out behavior with the one-dimensional surface diffusion impedance, a variety of distributions of source spacings would be required, which is probably more realistic than a single spacing.

Since a CW impedance appear to be a relatively good approximation of the surface diffusion impedance, the electrode Faradaic impedance will therefore be represented by a parallel combination of WCR[†] branches coupling the solution resistance to the electrode. Some of the elements of a WCR branch could be unimportant depending on the experimental conditions.

To test out these ideas, we attempted to fit the electrode impedance spectra using a parallel combination of a fixed layer capacity and a WCR branch. The results of the corresponding fits are essentially similar to those of the basic equivalent circuit represented in Figure 1.1 except in some instances when the capacitive impedance of the WCR branch becomes significant. This provides, however, a rationale for ascribing large apparent fixed layer capacity values, which are sometimes observed, to a chemical capacity in a WCR branch where the corresponding reaction resistance and Warburg impedance are unimportant.

[†]Warburg-Capacity-Resistance in series.

4.3 Depolarization Experiments on Copper, Iron, and Sulfide Electrodes

Large decreases in impedance can be achieved by electrical treatment of the electrode surface. The method consists in sending anodic or cathodic current to both working electrodes for specified duration using graphite as common counter-electrode. Thereafter, the electrode impedance spectrum is measured. We call such procedure "depolarization" when the electrode impedance is lowered and "repolarization" when the electrode impedance is returned to its initial value or is left unaltered. Anodic current flow occurs when the electrodes are driven positive relative to the counter-electrode, and cathodic when the electrodes are driven negative. There is an important difference between the behavior of the metal electrodes and that of the sulfide electrodes. We have observed that copper and iron get depolarized only when subjected to anodic current. In contradistinction to these metal electrodes, the sulfide electrodes -- covellite, chalcocite, pyrite, chalcopyrite, pyrrhotite -- which we have studied in great detail get depolarized only when subjected to cathodic current.

The main result of the depolarization of all these electrodes is that the electrode impedance drops to a very low value, giving usually a very low Warburg impedance. Such low Warburg impedance is testimony that very common ionic species must be involved in the electrode reactions. Let us examine more specifically typical depolarization experiments

performed on the various electrodes.

4.3.1 Depolarization of Copper Electrodes

Typical experimental results corresponding to copper electrodes in chloride environments are shown in Table 4.1. The initial electrode impedance spectrum, which we shall henceforth call "background spectrum", gives a Warburg impedance of 14770 $\Omega \cdot cm^2$. This would correspond to active species concentration of about $10^{-5.37}$ mole/liter. We see that successive anodic depolarization of the electrodes progressively lowers the electrode impedance. Extreme depolarization of the electrode sends the Warburg impedance down to about 61 $\Omega \cdot cm^2$ corresponding to an active species concentration of about $10^{-2.99}$ mole/l. This Warburg impedance is very close to the solution contribution and therefore any surface diffusion phenomena must be unimportant. It can also be seen that there is a significant time variation associated with the electrode impedance as the experiment following the extreme depolarization testifies. Subsequent depolarization in more concentrated chloride environment drives the Warburg impedance substantially lower again with equivalent active species concentration mirroring somewhat the chloride concentration. We shall attempt to present some plausible electrode reactions corresponding to these experiments as well as provide some explanation for the time variation of the electrode impedance observed (repolarization).

4.3.2. Depolarization of Iron Electrodes

The experimental results corresponding to iron are presented in Table 4.2. Three points deserve special attention:

1. From a background Warburg of 19550 $\Omega \cdot cm^2$ corresponding to equivalent active ionic species concentration of $10^{-5.49}$ mole/l in solution of $10^{-4.30}$ mole/l KCl, the lowest Warburg reached through depolarization is about 500 $\Omega \cdot cm^2$ in a solution of $10^{-2.22}$ mole/l salt concentration which is a relatively high impedance level in comparison to the impedance levels reached with copper.

2. All the capacity and Warburg values are well resolved and their product in each spectral measurement appears fairly constant. As discussed in Section 4.2, an increase in effective surface area as a result of topography will decrease the level of impedance but not keep the product of the solution Warburg and the fixed layer capacity constant. However, the correlation high capacity/low Warburg can be explained if the capacity and Warburg represent surface diffusion impedance elements. This is why we favor an explanation of the iron electrode depolarization based on surface diffusion. The decreased level of impedance could occur on the basis of the existence of increased number of active sites on the electrodes and/or increased surface species' concentration. The level of the attached surface impedance

is higher than, but of the same order as, the lower bound of surface impedance (determined in Section 4.2), and also high enough so that the solution contribution is overriden because of the series' disposition of these two impedances.

3. The time variation of the iron electrode impedances appears less pronounced after depolarization. The explanation for the relative stability of the electrode impedance remains an open question, especially in view of the proposed electrode reactions in Section 4.4. This stability seems to imply the existence of active sites and surface concentration of species which remain relatively stable even after depolarization.

Our experiments on iron have been less exhaustive than on copper and further experimentation under various conditions may be needed in order to ascertain more firmly the behavior of the iron electrode impedance. Since, for the depolarized electrode reactions, we need some major ionic species to carry the Faradaic current in the solution, we have formulated, as we shall see in Section 4.4, for the iron electrode reactions, the hypothesis that chloride ions carry the Faradaic current in the solution in similarity to copper electrode reactions.

4.3.3 Depolarization of Sulfide Electrodes

All the sulfides studied have essentially similar behavior with regard to depolarization. They are depolarized

Experimental condition (in sequence)	Equivalent circuit parameters normalized to $1cm^2$				Apparent Conc. 10^{-x}	i_0 A/cm^2	Misfit %
	$R_{(\Omega)}$	$C_{(\mu F)}$	R_{react} (Ω)	$W(\Omega)$			
Initial use in .001N KCl $\equiv 10^{-3}$	1 085	2	2 906	14 770	5.37	$.86x10^{-5}$	7.91
Anod. depol. 4.5ma/15 sec.	1 058	3	180	5 061	4.91	$.14x10^{-3}$	3.88
Further anod. depol. 4.2ma/33 sec.	973	4	169	441	3.85	$.15x10^{-3}$	4.46
Further anod. depol. 4.2ma/1 min.	932	298	93	180	3.46	$.27x10^{-3}$	2.22
Further anod. depol. 4.2ma/1 min. 14 sec.	937	2 395	63	61	2.99	$.40x10^{-3}$	1.04
Left 15 min. self-repolarization	1 103	7	843	5 095	4.91	$.30x10^{-4}$	4.94
Increase conc. .0045N KCl $\equiv 10^{-2.35}$ Anod. depol. 11ma/30 sec.	283	4 587	27	24	2.59	$.93x10^{-3}$	1.57
Left 5 hours self-repolarization	294	2	41	2 861	4.66	$.60x10^{-3}$	8.28
Anod. depol. 11.6ma/30 sec.	287	542	68	49	2.90	$.37x10^{-3}$	3.36

Table 4.1 Depolarization Experiments on Copper Electrodes.
Underlined values indicate the parameter was significant in the equivalent circuit fit.

Experimental condition (in sequence) very small spacing	Equivalent circuit parameters normalized to $1cm^2$				Apparent Conc. 10^{-x}	i_0 A/cm^2	Misfit %
	R (Ω)	C (μF)	Rreact (Ω)	W (Ω)			
Initial use in $5x10^{-5}$N KCl ≡ $10^{-4.3}$	2 251	13	462	19 560	5.49	$.54x10^{-4}$	6.28
Anod. depol. .18ma/5 min.	1 643	24	463	7 144	5.05	$.54x10^{-4}$	4.34
Increase KCl concentr. $5.5x10^{-4}$N KCl ≡ $10^{-3.26}$	219	52	28	4 669	4.87	$.90x10^{-3}$	5.51
Anod. depol. 1.3ma/10 min.	88	143	11	1 502	4.38	$.22x10^{-2}$	6.67
Left 11 min. self-repolarization	162	98	32	2 272	4.55	$.77x10^{-3}$	3.52
Increase KCl concentr. .0015N KCl ≡ $10^{-2.82}$	81	117	45	1 867	4.47	$.55x10^{-3}$	5.96
Increase KCl concentr. .0035N KCl ≡ $10^{-2.46}$	41	144	7	1 102	4.24	$.34x10^{-2}$	10.75
Stop stirring 30 min. time variation	34	453	3	941	4.17	$.79x10^{-2}$	7.61
Increase KCl concentr. .006N KCl ≡ $10^{-2.22}$	24	100	0	1 158	4.26	.18	13.07
Stop stirring 10 min. time variation	23	455	2	854	4.13	10^{-2}	7.18
Anod. depol. 3.8ma/10 min.	20	676	2	588	3.97	$.13x10^{-1}$	8.78
Time variation (10 min)	21	494	4	595	3.97	$.64x10^{-2}$	11.36
Left overnight	23	736	3	482	3.88	$.92x10^{-2}$	9.41

Table 4.2 Depolarization Experiments on Iron Electrodes

after sufficient cathodic currents are applied to them. The experimental results for covellite, chalcocite, chalcopyrite, pyrite and pyrrhotite are shown in Tables 4.3 through 4.7. Some general observations hold in all these cases:

(i) There is a significant time factor affecting the electrode impedance after depolarization.

(ii) The capacity of the equivalent circuit increases quite substantially for depolarized electrodes.

(iii) Stirring after depolarization is often seen to accelerate the initial rate of increase of the electrode impedance.

(iv) Reverse polarization or repolarization can return the induced large capacity and low Warburg values to almost normal background values.

Close examination of the Tables 4.3 through 4.7 shows that while the background Warburg impedances are of the order of several thousands of $\Omega \cdot cm^2$, they are seen to drop by almost one to two orders of magnitude when the electrodes are depolarized.

Table 4.3 shows covellite electrode initially in 10^{-3} mole/l KCl. The background Warburg impedance is 2760 $\Omega \cdot cm^2$. Impression of a cathodic current of 6.4 ma for 2 min brings the Warburg impedance down to 689 $\Omega \cdot cm^2$ equivalent to $10^{-4.04}$ mole/l. Whereas the time factor repolarized the electrode to 4514 $\Omega \cdot cm^2$ overnight, a further cathodic current of 4.5 ma for 5 minutes

Experimental condition (in sequence)	Equivalent circuit parameters normalized to $1cm^2$				Apparent Conc. 10^{-x}	i_0 A/cm^2	Misfit %
	R (Ω)	C (μF)	Rreact (Ω)	W (Ω)			
Initial experiment .001N KCl ≡ 10^{-3}	1 097	59	126	2 760	4.64	$.20x10^{-3}$	3.38
Cathodic depol. 4.6ma/30 sec.	1 071	292	158	2 457	4.59	$.16x10^{-3}$	2.96
Further cathodic depol. 4.6ma/30 sec.	1 073	417	150	2 301	4.56	$.17x10^{-3}$	3.38
Further cathodic depol. 4.6ma/2 min.	1 041	386	103	689	4.04	$.24x10^{-3}$	1.13
After 1 hour time variation	1 066	505	160	2 338	4.57	$.16x10^{-3}$	2.77
Left overnight	1 034	151	17	4 514	4.86	$.14x10^{-2}$	3.46
Cathodic depol. 4.7ma/5 min.	973	540	85	506	3.91	$.29x10^{-3}$	1.37
Add NaCl → .002N Cl^- ≡ $10^{-2.9}$	551	880	155	2 253	4.56	$.16x10^{-3}$	1.25
Further cathodic depol. 7.8ma/2 min. 32 sec.	553	988	84	504	3.90	$.30x10^{-3}$	1.37
Add NaCl → .004N Cl^- ≡ $10^{-2.4}$	291	1 355	89	1 460	4.37	$.28x10^{-3}$	2.92
Cathodic depol. 11.6ma/3 min.	278	1 136	43	422	3.83	$.58x10^{-3}$	2.38
Add NaCl → .006N Cl^- ≡ $10^{-2.22}$	191	1 883	59	962	4.19	$.42x10^{-3}$	2.69
Cathodic depol. 14.3ma/4 min.	190	1 747	44	576	3.96	$.57x10^{-3}$	4.35

Table 4.3 Depolarization Experiments on Covellite Electrodes

Experimental condition (in sequence)	Equivalent circuit parameters normalized to $1cm^2$				Apparent Conc. 10^{-x}	i_0 A/cm^2	Misfit %
	R (Ω)	C (μF)	Rreact (Ω)	W (Ω)			
Initial run in .001N KCl ≡ 10^{-3}	1 289	3	401	38 200	5.78	$.62x10^{-4}$	5.88
Anod. current* 5.1ma/2 min.	1 297	5	1 108	8 186	5.12	$.23x10^{-4}$	6.62
Further anod. current* 5.1ma/8 min.	1 279	4	590	5 554	4.95	$.42x10^{-4}$	4.07
Cathodic depol. 5.1 ma/2 min.	1 280	213	203	2 855	4.66	$.12x10^{-3}$	2.88
Further cathodic depol. 5.1ma/8 min.	1 255	306	1 101	861	4.14	$.25x10^{-4}$	2.35
Add NaCl → .002N Cl^- ≡ $10^{-2.7}$	663	255	225	1 434	4.36	$.11x10^{-3}$	3.27
Add NaCl → .004N Cl^- ≡ $10^{-2.4}$	342	311	95	1 234	4.29	$.26x10^{-3}$	1.52
Add NaCl → .009N Cl^- ≡ $10^{-2.06}$	159	415	27	947	4.18	$.94x10^{-3}$	3.19

Table 4.4 Depolarization Experiments on Chalcocite Electrodes

*Repolarization is expected with anodic current, but the initial impedance was higher than usual in this run and the apparent depolarization may not be significant.

Experimental condition (in sequence)	Equivalent circuit parameters normalized to $1cm^2$				Apparent Conc. 10^{-x}	i_0 A/cm^2	Misfit %
	R (Ω)	C (μF)	Rreact (Ω)	W (Ω)			
Initial run in .001N KCl ≡ 10^{-3}	1 190	49	89	8 567	5.14	$.28x10^{-3}$	5.45
Cathodic depol. 4.4ma/30 sec.	1 130	57	72	6 529	5.02	$.34x10^{-3}$	6.23
Further cathodic depol. 4.5ma/2 min.	1 130	78	313	4 940	4.90	$.80x10^{-4}$	6.91
Outside cathodic depol. 26.9ma/4 min.	1 103	250	853	949	4.18	$.29x10^{-4}$	4.53
Inside anod. repolarization 4.5ma/5 min. 30 sec.	1 092	39	295	7 397	5.07	$.85x10^{-4}$	4.97
Cathodic depol. 4.5ma/23 min.	1 022	436	85	643	4.01	$.29x10^{-3}$	1.81
Add NaCl → .002N Cl^- ≡ $10^{-2.7}$	587	98	8	1 700	4.43	$.33x10^{-2}$	3.62
Add NaCl → .00 N Cl^- ≡ $10^{-2.4}$	327	97	30	3 046	4.69	$.82x10^{-3}$	5.85
Add NaCl → .006N Cl^- ≡ $10^{-2.22}$	233	75	27	4 507	4.86	$.91x10^{-3}$	5.96
Cathodic depol. 13.9ma/4 min.	226	1 188	463	257	3.61	$.54x10^{-4}$	3.51
Anod. repolarization 14ma/5 min.	233	54	28	3 195	4.71	$.90x10^{-3}$	4.01

Table 4.5 Depolarization Experiments on Pyrite Electrodes

Experimental condition (in sequence)	Equivalent circuit parameters normalized to $1cm^2$				Apparent Conc. 10^{-x}	i_0 A/cm^2	Misfit %
	R (Ω)	C (μF)	Rreact (Ω)	W (Ω)			
Initial run in .001N NH_4Cl ≡ 10^{-3}	1 117	35	80	15 310	5.39	$.31x10^{-3}$	6.39
Add NH_4Cl →.0035N Cl^- ≡ $10^{-2.46}$	381	57	11	17 410	5.44	$.22x10^{-2}$	10.32
Cathodic depol. 4ma/45 sec.	356	1 092	244	780	4.09	$.10x10^{-3}$	5.58
After 4 hours time variation	358	171	40	4 346	4.84	$.62x10^{-3}$	11.25
Cathodic depol. 3.5ma/4 min.	323	9 195	24	141	3.35	$.10x10^{-2}$	1.47
Add NH_4Cl Further cathodic depol. 4.5ma/4 min.	208	5 576	19	83	3.12	$.13x10^{-2}$	1.57
Left overnight	213	591	12	3 094	4.69	$.21x10^{-2}$	4.95
Cathodic depol. 4.3ma/8 min.	206	5 380	24	83	3.12	$.10x10^{-2}$	1.42

Table 4.6 Depolarization Experiments on Chalcopyrite Electrodes

Experimental condition (in sequence)	Equivalent circuit parameters normalized to $1cm^2$				Apparent Conc. 10^{-x}	i_0 A/cm^2	Misfit %
	R (Ω)	$C_{(\mu F)}$	Rreact (Ω)	W (Ω)			
Initial run in .001N KCl ≡ 10^{-3}	1 336	59	2 175	2 510	4.60	$.11x10^{-4}$	4.27
Add NaCl →.002N Cl^- ≡ $10^{-2.7}$	721	64	2 486	2 988	4.68	$.10x10^{-4}$	7.65
Add NaCl →.004N Cl^- ≡ $10^{-2.40}$	371	31	42	5 767	4.96	$.59x10^{-3}$	8.54
Add NaCl →.006N Cl^- ≡ $10^{-2.22}$	254	34	36	5 730	4.96	$.69x10^{-3}$	7.88
Add NaCl →.008N Cl^- ≡ $10^{-2.1}$	196	37	96	5 496	4.94	$.26x10^{-3}$	8.14
Left overnight	198	33	27	8 451	5.13	$.94x10^{-3}$	8.61
Cathodic depol. 15.3ma/15 sec.	184	86	20	1 346	4.33	$.12x10^{-2}$	8.34
After 25 min. time variation	185	40	31	4 102	4.82	$.80x10^{-3}$	7.90
Further cathodic depol. 15.3ma/30 sec.	184	805	40	607,	3.99	$.63x10^{-3}$	4.01
After 35 min. time variation	195	66	1 704	2 736	4.64	$.15x10^{-4}$	10.85
Further cathodic depol. 15.4ma/1 min.	184	1 047	28	372	3.77	$.88x10^{-3}$	2.82
After 20 min. time variation	193	88	1 393	1 283	4.31	$.18x10^{-4}$	9.81
Further cathodic depol. 15.4ma/2 min.	180	1 352	96	122	3.29	$.26x10^{-3}$	2.73
After 30 min. time variation	193	96	1 802	1 428	4.36	$.14x10^{-4}$	9.96
Further cathodic depol. 15.5ma/4 min.	179	1 759	89	153	3.39	$.28x10^{-3}$	2.36

Table 4.7 Depolarization Experiments on Pyrrhotite Electrodes

lowered the electrode impedance to 506 $\Omega \cdot cm^2$. The electrode repolarizes spontaneously but subsequent cathodic depolarization drops again the Warburg impedance. It appears, however, that the resulting Warburg impedance of depolarized covellite remains relatively high in comparison to the diffusion impedance level that would be generated by major ionic species in solution, but is still low compared to the solution Warburg of minor constituents.

For a chalcocite electrode in Table 4.4, the background Warburg impedance of 38200 $\Omega \cdot cm^2$ is somewhat larger than usual. The apparent depolarization observed following impression of anodic current is not significant because the resulting Warburg of 5554 $\Omega \cdot cm^2$ is within the range of typical background values. Subsequent impression of cathodic current of 5.1 ma for 8 minutes lowers the impedance to about 861 $\Omega \cdot cm^2$.

We can see in Table 4.5 similar depolarization results on pyrite electrodes. It is seen that the large capacity induced by the cathodic depolarization of the electrode outside the cell has been reduced back to "normal" values when reverse polarity of 4.5 ma anodic current for 5 minutes was applied to the electrodes (repolarization). The same result can be seen by comparing the last two experiments shown in Table 4.5. Such observation gives additional support to ascribing any large capacity value obtained in the basic

equivalent circuit to a form of chemical capacity since it is unlikely that an increase in the fixed layer capacity due to induced surface topography will so readily be adversely affected by the reverse polarity imposed.

Table 4.6 shows a chalcopyrite electrode in NH_4Cl solution with background Warburg impedance of 15310 $\Omega \cdot cm^2$. Cathodic depolarization brings the impedance level down to as low as 83 $\Omega \cdot cm^2$ with significant time variation, however. Crude estimates of time variations can be seen from corresponding measurements in the table.

Similar results hold for pyrrhotite electrodes in Table 4.7. We can see that the Warburg impedance has been driven down to 122 $\Omega \cdot cm^2$ corresponding to equivalent active species concentration of $10^{-3.29}$ mole/l still somewhat below the concentration of any major ionic species in solution. All these substantial drops of electrode impedances seem to imply the occurrence of electrode reactions prompted by the depolarization conditions which must involve relatively common ionic species because of the low overall Warburg impedance induced. These depolarization experiments provide a means to decrease significantly the electrode impedance without affecting significantly the solution chemistry. The decisive change must therefore be an alteration of the condition of the electrode surface. A very convenient way to describe the state of the electrode surface is through analysis by the electron microprobe. We shall look in the next section at

typical analyses we achieved using the electron microprobe of the M.I.T. Department of Earth and Planetary Sciences.

4.3.4 Electrode Reactions in Light of the Electron Microprobe Analysis

The electron microprobe is very appropriate for the analysis of very small areas. The typical electron beam focused on the sample having a diameter of the order of one micron (10^{-6} m), a very detailed analysis of the electrode surface can be easily achieved. The most important step, however, in the analysis procedure is the standardization for the elements to be searched for. To decide which elements we ought to look for, we were guided by the range of composition of the variety of electrodes we were to use as well as the chemical composition of the solutions in which the electrode reactions would take place: the first important elements chosen for analysis were copper (Cu), iron (Fe), sulfur (S), and chlorine (Cl). In addition to these, we decided to analyze for potassium (K), calcium (Ca) and sodium (Na) because we wanted to see if the cathodic depolarization of sulfides could possibly be the result of cations K^+, Ca^{++}, or Na^+, reacting at the sulfide electrodes. Finally we included nickel in the list because some sulfides were ostensibly nickeliferous, and zinc for some brass electrodes studied. A chalcopyrite standard sample was used for standardizing copper, iron, and sulfur; an orthoclase standard for potassium, a sodium chloride standard for chlorine, a

pyroxene glass for sodium and calcium; MAC* standards were used for nickel and zinc.

The results of the analyses of various electrodes are shown in Tables 4.8 through 4.13. Each row represents one analysis of a given area of the electrode where the electron beam has been focused. All numbers represent weight fraction of corresponding element except the ones in parenthesis which represent the mole fraction of the element in the corresponding column. For example in the first row of Table 4.8, the analysis shows 20.88% weight fraction of sulfur and 84.06% weight fraction of copper with respective mole fractions of .33 and .67. The chemical formula of the compound should therefore be $Cu_{.67}S_{.33}$ which is easily recognized as chalcocite Cu_2S.

We have indicated in Tables 4.8 through 4.13 the degree of depolarization of the electrode (whenever it is the case) by reporting the Warburg impedance. Thus we can observe that in Table 4.8, the chalcocite electrode #332 has been more intensely depolarized than the chalcocite #331.

Two important results emerge from close examination of the tables:

(i) Intensely depolarized copper electrodes are loaded with chlorine

(ii) Depolarized sulfide electrodes are partially de-

---

*Materials Analysis Co.

pleted of sulfur, show an increase in metal-to-sulfur ratio and sometimes exhibit the presence of some attached chlorine.

These two results coupled to the low level of Warburg impedance induced by the depolarization of the electrodes, will provide the basis for the inference of plausible reactions which might control the electrode impedance.

Table 4.8 shows the results of analysis of chalcocite electrodes under three different conditions. The analysis of the original sample shows relatively pure chalcocite minerals Cu_2S. The sample #332 shows a significant depletion of sulfur consecutive to depolarization; the copper-to-sulfur ratio jumps from 2 to 5 while we can see some chlorine in the analysis. We suspect the iron shown to be due to impurities in the electrode. However, the sample #331 which is mildly depolarized shows almost no depletion of sulfur.

Table 4.9 shows results corresponding to covellite CuS electrodes. Here again we can see some depletion of sulfur consecutive to depolarization in electrode #335 and almost none in #338.

Table 4.10 shows chalcopyrite $CuFeS_2$ and pyrrhotite FeS electrodes where the depolarized ones show significant depletion of sulfur.

In Table 4.11 pyrite FeS_2 electrodes are analyzed. The sample #341 depolarized intensely in ferrous chloride shows

Electrodes	Condition	S	Cl	K	Ca	Na	Fe	Ni	Cu	Zn
Chalcocite, Ajo, Arizona	New original Sample	20.88 (.33)	.01	.01	.0	.0	.08	.04	84.06 (.67)	.0
		20.69 (.34)	.0	.0	.0	.0	.16	.10	80.50 (.66)	.0
		21.26 (.34)	.0	.0	.0	.0	.0	.07	80.98 (.66)	.0
	Average →	20.95 (.34)	.0	.0	.0	.0	.08	.07	81.85 (.66)	.0
	#332 Electrode cathodically depolarized externally and used thereafter in up to .008N Cl (.001N KCl + .007N NaCl) 87 Ωxcm^2 of Warburg	.24 (.01)	.01	.0	.0	.0	4.25	.07	77.89 (.94)	.0
		13.54 (.25)	.07	.10	.11	.22	1.05	.07	79.12 (.73)	.0
		13.90 (.26)	.09	.09	.11	.36	.22	.13	77.90 (.73)	.0
		4.25 (.09)	.88	.15	.16	.59	2.01	.02	76.26 (.84)	.0
	Average →	7.88 (.16)	.27	.08	.09	.27	1.92	.08	77.84 (.80)	.0
	#331 Electrode mildly cathodically depolarized in .009N Cl (.001N KCl + .008N NaCl) 948 Ωxcm^2 of Warburg	20.09 (.33)	.12	.05	.0	.0	.22	.07	78.74 (.66)	.0
		19.76 (.33)	.27	.04	.0	.04	.22	.04	79.31 (.66)	.0
		21.04 (.34)	.07	.04	.0	.0	.23	.06	78.84 (.65)	.0
	Average →	20.30 (.34)	.15	.04	.0	.0	.22	.05	78.95 (.66)	.0

Table 4.8 Electron Microprobe Analysis of Chalcocite Electrodes

Electrodes	Condition	S	Cl	K	Ca	Na	Fe	Ni	Cu	Zn
Covellite, Butte, Montana	New original Sample	24.96 (.42)	.02	.01	.02	.0	.0	.0	68.21 (.58)	.0
		27.57 (.45)	.03	.01	.0	.0	.0	.0	65.75 (.55)	.0
		23.92 (.41)	.11	.04	.04	.0	.0	.0	69.22 (.59)	.0
		19.13 (.37)	.0	.0	.0	.0	.0	.0	63.88 (.63)	.0
	Average →	23.87 (.41)	.04	.01	.0	.0	.0	.0	66.77 (.58)	.0
	#335 Electrode mildly depolarized cathodically in .006N Cl (.001N KCl + .005N NaCl)	21.63 (.33)	.05	.04	.0	.16	.09	.19	84.45 (.66)	.0
		16.73 (.32)	.02	.02	.02	.0	.0	.0	69.57 (.68)	.0
		13.61 (.27)	.12	.04	.0	.16	.04	.0	71.29 (.72)	.0
	576 $\Omega x cm^2$ of Warburg impedance level	12.67 (.26)	.07	.03	.01	.05	.0	.0	69.70 (.73)	.0
	Average →	16.06 (.30)	.06	.03	.0	.06	.02	.0	73.73 (.70)	.0
	#338 Electrode mildly depolarized cathodically in solution .006N Cl (.001N KCl + .005N NaCl)	27.93 (.43)	.29	.25	.03	.85	.04	.05	70.88 (.55)	.0
		31.10 (.46)	.07	.12	.01	.39	.03	.0	70.15 (.53)	.0
		20.86 (.43)	.06	.05	.01	.17	.12	.02	69.15 (.56)	.0
	618 $\Omega x cm^2$ of Warburg Average →	28.62 (.44)	.14	.14	.02	.49	.06	.02	70.07 (.54)	.0

Table 4.9 Electron Microprobe Analysis of Covellite Electrodes

Electrodes	Condition	S	Cl	K	Ca	Na	Fe	Ni	Cu	Zn
Chalcopyrite, Messina, Transvaal	New original Sample	33.99 (.49)	.02	.0	.0	.0	30.51 (.25)	.03	34.57 (.25)	.0
		33.98 (.49)	.02	.0	.01	.0	30.72 (.25)	.13	35.02 (.25)	.02
		34.14 (.49)	.03	.0	.01	.0	31.12 (.26)	.04	34.53 (.25)	.0
	Average →	34.04 (.49)	.02	.0	.01	.0	30.78 (.26)	.06	34.70 (.25)	.0
	#344 Electrode cathodically depolarized in .006N NH_4Cl 84 Ωxcm^2 of Warburg	23.67 (.40)	.01	.0	.0	.10	30.09 (.29)	.07	35.42 (.30)	.04
		24.20 (.41)	.0	.0	.0	.08	28.71 (.28)	.13	34.63 (.30)	.06
		17.83 (.35)	.13	.0	.0	.0	28.36 (.32)	.02	33.34 (.33)	.05
	Average →	21.87 (.39)	.04	.0	.0	.05	29.05 (.30)	.07	34.46 (.31)	.04
Pyrrhotite, Falconbridge, Ontario	New original Sample	40.27 (.53)	.02	.0	.01	.08	59.80 (.46)	.99	.03	.09
		37.65 (.52)	.01	.0	.0	.16	60.38 (.47)	.77 (.01)	.02	.12
		36.43 (.51)	.0	.0	.0	.08	60.11 (.48)	1.07 (.01)	.11	.0
	Average →	38.11 (.52)	.01	.0	.0	.11	60.09 (.47)	.94 (.01)	.05	.06
	#336 Electrode depolarized cathodically in .008N Cl^- (.001N KCl + .007N NaCl) 153 Ωxcm^2 of Warburg	29.41 (.46)	.11	.0	.02	.34	58.83 (.53)	.64 (.01)	.0	.41
		36.28 (.46)	.08	.0	.0	.30	72.40 (.53)	.83 (.01)	.05	.48
		26.96 (.43)	.10	.0	.0	.17	60.55 (.56)	.60 (.01)	.14	.28
		36.74 (.50)	.0	.0	.08	.15	61.69 (.48)	.76 (.01)	.05	.32
	Average →	32.29 (.46)	.08	.0	.0	.23	63.36 (.52)	.71 (.01)	.05	.37

Table 4.10 Electron Microprobe Analysis of Chalcopyrite and Phrrhotite Electrodes

Electrodes	Condition	S	Cl	K	Ca	Na	Fe	Ni	Cu	Zn
Pyrite, Ambassaguas, Spain	New original Sample	52.55 (.66)	.03	.0	.01	.0	46.82 (.34)	.02	.06	.19
		50.46 (.66)	.04	.0	.02	.10	45.31 (.34)	.03	.17	.11
		53.61 (.66)	.01	.0	.0	.09	47.50 (.34)	.05	.26	.26
	Average →	52.20 (.66)	.02	.0	.01	.06	46.54 (.34)	.03	.17	.19
	#341 Electrodes depolarized cathodically in .008N $FeCl_2$	9.45 (.22)	.12	.0	.0	.08	58.46 (.77)	.04	.23	.37
		7.01 (.17)	.16	.0	.01	.0	57.87 (.82)	.0	.09	.20
	16 Ωxcm^2 Warburg Average →	8.23 (.20)	.14	.0	.0	.04	58.17 (.79)	.01	.16	.28
	#342 Electrodes mildly depolarized cathodically in .008N Cl (.001N KCl + .007N NaCl) + KOH →pH≈ 9.2	49.30 (.64)	.44	.16	.0	.0	47.92 (.36)	.0	.13	.11
		48.30 (.64)	.02	.0	.0	.0	48.00 (.36)	.0	.04	.06
		51.45 (.65)	.06	.0	.02	.0	47.95 (.35)	.0	.05	.0
	702 Ωxcm^2 of Warburg Average →	49.68 (.64)	.17	.02	.0	.0	47.95 (.36)	.0	.07	.05
	#347 Electrodes depolarized cathodically in .005 NaCl + KOH→pH=8.6	45.90 (.62)	.17	.0	.01	.13	47.44 (.37)	.18	.10	.29
		39.24 (.60)	.10	.0	.01	.0	45.43 (.40)	.01	.0	.13
	1144 Ωxcm^2 of Warburg	32.34 (.52)	1.10 (.02)	.0	.04	1.53 (.03)	46.25 (.43)	.0	.07	.09
		26.55 (.54)	3.11 (.06)	.0	.0	2.33 (.07)	28.90 (.34)	.0	.0	.0
		43.80 (.61)	.29	.0	.02	.44 (.01)	46.71 (.37)	.11	.10	.16
	Average →	37.41 (.58)	1.01 (.01)	.0	.01	1.00 (.02)	42.96 (.38)	.04	.0	.04

Table 4.11 Electron Microprobe Analysis of Pyrite Electrodes

Electrodes	Condition	S	Cl	K	Ca	Na	Fe	Ni	Cu	Zn
Pyrite, Sonora, Mexico	New original Sample	50.20 (.65)	.02	.0	.0	.0	46.70 (.35)	.03	.16	.15
		52.29 (.66)	.0	.0	.0	.0	47.13 (.34)	.0	.19	.17
		53.77 (.66)	.01	.0	.02	.0	47.12 (.33)	.0	.07	.09
	Average →	52.08 (.66)	.01	.0	.01	.0	46.99 (.34)	.0	.14	.13
	#333 Electrode depolarized cathodically then anodically in .006N Cl⁻ (.001N Cl + .005N NaCl) 3195 Ωxcm^2 of Warburg	47.32 (.63)	.05	.0	.03	.13	46.90 (.36)	.0	.0	.11
		49.91 (.64)	.02	.0	.0	.09	47.83 (.35)	.0	.05	.18
		51.92 (.65)	.05	.0	.0	.06	47.44 (.34)	.0	.0	.11
	Average →	49.71 (.64)	.04	.0	.01	.10	47.39 (.35)	.0	.0	.13
Copper	New original Sample	.04	.03	.0	.02	.0	.03	.0	100.53 (1.00)	.0
		.01	.04	.0	.02	.0	.0	.03	102.14 (1.00)	.0
	Average →	.02	.03	.0	.02	.0	.02	.0	101.33 (1.00)	.0
	#334 Electrode depolarized anodically in .0045N Cl⁻ (.001N KCl+.0035N NaCl) 49 Ωxcm^2 of Warburg	.15	1.08 (.02)	.03	.01	.23 (.01)	.01	.07	89.62 (.97)	.0
		.03	1.04 (.02)	.0	.01	.0	.0	.02	91.83 (.97)	.0
		.13	1.16 (.02)	.05	.02	.26 (.01)	.01	.06	92.70 (.97)	.0
	Average →	.10	1.09 (.02)	.03	.02	.15	.0	.05	91.38 (.97)	.0

Table 4.12 Electron Microprobe Analysis of Pyrite and Copper Electrodes

Electrodes	Condition	S	Cl	K	Ca	Na	Fe	Ni	Cu	Zn
Copper	#329	.04	31.42 (.41)	.0	.0	.04	.06	.0	80.64 (.59)	.0
	Electrode heavily depolarized outside cell in NaCl anodically in .001N KCl	.02	23.28 (.33)	.0	.0	.0	.02	.07	82.87 (.66)	.0
	19 Ωxcm^2 of Warburg (So low impedance possibly due to increase of effective area of electrode)	.01	19.29 (.29)	.0	.0	.0	.08	.04	84.94 (.71)	.0
		.02	19.25 (.31)	.0	.0	.0	.0	.0	77.18 (.69)	.0
		.0	18.34 (.28)	.0	.0	.0	.03	.06	85.83 (.72)	.0
	Average →	.02	22.29 (.33)	.0	.0	.0	.03	.01	82.32 (.67)	.0
Brass	New original Sample	.0	.02	.01	.02	.0	.13	.14	56.83 (.50)	57.43 (.49)
		.0	.0	.0	.02	.0	.07	.10	63.18 (.57)	48.13 (.42)
		.02	.02	.0	.01	.0	.10	.06	63.73 (.58)	46.83 (.42)
	Average →	.01	.01	.0	.01	.0	.10	.09	62.50 (.55)	51.70 (.45)
	#327	.14	.67 (.01)	.02	.02	.0	.05	.11	61.60 (.65)	33.10 (.34)
	Electrode depolarized anodically in .001N CKl	.12	.44 (.01)	.07	.0	.0	.09	.09	54.39 (.60)	35.36 (.38)
	98 Ωxcm^2 of Warburg	.14	.45 (.01)	.03	.02	.0	.08	.07	57.15 (.63)	32.72 (.35)
	Average →	.14	.52	.04	.02	.0	.07	.09	57.71 (.63)	33.73 (.36)

Table 4.13 Electron Microprobe Analysis of Copper and Brass Electrodes

extreme depletion in sulfur with the presence of incipient chlorine. The electrodes #342 and 347 mildly depolarized show less depletion of sulfur but some chlorine seems attached to them. The presence of some non-negligible amount of sodium analyzed seems hard to account for. This is especially striking in the sample #347. The sample #342 does not show, however, any sodium, and this eliminates the suspicion we had that we may be observing an evaporate deposit of NaCl from the solution onto the electrode.

Table 4.12 shows more pyrite samples with only very slight depletion of sulfur and essentially no depolarization because of the anodic current imposed on the electrodes after they were mildly depolarized cathodically. We see also copper electrodes #334 anodically depolarized and exhibiting substantial amounts of chlorine.

Finally, Table 4.13 shows a heavily depolarized copper electrode which is loaded with chlorine. The resulting impedance became extremely low. Brass electrodes were also found to behave essentially like copper.

4.4 Chloride and Activated Metals Reactions

We propose in this section several plausible mechanisms to explain the depolarization experiments with special reference to chloride environments. Needless to mention, in some other environments if there is any depolarization at all, different reactions will be operative. The processes involved in such depolarization are not fully understood. However, we

can state general requirements that must be fulfilled at the electrodes:

(i) Some major ionic species in the solution must be involved; this is the only way Faradaic current can be carried through the solution with very low overall Warburg impedance.

(ii) Since solution Warburg and surface Warburg act in series, both must be small when the electrode is depolarized.

(iii) Any non-abundant reacting species must be incorporated into a phase of unit activity so that the reaction product does not add a large impedance in series. In particular, such condition is satisfied if the product formed is solid.

For metal electrodes in a chloride environment, it appears that chloride ions are involved in the depolarized electrode reactions; the evidence is particularly strong for copper as shown in the electron microprobe analyses.

4.4.1 Catalytic Behavior of Metallic Chlorides

With regard to the depolarization of copper and iron electrodes, the required polarity on these electrodes is pre-

cisely the one favoring attraction of chloride ions to the metal electrodes with subsequent electrochemical reactions*:

$$Cu + Cl^- = \overline{CuCl} + \bar{e}$$

$$Fe + 3Cl^- = \overline{FeCl_3} + 3\bar{e}$$

The bar implies that the corresponding phase has essen-

---

*Another plausible reaction would be the formation of paratacamite with Cu and CuO reacting with chloride ions according to the electrochemical reaction

$$Cu + 2Cl^- + 3CuO + 3H_2O = 3Cu(OH)_2 \cdot CuCl_2 + 2\bar{e}$$

$$Eh = 85 - 59.1 \log [Cl^-]$$

No data are available for compounds similar to paratacamite but involving iron. $FeCl_3$ (or $FeCl_2$) are not stable at the conditions of the experiments, and we do not know better alternatives.

tially unit activity so that its relative amount does not critically determine the impedance. The presence, however, of these metallic chlorides catalyzes further metal and chloride reactions contributing thereby to the effective depolarization of the electrode, the Faradaic current in the solution being carried by the abundant chloride ions. Indeed, it is well known that silver chloride electrodes are essentially depolarized in chloride environments. The same mechanism will be operative for the depolarization of copper electrodes and iron electrodes.

We observed in Section 4.3.1 and 4.3.2 that the inferred active ionic species after depolarization tended to approach the chloride concentration in the solution. The case is striking for copper but somewhat less evident for iron. The time variation of the impedance of depolarized copper and sulfide electrodes are relatively well pronounced. However, the relative stability of the impedance of depolarized iron electrodes remains a puzzle which further experimentation as suggested in section 5.2 may attempt to clarify. Except for copper under extreme depolarization where they match, the inferred active ionic species concentrations are usually smaller than the Cl^- concentrations. At least two factors may contribute to the mismatch of the concentrations: first, the effective size of the electrode active area being much smaller than the area of the electrode; second, the surface diffusion impedance is acting in series with the solution

Warburg. The separation of all these factors is not an easy task. A most promising approach would be the careful monitoring of the temperature dependence of the Warburg impedance. The solution Warburg should have the same temperature dependence as the viscosity of the solution. Any departure from such behavior may be ascribed to the electrode surface processes.

It is also observed that stirring after depolarization contributes sometimes to an accelerated increase in the electrode impedance. We suspect that stirring helps polarize the electrode by destroying the effect of the depolarization, i.e. dissolving the metallic chloride. Further research may be needed to clarify the rate of the metallic chloride dissolution. A comparative study of depolarization in very concentrated solutions and dilute solutions could help to identify the catalytic behavior of the metallic chlorides. The discrete nature of our measurements makes it extremely hard to give good estimates of the induced rate of impedance changes associated with stirring. Through continuous monitoring of the electrode impedance, such rate could perhaps be conveniently estimated. In particular, it may be useful to know whether there exists a saturation effect whereby if the solution reaches the saturation level of metallic chloride, the time variation of the depolarized electrode impedance will be minimized.

4.4.2 Induced Activated Metals on Sulfide Electrodes

The cathodic current required to depolarize the sulphide

electrodes is such that the sulfide bonds must be superficially destroyed, allowing thereby local depletion of sulfur from the electrode surface with subsequent increase in metal to sulfur ratio. This conclusion has indeed been confirmed by the microprobe analyses discussed in Section 4.3.3. We call such exposed metals "activated metals" because we suspect them to be responsible for the electrode reactions with the abundant chloride ions as outlined in Section 4.4.1. The qualifier "activated" is to remind us of substantial difference in comparison to the behavior of ordinary metals which give relatively high electrode impedance in chloride environments. As a rule, it appears that the degree of depolarization of a copper or iron sulfide electrode is related to the extent to which the depletion of sulfur has been carried out. In addition, Table 4.5 gives a case of pyrite electrode submitted to cathodic current outside the cell and which exhibited a low level of impedance comparable to those of electrodes depolarized in the cell. This essentially eliminated any suspicion that the depolarization could be due to the sulfide ions getting into solution and becoming active at the electrodes as we have seen in Section 3.2.2.

Several hypothetical reaction mechanisms leading to the formation of activated metals can be derived. The required cathodic current for the depolarization of sulfide electrodes will prompt drift of cations H^+, K^+, and/or Na^+ towards the electrodes. Subsequently H_2S will evolve at the sulfide

electrodes as a result of the reduction of the metals and the depletion of the electrode in sulfur. To help the depletion in sulfur, K_2S and Na_2S could conceivably be formed but will be readily hydrolyzed yielding potassium and sodium hydroxides. More speculative compounds like incipient potassium copper sulfide $KCuS_4$ or potassium copper iron sulfide $K_3(Cu,Na)Fe_{12}S_{14}$ listed in the x-ray diffraction search manual[†] could conceivably be formed as the result of K^+ or Na^+ reactions. At covellite and chalcocite electrodes we could have:

$$4\ CuS + K^+ + \bar{e} = KCuS_4 + 3Cu^*$$
(covellite) (activated copper)

$$4\ Cu_2S + K^+ + \bar{e} = KCuS_4 + 7\ Cu^*$$

We tried to detect such exotic compounds looking for the corresponding x-ray diffraction spectral lines using test samples from depolarized chalcocite electrodes. Our attempts were unsuccessful since our observed spectral lines showed only lines corresponding to chalcocite. Other plausible reactions for the formation of "activated metals" are listed in the following:

$$CuS + 2\bar{e} = Cu^* + S^=$$

$$Cu_2S + 2\bar{e} = 2Cu^* + S^=$$

$$CuFeS_2 + 2\bar{e} = Cu^* + FeS + S^=$$
(chalcopyrite) (pyrrhotite)

[†]Powder Diffraction File, 1974.

$CuFeS_2 + 2\bar{e} = Fe^* + CuS + S^=$

$CuFeS_2 + 4\bar{e} = Fe^* + Cu^* + 2S^=$

$FeS_2 + 4\bar{e} = Fe^* + 2S^=$
(pyrite)

$FeS + 2\bar{e} = Fe^* + S^=$

Of course several intermediate compounds in the system Cu-Fe-S could possibly be formed in view of the complex nature of this system. Extreme depolarization of sulfide electrodes shows very substantial depletion of the electrode surface in sulfur. Typical examples can be seen in Table 4.8 for chalcocite #332, Table 4.10 for chalcopyrite #344, and Table 4.11 for pyrite #341. The exposed "activated metals" will essentially act like active sites where the chloride reactions could take place. If the distribution of active metal sites is dense enough to lower substantially the surface diffusion impedance, it could be possible to observe the contribution to the electrode impedance of the diffusion of chloride in the solution.

The surface diffusion impedance provides a plausible rationale for the explanation of the background electrode impedances as a small number of active sites will give a surface diffusion impedance high enough to shadow the contribution of the solution provided major ionic species carry the Faradaic current in the solution. As long as the solution chemistry is not affecting the surface phenomena and as long as the solution Warburg is small compared to the surface diffusion

Warburg, the measured electrode impedance will be independent of the solution chemistry.

CHAPTER V

SUMMARY AND CONCLUSIONS WITH IMPLICATIONS FOR MINERAL EXPLORATION

The purpose of this study was to identify the controlling factors in induced polarization of metallic minerals. Our electrochemical approach led to extensive investigation of electrode impedance behavior in various environments. Several results of geophysical and/or electrochemical interest emerge from this study.

A consistent and remarkable observation in all the variety of experimental conditions is that the electrode impedance is dominated by the Warburg impedance which confirms a result obtained by Madden in his thesis (Madden, 1961). The implication of this observation is that the electrode impedances are controlled by some diffusion processes. Such diffusion could occur either in the solution or along the surface of the electrode. We have shown that when the ionic species Cu^{++} or $S^{=}$ are in the solution, they could be active at the electrodes, i.e. control the electrode impedance. In such cases, the controlling diffusion processes occur in the solution and surface diffusion phenomena are not involved.

A large variety of ionic species do not appear to be active in this way. These include chlorides (Cl^{-}), sulfates ($SO_4^{=}$), carbonates ($CO_3^{=}$), nitrates (NO_3^{-}), hydroxides (OH^{-}), iron (Fe^{++}), calcium (Ca^{++}), potassium (K^{+}), sodium (Na^{+}), and hydronium (H^{+}). In such

environments, the electrode impedance appeared realtively independent of the solution chemistry. In such circumstances, we have formulated the hypothesis that the diffusion processes occur in the volume and/or surface of the electrodes. Of additional support to this hypothesis is the observation that the electrode impedance is heavily dependent on the surface condition of the electrode. Reactions may occur only at specific sites so that only a fraction of the electrode surface would have active sites for the charge transfer reactions.

We have shown that for copper electrode reactions in chloride environments, depolarization could bring the electrode impedance to a level equivalent to the chloride diffusion contribution in the solution. Iron does not reach this level, at least in the condition of our experiments, and we suspect that surface diffusion remains an important factor for the iron electrode impedance, somewhat overriding the chloride diffusion contribution.

Metallic chlorides like CuCl appear to catalyze the charge transfer reactions but a detailed analysis of this phenomenon is complicated by some non-equilibrium conditions leading to significant time variation of the electrode impedance. Continuous monitoring of the impedance may be a convenient approach for a better understanding of these time variations.

Our analyses show that the electrode reactions involve essentially no reaction resistance in almost all our

measurements. Such a result implies very high exchange current density i_0 for the electrode processes. Our estimates of i_0 give consistently values greater than 10^{-5} A/cm^2 with many examples of i_0 greater than 10^{-3} A/cm^2. It also must be remembered that these estimates are lower bounds due to the insignificance of the reaction resistance. It is, however, a common experience that the magnitude of measured exchange current densities varies between wide limits.

Reactions at sulfide electrodes will involve sulfide ions if these ions are present in the solution leading to electrode impedance control from diffusion processes in the solution. In absence of active ionic species the hypothesis of diffusion of ionic species in the volume and/or surface of the electrode still holds. This process may be operative in only a few active sites. The generation of these sites is fostered by limited impression of cathodic current onto the sulfide electrodes creating thereby activated metals resulting from the depletion of sulfur from the electrode surface. Thus the electrode reactions would involve, we believe, the exposed activated metals and the chloride ions leading to a dramatic drop of the electrode impedance.

5.1 Implications for Electrical Exploration of Minerals

The impedance determing property of cupric and sulfide ions may have important consequences for the induced polarization measurements in prospecting for metallic minerals. Ore deposit environments contain a wide variety of ionic species

as well as complexes of ore metals which provide a means for the transport of ore minerals leading to various zoning sequences (Barnes and Czamanske, 1967). As a rule, the environment in the ground above the water table is oxidizing and usually acidic because of appreciable carbon dioxide and humic acids existing in the soil waters (Park and McDiamird, 1975). This is also the zone of influence of meteoric waters which carry along various dissolved substances through the soils and rocks which may react with preexistant minerals, forming various compounds like carbonates, sulfates, and silicates. In particular, cupric ions may exist in such environments.

The environment in the vicinity of the water table is generally reducing and neutral or mildly alkaline due to progressive neutralization of the acids from the oxidized zones. The deeper environment below the water table is usually alkaline and reducing where sulfides are essentially stable. Microorganism activity and/or organic matter can, however, perturb this gradational sequence. For example, sulfate ions can be reduced by bacterial activity but not through simple inorganic reactions in aqueous solutions.

Motoaki Sato (1960) made several in-situ measurements of Eh and pH in some mining districts. We have summarized his results in Table 5.1 using our standard calomel reference electrode scale of oxidation potential. In this table, O stands for oxidized zones while P represents primary zones usually reducing or mildly so. From the measured values of

Mine District	# of Data Points	Location	Depth Range (ft)	pH Range	SCE Eh (mv) Range	Temperature Range °C	Zone
Magma Mine Superior, Arizona	7	Central	0-50	4.4 to 8.1	58 to 328	22-28	O
	8	East and West	2500 to 4800	6.2 to 8.5	-142 to 78	36-68	P
San Manuel Mine San Manuel, Arizona	13	North, South and Main	1475 to 2075	5.7 to 8.6	-172 to 128	27-33	P
Cole and Campbell Mines Bisbee, Arizona	4	Cole	600 to 900	7.5 to 8.3	- 22 to 98	22-31	O
	2	Campbell	2800	7.8 to 8.0	-132 to -112	30-31	P
Continental #1 Mine San Juan County, Utah	4	C-5 to C-45	100 to 250	8.1 to 8.7	-152 to - 32	12-13	P

Table 5.1 Eh-pH of Natural Waters in Mining Districts

(Adapted from Motoaki Sato, 1960)

O = Oxidized Zone

P = Primary Zone, usually reducing

Eh and pH, we can infer in each zone, some range of concentrations of cupric or sulfide ions if these ionic species were present in the environment.

We can see that in the Magma Mine of Table 5.1, the oxidized zone could allow the presence of some active species like Cu^{++} since any existing copper sulfide will be oxidized to give cupric and sulfate ions. A crude estimate of the cupric ion concentrations using the Eh-pH diagram from copper gives an upper limit of about 10^{-3} mole/l. Thus, IP measurements in this environment may show impedance values generally lower by one to two orders of magnitude in comparison to the typical background values outside this zone. On the basis of cupric ion activity, the O zone from the Cole mine (Table 5.1) will not show, however, any anomaly in the impedance level of IP measurements. Similarly, on the basis of sulfide activity, anomalous IP impedances are to be expected only in very alkaline and reducing environments where sulfide ions may be abundant (Pourbaix, 1966). Such conditions are not met even in the P zones of Table 5.1 and, therefore, we suspect that in most environments, IP will not show significant impedance anomalies due to sulfide ions.

It is of interest to see whether one could attempt to ascribe diagnostic characteristics to a given sulfide mineral on the basis of its electrode impedance spectrum. Table 5.2 shows some results for background spectra of covellite, chalcocite, chalcopyrite, pyrite and pyrrhotite. The values

Table 5.2 Comparison of Background Electrode Impedances for Sulfide Electrodes

Covellite		Chalcocite		Chalcopyrite		Pyrite		Pyrrhotite	
W	C	W	C	W	C	W	C	W	C
2950	237	7149	34	13580	56	8567	49	9099	23
2132	91	7005	25	15930	59	3046[C]	97[C]	1595	71
2175	94	8511	26	3506[C]	344	4507[C]	75[C]	2609	47
8304*	36*	18800*	4*	15310	35	3195[C]	54[C]	2510	59
2782	119	3225	11	4346[C]	171[C]	6977	84	5767	31
2760	59	976[A]	41[A]	3094[C]	591[C]	7856	115	8451	33
4514	151	808[A]	24[A]			6331	39	4102	40
1504	30	2368[B]	111[B]			6651	92	2736	66
		4911	38			13360	44	2137	67
		11720	14			18610	64	3989	39
		11390	22					3444	39
								17000[D]	16[D]
$\bar{w}$=2559	$\bar{c}$=94	$\bar{w}$=7079	$\bar{c}$=22	$\bar{w}$=14890	$\bar{c}$=49	$\bar{w}$=9036	$\bar{c}$=65	$\bar{w}$=3648	$\bar{c}$=44

* Diamond polish

A Possibility of low w due to OH^- as active ion

B Possibility of low w due to H^+ as active ion

C Self-repolarizing values after depolarization

D Left in oxidizing environment for 100 hours

$\bar{w}$ and $\bar{c}$ are geometric mean of Warburg and capacity exclusive of special cases indicated by superscripts

Table 5.2 Comparison of Background Electrode Impedances for Sulfide Electrodes

$\bar{w}$ and $\bar{c}$ presented for each electrode are, respectively, the geometric mean of the Warburg impedance, and fixed layer capacity values listed without taking into account the special cases indicated. This crude appraisal gives the following hierarchy of electrode impedances:

covellite CuS < pyrrhotite FeS < chalcocite Cu_2S < pyrite FeS_2 < chalcopyrite $CuFeS_2$

This hierarchy is systematic but not quite absolute. The differences, however, are probably not great enough to serve as diagnostic tools in interpreting field IP data as these differences can be overshadowed by factors such as the mineral habits and concentrations.

A better understanding of the importance of active species in field measurements will come from good geochemical control in areas covered by IP surveys in order to establish possible correlations between the measured IP values and corresponding geochemical data about the environment. Such empirical studies may be especially feasible in mining areas where clear zoning sequences are well established. It could therefore be possible to set some empirical guidelines for the interpretation of IP measurements.

5.2 Suggestions for Further Research

We have seen that the electrode impedance is a function both of the solution chemistry and the electrode surface condition. We have indeed seen both extreme cases when the electrode impedance is controlled by the solution chemistry

(proposed preeminance of active species contribution in solution when surface phenomena are not involved) and when the electrode impedance is controlled by the electrode surface condition and is independent of the solution chemistry (proposed preeminence of surface diffusion impedance overriding any solution contribution). The general situation, however, is a mixing of both diffusion processes and their separation appears a formidable task. An initial helpful experimental procedure would consist in making use of an impedance comparator which subtracts the solution resistance from the overall impedance on the basis of a high frequency measurement. Such a system would allow one to expose the interfacial impedance in cases when the overall impedance is dominated by the solution resistance and thus provide a more sensitive electrode impedance spectrum.

With such sensitive processes, one could attempt to test the conclusions relative to the analysis of the surface diffusion impedance outlined in Section 4.2 as well as measure the relative importance of the solution contribution: the first step would consist in a systematic investigation of the influence of the electrode surface topography. In particular one could test our conclusion that the fixed layer capacity will increase while the solution Warburg will remain unaffected if the diffusion lengths and the diffusion layer volume are respectively greater than the topography and the integrated volume of the crevices. There is, however, one loop-

hole in such a test because surface diffusion impedance must also be considered. Therefore, the second step which might be looked at concurrently with the previous one is the temperature dependence of the interfacial impedance. A careful investigation of the temperature dependence of the Warburg impedance will show the relative importance of the solution Warburg with respect to the surface Warburg. As mentioned in Section 4.4.1, the solution Warburg should have the same temperature dependence as the viscosity of the solution. Needless to say, care must be taken in order not to fall in a "Teufelkreis" whereby the temperature change affects substantially the electrode surface condition.

Our experiments have heavily stressed chloride environments (perhaps unfairly) for Cl^- is a common ionic species in natural waters. It is obvious that the straightforward extension of these experiments to various environments is feasible. In particular, depolarization experiments could be carried in different environments under different conditions and perhaps provide a basis for the inference of the corresponding electrode reactions. We must add that our proposed chloride reactions at iron electrodes need to be more extensively investigated. In particular, the relative stability of the depolarized iron electrode impedance requires further investigation. Comparative study of the iron electrode in oxidizing and reducing environments may perhaps help in understanding better the behavior of the iron electrode

impedance.

Lastly, it is very likely that valuable imformation for the IP phenomena lie in the nonlinear regime. Our method of electrical equivalent circuit is a consequence of the linear regime assumed throughout the study. Therefore, the study of nonlinearities will require a somewhat different approach which may open a new field contributing more specifically to a better understanding of borehole measurements.

APPENDIX A

INVERSION OF THE ELECTRODE IMPEDANCE SPECTRUM BY THE GENERALIZED INVERSE THEORY

Let the analytic expression of the impedance of the circuit simulating the electrode impedance be

$$Z = Z(\omega, P_1, P_2, \ldots P_m) \equiv Z(\omega, \underline{P})$$

where ω represents a frequency and P_1, P_2, $\ldots P_m$ are the elements of the electrical equivalent circuit. These elements are frequency independent but unknown. Their knowledge will provide a means to predict the electrode impedance at any given frequency within the frequency range prescribed in the text. The measured impedance spectrum would essentially be a sampling of $Z(\omega, \underline{P})$ at the given frequencies were the model ideal and the measurements error-free. Thus, a sufficient number of measurements of the electrode impedance at various frequencies ω_i, $(i = 1, 2, \ldots n)$ will give a sufficient number of presumably independent relations between the elements of the circuit and thence yield the values of these elements by the solution of the inverse boundary value problem.

Solution of the Inverse Problem

A set of n measurements of the electrode impedance at n frequencies ω_i $(i = 1, 2, \ldots n)$ generates n relations

$$Z(\omega_i, \underline{P}) = Z^{obs}(\omega_i)$$

This gives n complex nonlinear equations from which it is possible to find the values of the elements P_i which fit best

all the observed spectrum. This could be achieved by making a first order Taylor expansion of $Z(\omega,\underline{P})$ near some reasonable starting values of the parameter $\underline{P}$ and adjusting these parameters iteratively:

$$Z^{obs}(\omega_i) = Z_i + \frac{\partial Z_i}{\partial P_j} \Delta P_j + HOT^*$$

where Z_i represents $Z(\omega_i,\underline{P})$. Einstein's summation convention is used.

The relevant changes in theparameters are found by solving the system of linearized equations

$$\frac{\partial Z_i}{\partial P_j} \Delta P_j = Z^{obs}(\omega_i) - Z_i \qquad (i = 1, \ldots n)$$

The new values of the parameters are used as starting values for a new iteration and the process goes until the changes in the parameters appear insignificant.

A more efficient method to solve the above nonlinear problem is provided by the method of logarithmic variation (Madden, 1972) which reads

$$\frac{\partial \text{Log } Z_i}{\partial \text{Log } P_j} \Delta \text{ Log } P_j = \text{Log } \frac{Z^{obs}(\omega_i)}{Z_i} \qquad (i = 1, \ldots n)$$

It has several built in assets, the simplest of which is that it takes advantage of the positive nature of the parameters and weights the data and parameters uniformly. Since the im-

---

*Higher Order Terms

pedance $Z(\omega,\underline{P})$ is complex and can be put in the form

$$Z = |Z| \exp(i\phi)$$

where $|Z|$ represents the amplitude and ϕ the phase, both functions of the frequency ω and the parameters P_j. The above equations are split into equations involving amplitudes and equations involving phases:

$$\frac{\partial \text{Log } |Z_i|}{\partial \text{Log } P_j} \Delta \text{ Log } P_j = \text{Log} \frac{Z^{obs}(\omega_i)}{|Z_i|}$$

$$\frac{\partial \phi_i}{\partial \text{Log } P_j} \Delta \text{ Log } P_j = \phi^{obs}(\omega_i) - \phi_i \qquad \begin{matrix} i = 1, \ldots n \\ j = 1, \ldots m \end{matrix}$$

This system of 2n equations is of the form

$$Ay = b \tag{1}$$

where y and b are unicolumn matrices and A is a 2n x m matrix:

$$y \equiv [y_j] \qquad y_j = \Delta \text{ Log } P_j \qquad j = 1, \ldots m$$

$$b \equiv [b_k] \qquad b_{2i-1} = \text{Log} \frac{|Z^{obs}(\omega_i)|}{|Z_i|} \qquad i = 1, \ldots n$$

$$b_{2i} = \phi^{obs}(\omega_i) - \phi_i \qquad k = 1, \ldots 2n$$

$$A \equiv [a_{kj}] \qquad a_{2i-1j} = \frac{\partial \text{Log}|Z_i|}{\partial \text{Log } P_j} \qquad i = 1, \ldots n$$

$$a_{2ij} = \frac{\partial \phi_i}{\partial \text{Log } P_j} \qquad j = i, \ldots m$$

$$k = 1, \ldots 2n$$

A useful property of the A matrix in the process of computation is that when the parameters are all homogeneous circuit elements (all impedances or all admittances), the sum of the elements of A in a row is 0 or 1 respectively for even and odd rows. It can also be shown that all the eigenvalues of A are less than unity. When 2n is larger than m, the system (1) to be solved is overdetermined. A possible fit to the data is provided by the least square solution

A particular approximate solution to Equation (1) in the least-squares sense is given by (Madden, 1972)

$$y'' = (\tilde{A}A + \varepsilon^2 I)^{-1} \tilde{A}b$$

where $\tilde{A}$ is the matrix A transposed, I the unit matrix of order m and ε^2, which we call the cutoff eigenvalue, is to minimize the influence of small eigenvalues of A generating instabilities. This solution represents the relevant changes of the logarithm of the parameters so that new values can be assigned to the parameters for a new iteration process. This "ε^2 method" which provides an approximate generalized inverse is very practical since it does not require a complete eigenvalue analysis of the A matrix for each iteration.

A feeling for the relevance of each parameter is given by the examination of the resolution matrix

$$R = (\tilde{A}A + \varepsilon^2 I)^{-1}\tilde{A}\,A$$

after a sufficient number of iterations.

When elements are well resolved, the corresponding rows

look like delta functions, i.e. all the elements are zero except the one on the diagonal of R, which is close to unity. When elements are poorly resolved, they may be: significant, in which case the corresponding rows contain scattered values addin up to a finite number less than unity; or, insignificant, in which case all the elements in the corresponding rows are zero. The choice of the cutoff eigenvalue is dictated by the quality of the fits obtained. Our fits were good enough so that we could allow a cutoff eigenvalue as small as .01.

REFERENCES

Antropov, L. I., 1972, Theoretical Electrochemistry, Mir Publishers, Moscow.

Baas Becking, L.G.M., Kaplan, I. R. and Moore, D., 1960, "Limits of the Natural Environment in Terms of pH and Oxidation-Reduction Potentials", *The Journal of Geology*, 68, No. 3, 243-284.

Bacon, L. O., 1965, "Induced Polarization Logging in the Search for Native Copper", *Geophysics*, 30, No. 2, 246-256.

Barnes, L. H., and Czamanske, G. K., 1967, "Solubilities and Transport of Ore Minerals", in Geochemistry of Hydrothermal Ore Deposits, L. H. Barnes, Ed., Holt, Rinehart and Winston, Inc., New York.

Bertin, Jacques, 1968, "Some Aspects of Induced Polarization", *Geophys. Prosp.*, 16, No. 4, 401.

Bertin, J. and Loeb, J., 1969, "Transients and Field Behavior in Induced Polarization", *Geophys. Prosp.*, 17, No. 4, 488.

Bleil, D. F., 1953, "Induced Polarization: a Method of Geophysical Prospecting", *Geophysics*, 18, 636-661.

Brant, A. A., 1959, in Overvoltage Research and Geophysical Applications, J. R. Wait, Ed., Pergamon Press.

Craig, J. R. and Scott, S. D., 1974, "Sulfide Phase Equilibria" in Sulfide Mineralogy , *Miner. soc. Amer. Short Course Notes*, P. H. Ribbe, Ed., 1.

Erdey-Grúz, Tibor, 1972, Kinetics of Electrode Processes, Wiley-Interscience Division, New York.

Frische, Richard H. and von Buttlar, H., 1957, "A Theoretical Study of Induced Electrical Polarization", *Geophysics*, 22, 688-706.

Garrels, R. M. and Christ, C. L., 1965, Solutions, Minerals and Equilibria, Harper and Row, Publ., New York.

Grahame, D. C., 1952, "Mathematical Theory of Faradaic Admittance", *J. of Electrochem. Soc.*, 99, 370C.

References (continued)

Hallof, P. G., 1957, "On the Interpretation of Resistivity and Induced Polarization Field Measurements", Ph.D. Thesis, MIT.

Hallof, P. G., 1966, "A Comparison of Variable Frequency IP Results with Turam Electromagnetic Conductors", *Mining Geophysics*, 1, 172.

Henkel, J. H. and Van Nostrand, R. G., 1957, "Experiments in Induced Polarization", *A.I.M.E. Trans.*, 9, 355-359.

Henkel, J. H., 1958, "Some Theoretical Considerations on Induced Polarization", *Geophysics*, 23, No. 2, 299-304.

Ives, D. J. G. and Janz, G. J., 1961, Reference Electrodes, Theory and Practice, Academic Press, New York.

Kaspers, C., 1940, "The Theory of the Potential and the Technical Practice of Electrodeposition (Parts I, II)", *Trans. Electrochem. Soc.*, 77, 353 and 365.

_____, 1940, "The Theory of the Potential and the Technical Practice of Electrodeposition (Parts III, IV), *Trans. Electrochem. Soc.*, 78, 131 and 147.

_____, 1942, "The Theory of the Potential and the Technical Practice of Electrodeposition (Part V)", *Trans. Electrochem. Soc.*, 82, 153.

Komarov, V. A., Pishpareva, N. A., Semenov, M. V., and Khloponina, L. S., 1966, Teoretisheskie Osnovi Interpretatsii Nabludenie v Metode Vizvannoy Polarizatsii (in Russian), Niedra, Leningrad.

de Levie, R., 1963, "On Porous Electrodes in Electrolyte Solutions", *Electrochemica Acta*, 8, 751.

_____, 1964, "On Porous Electrodes in Electrolyte Solutions", *Electrochemica Acta*, 9, 1231.

_____, 1965, "Influence of Surface Roughness of Solid Electrodes on Electrochemical Measurements", *Electrochemica Acta*, 10, 113.

_____, 1967, "Electrochemical Response of Porous and Rough Electrodes", in Advances in Electrochemistry and Electrochemical Engineering, Delahay, P. and Tobias, C. W., Eds, 6, 329.

Madden, T. R., Marshall, D. J., Fahlquist, D. A., Neves, A. S., 1957, "Background Effects in the IP Method of Geophysical Exploration", *AEC Report RME*, M.I.T., 3150.

Madden, T. R., and Marshall, D. J., 1958, "A Laboratory Investigation of IP", *AEC Report RME*, M.I.T., 3156.

Madden, T. R., and Marshall, D. J., 1959, "Electrode and Membrane Polarization", *M.I.T. Interim Report RME*, 3157.

Madden, T. R., and Marshall, D. J., 1959, "Induced Polarization: a Study of its Causes and Magnitudes in Geologic Materials", *AEC Report RME*, 3169.

Madden, T. R., "Electrode Polarization and its Influence on the Electrical Properties of Mineralized Rocks", Ph.D. Thesis, M.I.T., 1961.

Madden, T. R., and Cantwell, T., 1967, "IP, a Review", *Mining Geophysics*, II, SEG, Tulsa.

Madden, T. R., 1967, "Induced Polarization and its Application to Mineral Exploration", a lecture read at the Interregional Seminar of UNO on New Methods for Mineral Exploration with Emphasis on Geophysical Techniques, held in Moscow in July 1967.

Madden, T. R., 1972, "Transmission Systems and Network Analogies to Geophysical Forward and Inverse Problems", *Technical Report No. 72-3*, M.I.T.

Marshall, D. J., 1959, "Interfacial Polarization in Membranes and Its Significance in the Induced Polarization of Geologic Materials", Ph.D. Thesis, M. I. T.

Marshall, D. J. and Madden, T. R. 1959, "Induced Polarization: a Study of Its Causes", *Geophysics*, 24, 790-816.

Neuman, G. and Neumann, G. M., "Surface Self-Diffusion of Metals", *Diffusion Monograph Series No. 1.*

Oriani, R. A. and Frankenthal, R. P., 1962, in Metal Surfaces, Americ. Soc. for Metals, Metals Park, Ohio.

Park, C. F. and McDiamird, R. A., 1975, Ore Deposits, 3rd Edition, Freeman Press, New York.

Pourbaix, M., 1945, "Thermodynamique des Solutions Aqueuses Diluées", Representation Graphique du Rôle du pH et du Potentiel", Thesis, Delft, CEBELCOR Reprint (1963).

Pourbaix et al., 1966, Atlas of Electrochemical Equilibria in Aqueous Solutions, Pergamon Press, New York.

Pourbaix, M., 1973, Lectures on Electrochemical Corrosion, Plenum Press, New York.

Sato, Motoaki, 1960, "Oxidation of Sulfide Ore Bodies, I, Geochemical Environments in Terms of Eh and pH", *Economic Geology*, 55, 928-961.

Schlumberger, C., 1920, "Etude Sur la Prospection Electrique du Sous-Sol", Gauthier-Villars et Cie, Editeurs, 70-72.

Siegel, H. O., 1959, "A Theory of IP Effects for Step-Function Excitation", in Overvoltage Research and Geophysical Applications, J. R. Wait, Ed., Pergamon Press, New York.

Siegel, H. O., Hill, H. L., and Baird, J. G., 1968, "Discovery Case History of the Pyramid Ore Bodies Fine Point, Northwest Territories, Canada", *Geophysics*, 33, No. 4, 645-656.

Sumi, F., 1959, "Geophysical Exploration in Mining by Induced Polarization", *Geophys. Prosp.*, 7, No. 3, 300.

Sumi, F., 1961, "The Induced Polarization Method in Ore Investigation", *Geophys. Prosp.*, 9, No. 3, 459.

Sumi, F., 1965, "Prospecting for Non-Metallic Minerals by Induced Polarization", *Geophys. Prosp.*, 13, No. 4, 603.

Swift, C. M., 1973, "The L/M Parameter of Time-Domain IP Measurements - A Computational Analysis", *Geophysics*, 38, No. 1, 61.

Uhlig, H. H., 1971, Corrosion and Corrosion Control, 2nd Ed., John Wiley and Sons, Inc., New York.

Vacquier, V., Holmes, C. R., Kitzinger, P., and Lavergne, M., 1957, "Prospecting for Ground Water by Induced Electrical Polarization", *Geophysics*, 22, No. 3, 660.

Vetter, K. J., 1967, Electrochemical Kinetics, Academic Press, New York.

Van Voorhis, G. D., Nelson, P. H., and Drake, T. L., 1973, "Complex Resistivity Spectra of Porphyry Copper Mineralization", *Geophysics*, 38, No. 1, 49-60.

Wagner, C., 1933, "Beitrag Zur Theorie des Anlaufvorgangs I", *Z. Physikal Chem. Abt. B.*, 21, Heft 1-2.

_____, 1936, "Beitrag Zur Theorie des Anlaufvorgangs II", *Z. Physikal Chem. Abt. B.*, 32, Heft 6.

Wagner, C. and Grünewald, K., 1938, "Beitrag Zur Theorie des Aulaufvorgangs III", *Z. Physikal Chem. Abt. B.*, 40, 6.

Wagner, C., 1951, "Theoretical Analysis of the Current Density Distribution in Electrolyte Cells", *J. of Electrochem. Soc.*, 98, 116.

Wagner, C., 1961, "Calculation of the Current Distribution at Electrodes Involving Slots", *Plating*, 48, 997.

Wait, R., 1959, Overvoltage Research and Geophysical Applications, J. R. Wait, Ed., Pergamon Press, New York.

West, J. M., 1971, Electrodeposition and Corrosion Processes, Van Nostrand Reinhold Company, London.

Zonge, K. L., Sauck, W. A., and Sumner, J. S., 1972, "Comparison of Time, Frequency, and Phase Measurements in Induced Polarization", *Geophys. Prosp.*, 20, No. 3, 626.

de Zoubov, N., Vanleugenhaghe, C., and Pourbaix, M., 1963, "Copper", in Atlas of Electrochemical Equilibria in Aqueous Solutions, Pergamon Press, New York.

LIST OF SYMBOLS

c_i	concentration of i^{th} ionic species
C_o	salt concentration
c_f	fixed layer capacity
c_1, c_2	chemical capacity
D_n	diffusivity of negatively charged ionic species
D_p	diffusivity of positively charged ionic species
D_s	diffusivity of surface species
E	electric field
Eh	oxidation-reduction potential
F	Faraday
$\Delta\vec{G}_o^{\dagger}, \Delta\overleftarrow{G}_o^{\dagger}$	free energy change involving activated complex
h	Planck's constant
$H_0^{(1)}(z)$, $H_1^{(2)}(z)$	Hankel's function of second kind of order 0 and 1
i_∞	total current
i_{α_i}	current associated to electrode reaction involving i^{th} ionic species
i_0	exchange current density
i_x	current for reaction of species x
j	$\sqrt{-1}$
K	diffuse layer parameter
k	Boltzmann's constant
mV	millivolt

n	concentration of negatively charged ionic species
n_1	concentration change of negatively charged ionic species
p	concentration of positively charged ionic species
p_1	concentration change of positively charged ionic species
q_0	active species concentration
Q	active ionic species
q_1	concentration change of active species
R	perfect gas constant
R, R_1, R_2	reaction resistance
R_s	solution resistance
r_1^{-1}	diffuse zone distance
r_2^{-1}	diffusion length
SCE	standard calomel electrode
T	absolute temperature (°K)
t	time
V_f	voltage drop across fixed layer
CW	capacity-Warburg in series
W, W_1, W_2	Warburg impedance amplitude
WCR	Warburg-capacity-resistance in series
W_s	surface Warburg amplitude
W_{sol}	solution Warburg
Z_W	Warburg impedance
Z_{W_s}	surface Warburg impedance

α	reaction rate parameter
α_i	fraction of total current carried by i^{th} ionic species reaction
β, γ, ξ	reaction rate coefficients
ε	dielectric constant
ϕ	phase of impedance
η θ	reaction rate parameters
μ_i	mobility of i^{th} ionic species
μ_F	microfarad
ν	reaction rate coefficient
ν_i	stochiometric coefficient
σ	ratio of negative and positive ionic species mobilities
Ω	Ohm
ω	angular frequency